STUDY OF POLY(ACRYLIC ACID) AND LITHIUM TETRAFLUOROBORATE/LITHIUM PERCHLORATE BASED POLYMER ELECTROLYTES

NGAI KOH SING

FACULTY SCIENCE
UNIVERSITI MALAYA
KUALA LUMPUR

2023

STUDY OF POLY(ACRYLIC ACID) AND LITHIUM TETRAFLUOROBORATE/LITHIUM PERCHLORATE BASED POLYMER ELECTROLYTES

NGAI KOH SING

THESIS SUBMITTED IN FULFILMENT OF THE REQUIREMENTS FOR THE DEGREE OF DOCTOR OF PHILOSOPHY

DEPARTMENT OF PHYSICS
FACULTY SCIENCE
UNIVERSITI MALAYA
KUALA LUMPUR

2023

UNIVERSITI MALAYA

ORIGINAL LITERARY WORK DECLARATION

Name of Candidate: **NGAI KOH SING**

Registration No: **17006027/1**

Name of Degree: **DOCTOR OF PHILOSOPHY**

Title of Thesis:
STUDY OF POLY(ACRYLIC ACID) AND LITHIUM TETRAFLUOROBORATE/LITHIUM PERCHLORATE BASED POLYMER ELECTROLYTES

Field of Study: **EXPERIMENTAL PHYSICS**

I do solemnly and sincerely declare that:

(1) I am the sole author/writer of this Work;
(2) This Work is original;
(3) Any use of any work which copyright exists was done by way of fair dealing and for permitted purposes and any except or extract from, or reference to or reproduction of any copyright work has been disclosed expressly and sufficiently and the title of the Work and its authorship have been acknowledged in this Work;
(4) I do not have any actual knowledge nor do I ought reasonably to know that the making of this work constitutes an infringement of any copyright work;
(5) I hereby assign all and every rights in the copyright to this Work to the Universiti Malaya ("UM"), who henceforth shall be owner of the copyright in this Work and that any reproduction or use in any form or by any means whatsoever is prohibited without the written consent of UM having been first had and obtained;
(6) I am fully aware that if in the course of making this Work I have infringed any copyright whether intentionally or otherwise, I may be subject to legal action or any other actions as may be determined by UM.

Candidate's Signature Date: 19-06-2023

Subscribed and solemnly declared before,

Witness's Signature Date: 19-06-2023

Name:
Designation:

STUDY OF POLY(ACRYLIC ACID) AND LITHIUM TETRAFLUOROBORATE/LITHIUM PERCHLORATE BASED POLYMER ELECTROLYTES

ABSTRACT

Polymer electrolytes are among the most potential materials used in electrical double layer capacitor and thus the characteristics of these electrolyte exert great impacts on the performance of the electrochemical devices. In this study, four types of poly(acrylic acid)-based electrolytes were synthesized via solvent casting, namely poly(acrylic acid)/lithium tetrafluoroborate, poly(acrylic acid)/lithium tetrafluoroborate/barium titanate, poly(acrylic acid)/lithium perchlorate, and poly(acrylic acid)/lithium perchlorate/barium titanate. The physicochemical properties such as ionic conductivity, structural and thermal stability were evaluated by electrochemical spectroscopy, themogravimetric analysis, X-ray diffraction and fourier transform infrared analysis.

Poly(acrylic acid) (PAA) managed to host up to 30 wt.% of $LiBF_4$ and exhibit the highest conductivity of 6.61×10^{-4} S cm^{-1}. The ionic conductivity of 8.95×10^{-4} S cm^{-1} is obtained after 10 wt.% of $BaTiO_3$ was added in PAA/$LiBF_4$. The incorporation of 10 wt.% $LiClO_4$ in the PAA matrix demonstrated a highest ionic conductivity, which is 2.40×10^{-6} S cm^{-1}. The ionic conductivity of 1.0×10^{-5} S cm^{-1} was obtained for PAA-$LiClO_4$-$BaTiO_3$ electrolyte. Arrhenius equation was employed to examine the effects of temperature on the ionic conductivity of the polymer electrolytes. The results shown that all the electrolyte systems obey Arrhenius theory where the ionic conductivity is corresponded to the elevation of temperature.

The variation of dielectric constant values with frequency in PAA-based electrolyte systems confirm the presence of polarization process at electrode interface. The variation of dielectric constant with frequency is more prominent with the effect of conducting salt or dopant addition. In the addition of more conducting salt into PAA electrolyte matrix, the loss tangent peaks shift towards higher frequency suggesting the speed up of relaxation time.

Polymer electrolytes with wide electrochemical stability window (ESW) are potentially to be applied for electrochemical devices. PAA-$LiBF_4$ and PAA-$LiBF_4$-$BaTiO_3$ electrolyte demonstrated ESW at 3.2 V and 4.0 V respectively. However, the electrolyte systems using $LiClO_4$ as conducting salt portrays a wider ESW which are about 10.0 V and 11.5 V for PAA-$LiClO_4$ and PAA-$LiClO_4$-$BaTiO_3$, respectively. The study confirmed that incorporation of conducting salt of $LiBF_4$/$LiClO_4$ and $BaTiO_3$ improves the thermal stability of polymer electrolyte. The XRD study indicates that higher loading of $LiBF_4$/$LiClO_4$ and $BaTiO_3$ indicates a higher degree in amorphous nature which improves the ionic conductivity in the PAA electrolytes. The FTIR study showed evident on the interaction between Li^+ and PAA.

The characterization study indicates that all the polymer electrolyte prepared in my study can be used as promising electrolyte materials for EDLC application especially the PAA-$LiClO_4$ based electrolytes with excellence electrochemical stability window.

Keywords: Poly(acrylic acid), lithium tetrafluoroborate, lithium perchlorate, barium titanate, ionic conductivity

KAJIAN MENGENAI POLIMER ELEKTROLIT BERASASKAN POLI(ASID AKRILIK) DAN TETRAFLUOROBORATE LITIUM/PERKLORAT LITIUM

ABSTRAK

Elektrolit polimer adalah antara bahan yang paling berpotensi digunakan dalam kapasitor lapisan berganda elektrik dan dengan itu ciri-ciri elektrolit ini memberi kesan yang besar terhadap prestasi peranti elektrokimia. Di dalam kajian ini, empat jenis bahan elektrolit berasaskan poli(asid akrilik) telah disintesis iaitu poli(asid akrilik)/tetrafluoroborate litium, poli(asid akrilik)/ tetrafluoroborate litium/barium titanat, poli(asid akrilik)/perklorat litium dan poli(asid akrilik)/perklorat litium/barium titanat menggunakan teknik acuan pelarut. Sifat fizikal dan kimia seperti kekonduksian ionik, kestabilan struktur dan haba telah dikaji mengunakan spektroskopi elektrokimia, analisis temogravimetrik, pembelauan X-ray dan spektroskopi inframerah transformasi.

Sampel PAA didapati boleh mengisi sebanyak 30 wt.% $LiBF_4$ dan mencapai kekonduksian yang tertinggi iaitu 6.61×10^{-4} S cm^{-1}. Kekonduksian ionik sebanyak 8.95×10^{-4} S cm^{-1} diperolehi dengan menggunakan 10 wt.% $BaTiO_3$ dalam komposisi PAA/ $LiBF_4$. Penambahan sebanyak 10 wt.% $LiClO_4$ di dalam PAA juga telah menunjukkan kekonduksian ionik tertinggi iaitu 2.40×10^{-6} S cm^{-1}. Kekonduksian ionik 1.0×10^{-5} S cm^{-1} diperolehi untuk elektrolit PAA-$LiClO_4$-$BaTiO_3$. Persamaan Arrhenius digunakan untuk mengkaji kesan suhu pada kekonduksian ionik elektrolit polimer. Hasil kajian menunjukkan bahawa semua sistem elektrolit mematuhi teori Arrhenius di mana kekonduksian ionik bersepadan dengan kenaikan suhu.

Variasi nilai malar dielektrik dengan kekerapan dalam sistem elektrolit berasaskan PAA mengesahkan kehadiran proses polarisasi pada permukaan elektrod. Variasi pemalar dielektrik dengan kekerapan adalah lebih menonjol dengan kesan penambahan konduksi garam atau dopant. Apabila lebih banyak garam kokunduksi ditambahkan ke dalam matriks elektrolit PAA, puncak tangen hilang beralih ke arah frekuensi yang lebih tinggi mencadangkan mempercepatkan masa relaksasi.

Elektrolit polimer dengan tetingkap kestabilan elektrokimia (ESW) yang luas berpotensi untuk digunakan untuk peranti elektrokimia. Elektrolit. Elektrolit PAA-$LiBF_4$ dan PAA-$LiBF_4$-$BaTiO_3$ menunjukkan ESW pada 3.2 V dan 4.0 V masing-masing. Walau bagaimanapun, sistem elektrolit yang menggunakan $LiClO_4$ sebagai garam konduktif mempamerkan ESW yang lebih luas iaitu kira-kira 10.0 V dan 11.5 V untuk PAA-$LiClO_4$ dan PAA-$LiClO_4$-$BaTiO_3$, masing-masing. Kajian ini mengesahkan bahawa penggabungan garam konduksi $LiBF_4$ / $LiClO_4$ dan $BaTiO_3$ meningkatkan kestabilan haba elektrolit polimer. Kajian XRD menunjukkan bahawa pemuatan $LiBF_4$ / $LiClO_4$ dan $BaTiO_3$ yang tinggi mengakibatkan tahap amorf yang lebih tinggi untuk meningkatkan kekonduksian ionik dalam elektrolit PAA. Kajian FTIR membuktikan mengenai interaksi antara Li^+ dan PAA.

Kajian pencirian menunjukkan bahawa semua elektrolit polimer yang disediakan dalam penyelidikan ini boleh digunakan sebagai bahan elektrolit yang terjamin untuk aplikasi EDLC terutamanya elektrolit berasaskan PAA-$LiClO_4$ dengan tetingkap kestabilan elektrokimia yang cemerlang.

Kata kunci: Poli(asid akrilik), tetrafluoroborate litium, perklorat litium, barium titanat, kekonduksian ionic

ACKNOWLEDGEMENTS

First and foremost, I would like to express my deepest gratitude to my supervisors, Professor Dr. Ramesh A/L T. Subramaniam and Associate Professor Dr. Ramesh Kasi, who expertly guided me and supported me throughout my PhD research journey.

Most importantly, I thank Associate Professor Dr. Loh Yen Lee for inspired me to do PhD in Physics. His genuine interest in Natural Science and unwavering enthusiasm for physics impressed and impacted me; kept me persistently building up my scientific and scholaric profile and engaging research work with an unbeatable perseverance.

I am extremely thankful and pay my sincere gratitude to Associate Professor Dr Juan Joon Ching, Associate Professor IR. TS. Dr. Lai Chin Wei and Datuk Dr Soon Ting Kueh for valuable guidance and support in research publication and the participation of proceedings presentation in various International Conferences.

I acknowledge Department of Physics, University of Malaya for offering a platform in pursuing PhD in Physics and also giving me the opportunity to complete the study. I also acknowledge Ministry of Higher Education Malaysia, University of Malaya, Malaysian Institute of Chemistry and Royal Society of Chemistry for offering financial support to the research work and also participation in the International Conferences especially to the 47th IUPAC World Chemistry Congress in Paris, France.

I would like to extend my sincere appreciation towards all the researchmates who have supported me throughout my research journey.

Thank you.

TABLE OF CONTENTS

Abstract iii

Abstrak v

Acknowledgements vii

Table of Contents viii

List of Figures xv

List of Tables xviii

List of Symbols and Abbreviations xix

CHAPTER 1: INTRODUCTION 1

1.1 Introduction 1

1.2 Research Background 2

1.3 Problem Statements 3

1.4 Research Objectives 5

1.5 Scope of Research 5

1.6 Outline of Thesis 6

CHAPTER 2: LITERATURE REVIEW 8

2.1 Introduction of Electrical Double Layer Capacitors 8

2.2 Configuration of Electrical Double Layer Capacitors 8

2.2.1 Electrode Materials 9

2.2.1.1 Carbonaceous Materials 10

2.2.1.2 Metal Oxides 13

2.2.1.3 Polymers 17

2.2.1.4 Composite Materials 18

2.2.2 Electrolyte Materials 20

2.2.2.1 Introduction of Polymer Electrolytes 21
2.2.2.2 Advantages of Polymer Electrolytes 21
2.2.2.3 Applications of Polymer Electrolytes 22
2.2.2.4 History of Polymer Electrolytes Development 22
2.2.2.5 Three Types of Polymer Electrolytes 23
2.2.2.6 Approaches to Improve Polymer Electrolytes 24
2.2.2.7 Composite Polymer Electrolytes 25
2.2.2.8 Polymer Hosts 26
2.2.2.9 Fillers 27
2.2.3 Separator Materials 28
2.3 Storage Technology and Basic Principle of Electrical Double Layer Capacitors 28
2.4 Factors Affecting the Performance of Electrical Double Layer Capacitors 30
2.5 Desired Characteristics of Electrolyte Materials 31
2.6 Selection Criteria of Polymer Host, Inorganic Salt and Dopant 33
2.6.1 Selection Criteria and the Choice of Polymer Host 33
2.6.2 Selection Criteria and the Choice of Inorganic Salt 34
2.6.3 Selection Criteria and the Choice of Dopant 37
2.7 The Stand of Polymer Electrolytes in the Past, Recent and Future Developments of Electrical Double Layer Capacitors 38
2.7.1 In the Previous Development of Electrical Double Layer Capacitors 38
2.7.2 In the Recent Development of Electrical Double Layer Capacitors 39
2.7.3 In the Future Development of Electrical Double Layer Capacitors 40

CHAPTER 3: MATERIAL AND METHODOLOGY 41

3.1 Introduction 41

3.2 Material 41

3.2.1 Poly(acrylic acid) 41

3.2.2 Lithium Tetrafluoroborate 41

3.2.3 Lithium Perchlorate 41

3.2.4 Barium Titanate 42

3.2.5 Deionized Water 42

3.3 Methodology 42

3.3.1 Preparation of Polymer Electrolytes 42

3.3.1.1 Preparation of PAA-$LiBF_4$ 43

3.3.1.2 Preparation of PAA-$LiClO_4$ 44

3.3.2 Preparation of Composite Polymer Electrolytes 45

3.3.2.1 Preparation of PAA-$LiBF_4$-$BaTiO_3$ 45

3.3.2.2 Preparation of PAA-$LiClO_4$-$BaTiO_3$ 46

3.4 Characterization 47

3.4.1 Effect of Conducting Salt and Dopant Concentration Studies 47

3.4.1.1 Effect of Conducting Salt Concentration Studies 47

3.4.1.2 Effect of Dopant Concentration Studies 48

3.4.2 Ambient Temperature-Ionic Conductivity Studies 48

3.4.3 Temperature Dependent-Ionic Conductivity Studies 49

3.4.4 Dielectric Studies 50

3.4.5 Electrochemical Stability Studies 51

3.4.6 Thermogravimetric Analysis 52

3.4.7 X-ray Diffraction Studies 52

3.4.8 ATR-FTIR Analysis 52

CHAPTER 4: PAA-$LiBF_4$ ELECTROLYTES CHARACTERIZATION 54

4.1 Introduction 54

4.2 Results and Discussion 56

4.2.1 Electrical Properties 56

4.2.1.1 Ambient Temperature-Ionic Conductivity Studies of PAA-$LiBF_4$ 56

4.2.1.2 Ambient Temperature-Ionic Conductivity Studies of PAA- $LiBF_4$-$BaTiO_3$ 59

4.2.1.3 Temperature Dependent-Ionic Conductivity Studies of PAA-$LiBF_4$ 61

4.2.1.4 Temperature Dependent-Ionic Conductivity Studies of PAA-$LiBF_4$-$BaTiO_3$ 64

4.2.1.5 Dielectric Permittivity Studies of PAA-$LiBF_4$ 65

4.2.1.6 Dielectric Permittivity Studies of PAA-$LiBF_4$-$BaTiO_3$ 68

4.2.1.7 Modulus Studies of PAA-$LiBF_4$ 70

4.2.1.8 Modulus Studies of PAA-$LiBF_4$-$BaTiO_3$ 72

4.2.2 Electrochemical Properties 74

4.2.2.1 Electrochemical Stability Window of PAA-$LiBF_4$ 74

4.2.2.2 Electrochemical Stability Window of PAA-$LiBF_4$-$BaTiO_3$ 75

4.2.3 Thermal Properties 76

4.2.3.1 Thermal Studies of PAA-$LiBF_4$ 76

4.2.3.2 Thermal Studies of PAA-$LiBF_4$-$BaTiO_3$ 79

4.2.4 Structural Properties 80

4.2.4.1 X-ray Diffraction Studies of PAA-$LiBF_4$ 80

4.2.4.2 X-ray Diffraction Studies of PAA-$LiBF_4$-$BaTiO_3$ 82

4.2.4.3 ATR-FTIR Studies of PAA-$LiBF_4$ 84

4.2.4.4 ATR-FTIR Studies of PAA-$LiBF_4$-$BaTiO_3$ 85

4.3 Conclusion 87

CHAPTER 5: PAA-$LiClO_4$ ELECTROLYTES CHARACTERIZATION 89

5.1 Introduction 89

5.2 Results and Discussion 90

5.2.1 Electrical Properties 90

5.2.1.1 Ambient Temperature-Ionic Conductivity Studies of PAA- $LiClO_4$ 90

5.2.1.2 Ambient Temperature-Ionic Conductivity Studies of PAA-$LiClO_4$-$BaTiO_3$ 92

5.2.1.3 Temperature Dependent-Ionic Conductivity Studies of PAA-$LiClO_4$ 96

5.2.1.4 Temperature Dependent-Ionic Conductivity Studies of PAA-$LiClO_4$-$BaTiO_3$ 97

5.2.1.5 Dielectric Permittivity Studies of PAA-$LiClO_4$ 99

5.2.1.6 Dielectric Permittivity Studies of PAA-$LiClO_4$-$BaTiO_3$ 101

5.2.1.7 Loss Tangent Studies of PAA-$LiClO_4$ 103

5.2.1.8 Loss Tangent Studies of PAA-$LiClO_4$-$BaTiO_3$ 105

5.2.1.9 Modulus Studies of PAA-$LiClO_4$ 106

5.2.1.10 Modulus Studies of PAA-$LiClO_4$-$BaTiO_3$ 108

5.2.2 Electrochemical Properties 109

5.2.2.1 Electrochemical Stability Window of PAA-$LiClO_4$ 109

5.2.2.2 Electrochemical Stability Window of PAA-$LiClO_4$-$BaTiO_3$ 110

5.2.3 Thermal Properties 111

5.2.3.1 Thermal Studies of PAA-$LiClO_4$ 111

5.2.3.2 Thermal Studies of PAA-$LiClO_4$-$BaTiO_3$ 113

5.2.4 Structural Properties 114

5.2.4.1 X-ray Diffraction Studies of PAA-$LiClO_4$ 114

5.2.4.2 X-ray Diffraction Studies of PAA-$LiClO_4$-$BaTiO_3$ 116

5.2.4.3 ATR-FTIR Studies of PAA-$LiClO_4$ 118

5.2.4.4 ATR-FTIR Studies of PAA-$LiClO_4$-$BaTiO_3$ 119

5.3 Conclusion 120

CHAPTER 6: COMPARATIVE STUDIES BETWEEN DIFFERENT ELECTROLYTE SYSTEMS 121

6.1 Introduction 121

6.2 Results and Discussion 121

6.2.1 Ambient Temperature-Ionic Conductivity Studies 121

6.2.1.1 Comparison between Polymer electrolytes with Different Conducting Salts 121

6.2.1.2 Comparison between Polymer Electrolytes with Respective Composite Polymer Electrolytes 123

6.2.2 Temperature Dependent-Ionic Conductivity Studies 124

6.2.3 Dielectric Permittivity Studies 124

6.2.4 Modulus Studies 125

6.2.5 Electrochemical Stability Window 126

6.2.6 Thermal Studies 127

6.2.7 Structural Studies 128

6.3 Conclusion 139

CHAPTER 7: CONCLUSION 131

7.1 Preamble 131

7.2 Recommendations for Further Research 135

REFERENCES **138**

LIST OF PUBLICATIONS AND PAPERS PRESENTED **149**

LIST OF FIGURES

Figure 2.1: A typical configuration of capacitor and electrical double layer capacitor 9

Figure 2.2: The chemical structure of the lithium salts used in the study: (a) $LiBF_4$ and (b) $LiClO_4$ 36

Figure 4.1: Repeated unit of poly(acrylic acid), the polymer host used in this research study 54

Figure 4.2: Impedance plot of PAA-$LiBF_4$ electrolyte film at ambient temperature. The inset: Magnified axis in a higher frequency region of the real part of complex impedance (x-axis). The imaginary part of complex impedance is the y-axis 57

Figure 4.3: Effect of $LiBF_4$ salt content on the ionic conductivity of PAA-based electrolytes at ambient temperature 58

Figure 4.4: Impedance plot of PAA-$LiBF_4$-$BaTiO_3$ electrolyte film at ambient temperature 59

Figure 4.5: Effect of $BaTiO_3$ content on the ionic conductivity of PAA- $LiBF_4$ electrolytes at ambient temperature 61

Figure 4.6: Arrhenius plot of ionic conductivity for P80-LB20, P75-LB25, and P70-LB30 with frequency ranging from 50 Hz to 5 MHz at temperatures from 303 K to 393 K 63

Figure 4.7: Arrhenius plot of ionic conductivity for PAA-$LiBF_4$-$BaTiO_3$ CPE6B, CPE8B, and CPE10B with frequency ranging from 50 Hz to 5 MHz at temperatures from 303 K to 393 K 65

Figure 4.8: Variation of (a) dielectric permittivity and (b) dielectric loss for P90-LB10, P80-LB20, and P70-LB30 as a function of frequency at ambient temperature 67

Figure 4.9: Variation of (a) dielectric permittivity and (b) dielectric loss for PAA-$LiBF_4$-$BaTiO_3$ CPE2B (low), CPE6B (medium), and CPE10B (high) as a function of frequency at ambient temperature 70

Figure 4.10: The (a) real part and (b) imaginary part of dielectric moduli as a function of logarithmic frequency for P90-LB10, P80-LB20, and P70-LB30 in the frequency range of 50 Hz – 5 MHz at ambient temperature 72

Figure 4.11: The (a) real part and (b) imaginary part of dielectric moduli as a function of logarithmic frequency for PAA-$LiBF_4$-$BaTiO_3$: CPE2B, CPE6B and CPE10B in the frequency range of 50 Hz – 5 MHz at ambient temperature 73

Figure 4.12: Linear Sweep voltammogram of PAA-$LiBF_4$ (30 wt.% $LiBF_4$) electrolyte system at ambient temperature. Scan rate: 5 mV s^{-1} 75

Figure 4.13: Linear Sweep voltammogram of PAA-$LiBF_4$-$BaTiO_3$ electrolyte (with 10 wt.% $BaTiO_3$) at ambient temperature. Scan rate: 5 mV s^{-1} 76

Figure 4.14: TGA thermograms of pure PAA, P70-LB30, P75-LB25, and P80-LB20 in the temperature range of 30–600 °C under inert condition 78

Figure 4.15: TGA thermograms of pure PAA, PAA-$LiBF_4$-$BaTiO_3$ in 6 wt.% (CPE6B), 8 wt% (CPE8B) and 10 wt.% (CPE10B) in the temperature range of 20–600 °C under inert condition 80

Figure 4.16: XRD pattern of (a) pure $LiBF_4$, (b) pure PAA, (c) P80-LB20, (d) P75-LB25, and (e) P70-LB30. The inset: Magnified axis between 2θ = 21.0 – 22.5 ^{o} 82

Figure 4.17: XRD patterns of (a) $BaTiO_3$, (b) $LiBF_4$, (c) PAA, (d) CPE10B, (e) CPE8B, and (f) CPE6B 84

Figure 4.18: ATR-FTIR Spectra of (a) pure PAA, (b) pure $LiBF_4$, (c) P80-LB20, (d) P75-LB25, and (e) P70-LB30 85

Figure 4.19: ATR-FTIR Spectra of (a) PAA, (b) $LiBF_4$, (c) $BaTiO_3$, (d) CPE10B, (e) CPE8B, and (f) CPE6B 87

Figure 5.1: Impedance plot of PAA-$LiClO_4$ electrolytes at ambient temperature 91

Figure 5.2: Effect of $LiClO_4$ content on the ionic conductivity of PAA-based electrolytes at ambient temperature 92

Figure 5.3: Impedance plot of PAA-$LiClO_4$-$BaTiO_3$ electrolyte at ambient temperature using AC-impedance spectroscopy 94

Figure 5.4: Effect of $BaTiO_3$ content on the ionic conductivity of PAA-$LiClO_4$ electrolytes at ambient temperature 95

Figure 5.5: Arrhenius plot of ionic conductivity for P90-LC10, P85-LC15 and P80-LC20 with frequency ranging from 50 Hz to 5 MHz at temperatures from 303 K to 393 K 97

Figure 5.6: Arrhenius plot of ionic conductivity for PAA-$LiClO_4$-$BaTiO_3$ CPE6C, CPE8C, and CPE10C with frequency ranging from 50 Hz to 5 MHz at temperatures from 303 K to 393 K 99

Figure 5.7: Variation of (a) dielectric permittivity and (b) dielectric loss for P90-LC10, P85-LC15, and P80-LC20 as a function of frequency at ambient temperature 101

Figure 5.8: Variation of (a) dielectric permittivity and (b) dielectric loss for PAA-$LiClO_4$-$BaTiO_3$ CPE2C (low), CPE6C (medium), and CPE10C (high) as a function of frequency at ambient temperature 103

Figure 5.9: Variation of loss tangent (tan δ) against the logarithm of angular frequency (log ω) for P90-LC10, P85-LC15, and P80-LC20 at ambient temperature 104

Figure 5.10: Variation of loss tangent (tan δ) against the logarithm of angular frequency (log ω) for PAA-$LiClO_4$-$BaTiO_3$: CPE2C at ambient temperature 106

Figure 5.11: The (a) real part and (b) imaginary part of dielectric moduli as a function of logarithmic frequency for P90-LC10, P85-LC15, and P80-LC20 in the frequency range of 50 Hz – 5 MHz at ambient temperature 107

Figure 5.12: The (a) real part and (b) imaginary part of dielectric moduli as a function of logarithmic frequency for PAA-$LiClO_4$-$BaTiO_3$: CPE2C, CPE6C and CPE10C in the frequency range of 50 Hz – 5 MHz at ambient temperature 109

Figure 5.13: Linear Sweep voltammogram of PAA-$LiClO_4$ (10 wt.% $LiClO_4$) electrolyte system (P90-LC10) at ambient temperature. Scan rate: 5 mV s^{-1} 110

Figure 5.14: Linear Sweep voltammogram of PAA-$LiClO_4$-$BaTiO_3$ electrolyte (with 10 wt.% $BaTiO_3$) at ambient temperature. Scan rate: 5 mV s^{-1} 111

Figure 5.15: TGA thermograms of pure PAA, P90-L10, P85-L15, and P80-L20 in the temperature range of 20–600 °C under inert condition 113

Figure 5.16: TGA thermograms of pure PAA, PAA-$LiClO_4$-$BaTiO_3$ in 6 wt.% (CPE6C), 8 wt% (CPE8C) and 10 wt.% (CPE10C) in the temperature range of 20–600 °C under inert condition 114

Figure 5.17: XRD patterns of (a) $LiClO_4$, (b) pure PAA, (c) P90-LC10, (d) P85-LC15, and (e) P80-LC20 116

Figure 5.18: XRD pattern of (a) $BaTiO_3$, (b) $LiClO_4$, (c) pure PAA, (d) CPE10C, (e) CPE8C, and (f) CPE6C 117

Figure 5.19: ATR-FTIR Spectra of (a) pure PAA, (b) pure $LiClO_4$, (c) P90-LC10, (d) P85-LC15, and (e) P80-LC20 118

Figure 5.20: ATR-FTIR Spectra of (a) PAA, (b) $LiClO_4$, (c) $BaTiO_3$, (d) CPE10C, (e) CPE8C, and (f) CPE6C 119

Figure 6.1: Effect of types of conducting salt and respective content on the ionic conductivity of PAA-based electrolytes at ambient temperature 122

Figure 6.2: The chemical structure of both conducting salts: (a) $LiBF_4$ and (b) $LiClO_4$ 123

LIST OF TABLES

Table 2.1: Average range of specific capacitance for some common electrode materials 11

Table 2.2: A summary of the properties, advantages, and applications of the polymer electrolytes 23

Table 3.1: Chemical composition for PAA-$LiBF_4$ electrolyte systems with different weight percentage of $LiBF_4$ at ambient temperature. 44

Table 3.2: Chemical composition for PAA-$LiClO_4$ electrolyte systems with different weight percentage of $LiClO_4$ at ambient temperature 45

Table 3.3: Chemical composition for PAA-$LiBF_4$-$BaTiO_3$ electrolyte systems with different $BaTiO_3$ weight percentages at ambient temperature 46

Table 3.4: Chemical composition for PAA-$LiClO_4$-$BaTiO_3$ electrolyte systems with different $BaTiO_3$ weight percentages at ambient temperature 47

Table 3.5: The applied potential range for various types of PE/CPE system in the LSV analysis 52

Table 4.1: The activation energy of the PAA-$LiBF_4$ electrolyte systems 63

Table 4.2: The activation energy of the PAA-$LiBF_4$-$BaTiO_3$ electrolyte systems 65

Table 5.1: The activation energy of the PAA-$LiClO_4$ electrolyte systems 97

Table 5.2: The activation energy of the PAA-$LiClO_4$-$BaTiO_3$ electrolyte systems 99

Table 5.3: Relaxation frequencies for P90-LC10, P85-LC15, and P80-LC20 with different $LiClO_4$ content 105

Table 6.1: Ionic conductivity of poly(acrylic acid) electrolyte systems with optimized lithium salt/barium titanate content at ambient temperature 123

Table 6.2: Effect of $BaTiO_3$ content on the ionic conductivity of (a) PAA- $LiBF_4$ and (b) PAA- $LiClO_4$ electrolytes at ambient temperature 124

Table 6.3: Electrochemical stability window for PAA-$LiBF_4$, PAA-$LiBF_4$-$BaTiO_3$, PAA-$LiClO_4$ and PAA-$LiClO_4$-$BaTiO_3$ with selected potential range at ambient temperature. Scan rate: 5 mV s^{-1} 126

Table 6.4: Summarized the residual mass of all tested PEs and CPEs at 600°C 128

LIST OF SYMBOLS AND ABBREVIATIONS

E_a	:	activation energy
R_b	:	bulk resistance
ATR-FTIR	:	attenuated total reflectance-fourier transform infrared
$BaTiO_3$	:	barium titanate
CNT	:	carbon nanotube
CPE	:	composite polymer electrolyte
EDLC	:	electrical double layer capacitor
EIS	:	electrochemical impedance spectroscopy
ESW	:	electrochemical stability window
FWHM	:	full width at half maximum
GPE	:	gel polymer electrolyte
$LiBF_4$	:	lithium tetrafluoroborate
$LiClO_4$	:	lithium perchlorate
LSV	:	linear sweep voltammetry
LiTFSI	:	lithium bis(trifluoromethane) sulfonimide
MnO_2	:	manganese oxide
NiO	:	nickel oxide
PAA	:	poly(acrylic acid)
PAA-$LiBF_4$	:	poly(acrylic acid)/lithium tetrafluoroborate
PAA-$LiBF_4$-$BaTiO_3$	:	poly(acrylic acid)/lithium tetrafluoroborate/barium titanate
PAA-$LiClO_4$	:	poly(acrylic acid)/lithium perchlorate
PAA-$LiClO_4$- $BaTiO_3$	:	poly(acrylic acid)/lithium perchlorate/barium titanate
PANI	:	polyaniline
PCL	:	poly(ε-caprolactone)
PE	:	polymer electrolyte

PEO:	poly(ethylene oxide)
PMMA:	poly(methyl methacrylate)
PPy:	polypyrrole
PSD:	pore size distribution
PVdF:	poly(vinylidene fluoride)
SPE:	solid polymer electrolyte
SS:	stainless steel
SSA:	specific surface area
TGA:	thermogravimetry analyzer
XRD:	X-ray diffraction

CHAPTER 1: INTRODUCTION

1.1 Introduction

In the scientific world, anything and everything in Universe are classified into two categories: matter and energy. As prescribed in the definition, matters are anything having mass and occupying space. Conversely, energy do not possess mass and do not occupy space. The Law of Conservation Energy states that energy can neither be created nor destroyed but it can be transferred from one form to another. There are different types of energy such as light energy, sound energy, heat energy, electrical energy, chemical energy, nuclear energy, kinetic energy, potential energy, wind energy, tide energy, hydrogen energy, geothermal energy, biochemical energy and hydroelectric energy. These forms of energy are classified into renewable energy and non-renewable energy. Fossil fuel is the most important non-renewable energy source and in the high consumption by human for various purposes. In the past few decades, the sourcing of renewable energy to replace fossil fuel become one of the most popular research areas for most scientists around the world. As the activities and life on Earth are mainly driven by the energy, the exhaustion of fossil fuel should lead to a global threat if the economical and commercially sound renewable energy sources still unable to replace the fossil fuel effectively.

Electrical and chemical energies are among the commonly found renewable energy sources in our daily life. Electrochemical energy is one of the renewable energy forms that convert the electrical energy to chemical energy, or vice versa. Conventionally, electrochemical energy is stored in the electrochemical cell, and also battery which comprised of one or more electrochemical cells. Nowadays, more electrochemical energy storage alternatives are found due to the enhancement of technology to fulfil the industrial

needs. Fuel cells and supercapacitors are among the most widely used electrochemical energy storing devices beside batteries.

Battery is the conventional electrochemical storing device which consists of electrodes and liquid electrolyte. Secondary or rechargeable battery is the upgraded form of primary battery with better properties and higher application voltage which can be charged and discharged many times. Modern batteries have advanced features due to the transformation from liquid electrolytes to solid electrolytes. Capacitor is also an electrochemical storing device and having some similarities features with battery in terms of structural, functional and application. Same like battery, enhanced versions of capacitors such as supercapacitor and electrical double layer capacitor (EDLC) are developed with enhanced properties such as higher power density and higher energy storing capacity.

1.2 Research Background

EDLC is composed by electrodes, electrolyte and a separator. In the field of electrochemistry, EDLC is one of the popular research subjects. The research scopes under EDLC ranging from the sourcing and characterization of novel electrode or electrolyte materials, and also the performance of the EDLC with the application of the newly found electrode or electrolyte materials. A wide range of the electrode and electrolyte materials are available to be selected as the research subject. The choice of the component used in electrolyte materials such as polymer host and inorganic salts, with or without the incorporation of dopants, making a wide research scope of EDLC which also extended the variety of this device enhancement to fulfil the various industrial needs.

1.3 Problem Statements

The consumption of fossil fuel as one of the important energy sources leads to many adverse effects such as air pollution, global warming, and climate change. The continuation of these effects will lead to some serious outcomes which endangered the continuous living of most living things, damage of our natural assets such as atmosphere and ecosystem, and also influence on the human and industrial activities. The depletion of the fossil fuel is also exerted a driver to scientists and researchers for sourcing renewable energy sources as a replacement. Renewable energy sources such as solar and hydroelectric energy required a huge start-up capital. Nuclear energy source beside posing high start-up and operational costs, the capability of the human in controlling of the nuclear plant, reducing the risk and post-accident handling is still uncertain. A reliable, low cost and effective source of renewable energy source is highly demanded not only to reduce and replace the consumption of fossil fuel, but also to overcome the disadvantages that facing by most forms of renewable energy such as cost, limitation in mobility and generation of low energy quantity.

Capacitor as one of the alternatives to battery is widely used in various electrochemical applications. Primary battery using the liquid electrolyte as one of the compositions posing a lot of adverse effects and disadvantages especially in the safety aspect and break down incident. Among the most commonly occur unwanted consequences in the utilization of liquid electrolytes are internal shorting, leaking of electrolyte, evaporation of excessive harmful liquid solvent, poor compatibility with electrodes and using of hazardous or corrosive solvents as electrolyte materials (Scrosati, 1993). The replacement of liquid electrolytes with solid electrolytes such as polymer electrolytes definitely creates a paradigm shift in the field of electrochemical devices, especially in the device performance and applications. Solid electrolytes can mitigate most of disadvantages and

drawbacks of liquid electrolytes. Solid electrolytes possess many favourite properties and enhanced characteristics such as solvent-free, light in weight, high ionic conductivity, thin configuration but flexible to shape into various configuration (Susan et al., 2005).

Both electrode and electrolyte materials in the EDLC play a vital role to determine the properties, characteristics, performance and applicability of the devices. The sourcing of a safe, reliable, highly performance electrode and electrolyte materials is highly demanded to enhance the properties and performance of modern capacitors. Some common unfavourite properties of electrolyte materials such as low ionic conductivity, poor thermal decomposition property, and narrow electrochemical stability window (ESW). The cost of the electrolyte materials and ease in the preparation process also among the consideration for the potentially of commercialize and production in bulk. The strategies used for further development of advanced electrolyte materials are the seeking of synergistic combination between polymer host, inorganic salt and/or incorporation of dopant. A promising electrolyte candidate is demanded not only to replace the liquid electrolyte but also to offer the desirable features such as high ionic conductivity, excellent thermal property, wide ESW, flexible configuration, excellent safe features, cost effective, better compatibility with the electrodes and such it could be predominates in commercialized devices (Xu et al., 1999; Fonseca, et al., 2006).

Despite the efforts over decades, the critical properties of the electrolyte materials are found below the requirements for various applications. Even though massive research activities have been carried out over last few decades, the electrochemical scientists and researchers still struggling to meet the global needs, market requirements and stringent safety requisites. However, the researchers still drive by a vision to pursue new

electrode and electrolyte materials for the achievement of a new EDLC components that offers a promising replacement of non-renewable energy source.

1.4 Research Objectives

The Research objectives of this research study are as follows:

1. To formulate polymer electrolytes and composite polymer electrolytes using poly(acrylic acid) as a polymer host, lithium tetrafluoroborate and lithium perchlorate as conducting salts, and barium titanate as dopant/filler;
2. To perform chemical, electrical, electrochemical, thermal and structural characterization of the prepared polymer electrolytes and composite polymer electrolytes;
3. To compare the chemical, electrical, electrochemical, thermal and structural properties between polymer electrolytes with different lithium salts; and between the polymer electrolyte with/without the incorporation of dopant.

1.5 Scope of Research

In this research study, various electrolyte materials are investigated. The selection of the electrolyte materials and the components are based on the intention to be used as electrolyte materials in the application of EDLCs. Poly(acrylic acid), PAA is used as the polymer host in this study. Lithium tetrafluoroborate, ($LiBF_4$) and lithium perchlorate ($LiClO_4$) are used as the inorganic salts. The effect of the doping of barium titanate ($BaTiO_3$) in both polymer electrolyte (PE) systems are also evaluated. The scope of this research is divided into two stages: preparation and characterization of the electrolyte systems. There are four electrolyte systems involved in the study: poly(acrylic acid)/lithium tetrafluoroborate electrolyte, poly(acrylic acid)/lithium tetrafluoroborate/barium titanate electrolyte, poly(acrylic acid)/lithium perchlorate

electrolyte, and poly(acrylic acid)/lithium perchlorate /barium titanate electrolyte systems. Among these four electrolyte systems, two systems are polymer electrolytes and two systems are composite polymer electrolytes. The scopes of the characterization study are the studies on the effect of conducting salt concentration, effect of selected dopant concentration, ambient temperature-ionic conductivity, temperature dependent-ionic conductivity, dielectric studies (including dielectric permittivity, loss tangent, and modulus studies), electrochemical stability window study, thermogravimetric analysis, X-ray diffraction study and attenuated total reflectance-fourier transform infrared analysis.

1.6 Outline of Thesis

This thesis aims to present a novel research work on the preparation and characterization studies of four electrolyte systems for the development of EDLC. Chapter 2 presents the components, storage technology, basic principles and factors affecting the performance of EDLC. This chapter also offers a concise review on the types of electrode materials and electrolyte materials used in EDLC applications. The introduction of PEs, basic components and the criteria for the selection of the PE components are also discussed in Chapter 2. Highly interesting are the types of chemicals used in the selection of electrolyte components especially the polymer hosts used in the preparation of PEs. Chapter 3 provides detail description of the materials used and specification of instrumentation analyses in the characterization of electrolyte materials by chemical, electrical, electrochemical, and thermal methods. Chapter 4 and 5 presents the results obtained and respective discussions for the characterization studies of the electrolytes via electrochemical impedance spectroscopy, dielectric study, linear sweep voltammetry, thermal and structural analyses. Chapter 6 makes comparison studies among the four electrolyte systems and highlights the system with significance performance in a specific

study. Chapter 7 draws the conclusion of the study which met the purpose of investigation. This Chapter also provides some future directions in PE development.

CHAPTER 2: LITERATURE REVIEW

2.1 Introduction of Electrical Double Layer Capacitors

Energy devices are classified into energy converting or storing devices. Batteries, fuel cells are energy converting devices whereas capacitors are energy storing devices. The capacitor is a fundamental electrical circuit component that stores energy in electric field when it is charged and then discharged the stored electrical energy to the loads. Conventional capacitor is made of two metallic electrodes with an insulating dielectric material placed between the electrodes for electric charge accumulation. Battery stores energy in the form of chemicals and utilize redox reactions in converting between chemicals and electrical energies. Electrical double layer capacitor (EDLC) is an enhanced version of conventional capacitor but also employ the working principles of both capacitor and battery. It stores electrical energy in the interface between a solid electrode and an electrolyte. This storage technology also fill-up the gap between battery and conventional capacitor. EDLC possesses higher power density and higher energy storing capacity than conventional capacitor; it is also able to deliver more power than conventional battery. Electrochemical capacitors have received high attention in the past two decades due to their excellent electrochemical energy storing capacity. Thus, EDLC is considering one of the most promising electrochemical energy storing devices.

2.2 Configuration of Electrical Double Layer Capacitors

A conventional EDLC consists of two porous carbon electrodes immersed into an electrolyte and separated by a membrane, as shown in Figure 2.1. A non-conventional EDLC exists when various choices of electrode material and electrolyte material are used in the fabrication of EDLC. Therefore, many literatures are published based on different combinations of electrode/electrolyte materials. Different materials possess their specific

characteristics whereas the combinations of them will definitely exert an impact on the device performance.

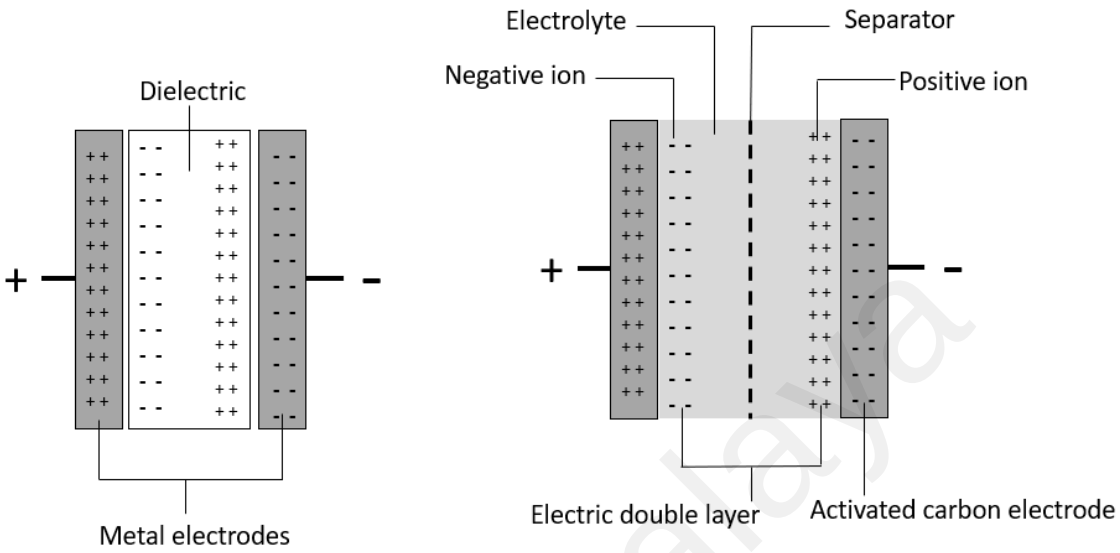

Figure 2.1. A typical configuration of capacitor and electrical double layer capacitor.

The electrodes in EDLC typical are two carbon electrodes with high surface area and porous. Porous carbon electrodes are low in cost, with better chemical stability and excellent electrical conductivity. The electrolyte used would be either aqueous or non-aqueous. The separator is a membrane which ionic conducting but electronic insulating.

2.2.1 Electrode Materials

The electrode material is crucial in determining the electrical properties of EDLC (You et al., 2018). Due to the fact that the charge storage mechanism in EDLC is a surface process, thus the capacitance of the EDLC is substantially affected by the surface characteristics of electrode used. Among the most commonly used electrode materials are carbon, metal oxides, conducting polymers, and composites. The characteristics of various electrode materials and their respective specific capacitances are reviewed. Table 2.1 presents the ranges of specific capacitances in reported electrode materials. Aerogel

carbon, foamed carbon and carbon materials having the specific capacitance ranges of 120 to 160 F g^{-1}, 70 to 180 F g^{-1}, and 150 to 350 F g^{-1}, respectively. Metal oxides, anhydrous ruthenium oxide and hydrous ruthenium oxides giving the specific capacitance ranging of 50 to 500 F g^{-1}, 100 to150 F g^{-1}, and 600 to 750 F g^{-1}, respectively. Conductive polymers, cellulose derivatives doped polymer, nitrogen doped carbon materials offer an average range of specific capacitance values of 300 to 750 F g^{-1}, 400 to 500 F g^{-1}, 150 to 300 F g^{-1}. Metal/carbon, polymer/carbon, metal/polymer composites demonstrated the specific capacitance range between 200 to 350 F g^{-1}, 500 to 1050 F g^{-1}, 500 to 600 F g^{-1}.

2.2.1.1 Carbonaceous Materials

Carbon is one of the commonly used electrode materials which is abundance, low cost, non-toxic, non-corrosive, mostly available, easily obtain from various resources and also can be altered in various forms. This poses no adverse effect to environment and ease to handle during the recycling process via dismantle of the electrical devices, separation of the electrode material and electrolyte material. The carbon-based electrode material and electrolyte material also lead to the commercial popularity due to their low in cost, longer life cycle, high recyclability, and possess a wider range of operating temperatures. This is due to their wide electrochemical stability window (ESW), inert with a broad spectrum of electroactive materials, conductive, low in cost, widely available and also potentially to be modified as highly porous and activated carbon electrode materials (50 F g^{-1}, 500 to 1050 F g^{-1}, 500 to 600 F g^{-1}. Carbon can be further modified and treated to become carbonaceous materials in the form of foams, fibers, mesoporous carbon, activated carbon, carbon aerogel, nanotubes, nanofibers, nanofibers, etc.

Table 2.1: Average range of specific capacitance for some common electrode materials.

Electrode Material	Specific Capacitance (F g^{-1})
Aerogel carbon	120 - 160
Foamed carbon	70 -180
Carbon materials	150 - 350
Metal oxides	50 - 500
Anhydrous ruthenium oxide	100 - 150
Hydrous ruthenium oxides	600 - 750
Polymers	300 - 750
Cellulose derivatives doped polymers	400 - 500
Nitrogen doped carbon materials	150 - 300
Metal/carbon composites	200 - 350
Polymer/carbon composites	500 - 1050
Metal/polymer composites	500 - 600

Most of the commercial EDLCs are utilized activated carbon as electrode materials. Activated carbon has a long historical utilization background, low in cost, easy to produce even in bulk quantity, great cycle stability, and also possess well-developed manufacturing technology. Thus, activated carbon is the longest and also widely used type of porous carbon materials. Petroleum coke, charcoal, pitch are examples of conventional carbon sources. Those have high carbon yields, low in price, high availability, thus they are most commonly precursors for the production of commercial activated carbons. Due to the growing global energy demand, the reducing of carbon sources such as fossil fuels, and also the increasing awareness of the environmental impact that led by the consumptions of fossil fuel, renewable and low-cost resources such as sucrose, cellulose, nutshell, corn grain are gaining attention and use to replace the

conventional carbon resources. Furthermore, these renewable resources possess uniform structure and high chemical purity. Thus, this allows uniform and reproducible features of the produced activated carbons. Further progress in the activated carbon synthesis technologies also lead to the achievement of controllable properties such as even pore size distribution, enhanced capacitance and low pore tortuosity.

Carbons are modified to derive some good characteristics in order to fulfil the commercial requirements such as better charge/discharge efficiency, longer life cycle, good charge retention and low self-discharge. Several methods have been used for the modification of carbons. Surface functionality can be enriched via oxidation of carbon surface via chemical, electrochemical, or plasma treatments. Electroactive materials such as transition metal oxides or metal oxides can be inserted into carbon materials for better capacitance properties. Chemical and electrochemical polymerization allows the formation of conducting polymer layers on carbon surface.

Carbon aerogels, foams, carbonaceous fibers, carbon nanotubes and nanofilms are produced via modification of carbon also applied as the electrode materials in EDLC. A modified carbon aerogel electrode was developed by activating the carbon under the flow of carbon dioxide (Wei et al., 2005). This follows by the surface modification via a surfactant. The activated carbon aerogel possesses lower internal resistance with a high usable surface area after the modification which is then used as electrode materials in EDLC. The resulting EDLC offers a high energy density, specific capacitance and power capability.

An activated carbon monolith is synthesized from mesophase pitch for supercapacitor (Ruiz et al., 2009). The resulting electrode materials possess large porosity and the device

developed from the new electrode material offers a capacitance value of 334 F g^{-1} in sulfuric acid medium. Other excellence characteristics such as high power density of 12000 W Kg^{-1} and excellence cycle stability indicating that the modified electrode can be used in the preparation of efficient energy storing devices.

An emerging potential electrode material of carbon nanosheet is prepared and investigated by cyclic voltammetry (Zhao et al., 2009). 1-7 graphene monolayers constituent a carbon nanosheet where numerous nanosheets are arranged vertically in respect to the substrate. A capacitance of 0.076 F cm^{-2} was determined via a typical electrochemical three-electrode cell. A total possible capacitance of 1.49 x 10^4 F in a virtual supercapacitor cell was simulated through a mathematical model.

A study was carried out to evaluate the electrochemical performance of an EDLC when graphene nanosheets (GNSs) were used as electrode materials (Du et al., 2010). From the literature, graphene nanosheets are prepared from the natural graphite via oxidation and rapid heating techniques. Graphene with larger surface areas and more edges are obtained via deeper oxidation which enhance the EDLC performance. Freestanding graphene nanosheets which offer good rate capability and reversibility are produced via coating method. A specific capacitance of 150 F g^{-1} was obtained with a surface area of 524 m^2 g^{-1}. The electrochemical performance of the EDLC is substantially affected by the specific surface area, pore characteristics, layer stacking and also the number of oxygen containing groups in electrode material.

2.2.1.2 Metal Oxides

Metal oxides among the most attractive alternative to be used as electrode materials in EDLCs due to their high specific capacitance and low resistivity. The charge storage is

critical in the bulk of metal oxide active materials. EDLCs with metal oxide electrode materials offers higher energy and power density when compared to the EDLCs with carbon electrode materials.

Hydrous ruthenium oxide

A capacitor was reported which constructed from hydrous ruthenium oxide ($RuO_2.xH_2O$) and sulfuric acid used as electrode and electrolyte materials, respectively (Zheng et al., 1995). It was found that the energy density of new electrode was 26.7 Wh kg^{-1} beside maintaining a good stability in the acid electrolyte.

Anhydrous ruthenium oxide

Anhydrous mesoporous ruthenium oxide (RuO_2) was prepared and applied as electrode materials in an electrochemical supercapacitor (Subramanian et al., 2004). The synthesis of anhydrous mesoporous ruthenium oxide was conducted in a surfactant templating process. The new electrode exhibited a capacitance value of 58 F g^{-1}. The study also demonstrated that the capacitance values reduce linearly when the scan rate is increasing. This concluded that the capacitance of anhydrous mesoporous ruthenium is strongly depending on the scan rate.

Vanadium oxide

Nanoporous vanadium oxide (V_2O_5) is synthesized through a sol-gel method (Reddy & Reddy, 2006). The electrochemical studies were conducted with three types of electrolytes: lithium chloride, sodium chloride and potassium chloride. When potassium chloride electrolyte solution is in used, a highest capacitance of 214 F g^{-1} was obtained at a scan rate of 5 mV s^{-1}. The study also concluded that the electrolyte solution concentration affects the nanoporous vanadium oxide electrode performance. The

specific capacitance reduced dramatically when the vanadium oxide electrode is subjected to 100 cycles with a scan rate of 5 mV s^{-1}.

Nickel oxide

Nickel oxide (NiO) was synthesized and assembled in supercapacitors as electrode material (Zheng et al., 2009). The NiO precursor is prepared first via hydrothermally synthesis at various temperatures, then followed by the formation of nanostructured NiO by heating at a low temperature. The resulting NiO possesses large surface area due to its unique flake-like nanostructure. The large surface area promotes the electrolyte ions transport during the charge/discharge processes. A specific capacitance of 137.7 F g^{-1} was obtained when potassium hydroxide (KOH) electrolyte solution is used. A capacitance retention of 91.6% was achieved when the device is subjected to 1000 charge/discharge processes.

Nanocrystalline NiO is formed by the liquid phase process (Zhang et al., 2004). When crystalline nickel oxide is applied as an electrode material in a c cyclic voltammetry study, 300 F g^{-1} was obtained as a specific capacitance when a scan rate ranging between 0.0 to 0.5 V is applied.

Manganese oxide

Manganese oxide (MnO_2) was used as an electrode material in supercapacitors (Zhang et al., 2011c). MnO_2 is synthesized from the solid-state reaction between $KMnO_4$ and $MnCl_2$ at low temperature. A specific capacitance of 258.7 F g^{-1} is measured when $KMnO_4$/$MnCl_2$ (molar ratio of 3:2) was in used. An excellent discharge capacitance of 145.9 F g^{-1} was obtained even after 200 cycles. The capacitance retention is 102.4% after 200 cycles inferred that the electrode material has excellent cycle stability.

Nano MnO_2 was designed and used as the electrode material in a supercapacitor (Ragupathy et al., 2009). Nanostructured MnO_2 is prepared by mixing of $KMnO_4$ and ethylene glycol under ambient conditions. The nano-MnO_2 resulting a capacity retention of 250 F g^{-1} and 1200 cycles stability. The excellent electrochemical properties of supercapacitors are due to the porosity and surface area of nano-MnO_2

Synthetic nano-material MnO_2 was synthesized via hydrothermal reaction under mild condition (Subramaniam et al., 2006). A good cycle stability and reversibility were achieved with a specific capacitance of 168 F g^{-1} when the nano-manganese oxide in a mild aqueous electrolyte solution was characterized using galvanostatic cycling and cyclic voltammetry.

Xerogel and ambigel are different forms of MnO_2 synthesized by Reddy & Reddy via a sol-gel method (Reddy & Reddy, 2003). The ambigel form exhibited a higher capacitance of 130 F g^{-1} in a sodium chloride electrolyte solution when compared to the xerogel form of manganese oxide.

Amorphous MnO_2, a mesoporous electroactive material was prepared by an improved reduction method (Xu et al., 2007). A specific capacitance of 299 F g^{-1} and good stability were obtained when this electrode material was studied in an aqueous KOH electrolyte solution.

Amorphous nanostructure MnO_2 was prepared and deposited on SS (Prasad, & Miura, 2004). In the deposition process, sulfuric acid and manganese(II) sulfate pentahydrate were mixed and used as an electrolyte solution. The electrochemical properties of the

material were alco characterized in supercapacitors which demonstrated a high power characteristic. A specific capacitance of 482 F g^{-1} was reached at a scan rate of 10 mV s^{-1} with a long-life cycle stability.

2.2.1.3 Polymers

Conductive polymers are also demonstrated good electrochemical performance as potential electrode materials. They can be produced in a competitive cost and the price is comparable to activated carbons. Kinetics of charge/discharge process is fast at conductive polymer electrodes. The charge is stored in the bulk of the material. Store and release charge in conducting polymers are undergo via redox processed. Doping is referring to the process when ions are transferred to the backbone of polymer during the oxidation. De-doping occurs when ions are released to the solution via reduction. Therefore, the charging of conducting polymer occurs throughout the bulk volume of the polymer film. In contrast with carbon electrode whereby the charging occurs on the electrode surface.

Polyaniline (PANI) is polymerized through the anodic electropolymerization of aniline. The electrochemical performance of a supercapacitor was evaluated when PANI was used as electrode material (Fusalba et al., 2000). The PANI was deposited on carbon paper electrode to form an electroactive film. An energy density and power density of 3.5 Wh kg^{-1} and 1300 W $kg^{-1,}$ respectively were obtained from the supercapacitor with applying this electrode material.

The PANI nanowire network is used as the electrode material and characterized in a sulfuric acid electrolyte solution. The performance was studied for a redox supercapacitor (Gupta and Miura, 2005). A specific capacitance of 742 F g^{-1} was reached at a

charge/discharge current density of 6 mA cm^{-2}. A specific power of 16 kW kg^{-1} was achieved with a long charge/discharge cycle stability.

Doped PANI nanofiber was applied as electrode materials in supercapacitors (Mi et al., 2008). It was fabricated using ferric chloride and ammonium persulfate in the template method. A specific capacitance of 428 F g^{-1} is obtained in a potential range of -0.2 to 0.8 V with sulfuric acid is used as an electrolyte solution. A capacitance retention of 83% and a discharge/charge efficiency of 93% were achieved. The study indicating that PANI electrode demonstrated good electrochemical properties.

Conjugated polymer poly(3,4-ethylenedioxythiophene) is prepared by chemical polymerization of a thin film on a non-conducting plastic substrate (Carlberg & Inganäs, 1997). This followed by the electrochemically reduction to reach a neutral state beside kept in the doped state. The polymer is used as an electrode material in electrochemical supercapacitors. A cell voltage of 0.8 V is achieved in the charged state of the measured supercapacitor.

2.2.1.4 Composite Materials

Composite material is an alternative choice of electrode material whereby a material is incorporated into another material within the same electrode. For examples, metal oxides/carbonaceous material; conducting polymer/carbonaceous material, metal oxide or conducting polymer/carbon nanotubes, etc.

MnO_2/activated carbon nanotube (MnO_2/A-CNT) composite was prepared using co-precipitation method. It was used as an electrode material for supercapacitors (Ko & Kim, 2009). The CNTs were activated in KOH aqueous solution, shown that the electrical

conductivity, specific capacitance, and specific surface area of A-CNTs were improved after the activation. The electrochemical evaluation was performed on the composite of MnO_2 and chemically activated CNTs demonstrated that the capacitance and cycle stability were improved. A specific capacitance of MnO_2/A-CNT composite electrode was 250 F g^{-1} at a scan rate of 10 mV s^{-1}, and 184 F g^{-1}, at scan rate of 100 mV s^{-1}.

The composite of MnO_2/graphene was synthesized via polymer-assisted chemical reduction (Qian et al., 2011). From this method, MnO_2 nanoparticles were uniformly distributed on the graphene nanosheets. A specific capacitance of 324 F g^{-1} is achieved by the prepared MnO_2/graphene composite electrode with sodium sulfate electrolyte used. The cyclic voltammetry showed that this electrode offered long-term cycle stability since the reduction of initial specific capacitance was 3.2% even after 1000 cycles.

The composite material of PANI and multi-walled carbon nanotubes (MWCNTs) was formed by *in-situ* chemical polymerization (Sivakkumar et al., 2007). The specific capacitances of 606 F g^{-1} was obtained by the supercapacitors with electrodes using composite materials of PANI-CNTs; which is higher than the supercapacitors with the PANI electrodes. Besides, the study also revealed that the specific capacitance decreased rapidly in repeating cycles when polyaniline electrodes were in used. Supercapacitors prepared from PANI-CNTs composite material have a better cyclability and good cycle retention compared with devices using only PANI.

Nitrogen-containing CNTs were synthesized by carbonizing of PANI nanotubes in a rapidly mixed reaction. The supercapacitor which assembled using electrode materials composed by PANI-based CNTs was reported (Yang et al., 2010). A high specific

capacitance of 163 F g^{-1} was obtained at 700 °C with a current density of 0.1 A g^{-1} when carbonized PANI nanotubes in potassium hydroxide solution was in used.

A composite material of graphene and polypyrrole (PPy/GNS) was synthesized from pyrrole monomer and graphene by in-situ polymerization under acidic conditions (Zhang et al., 2011a). Polypyrrole (PPy) was found to be an interesting electrode material due to its ductility, flexibility, good redox properties and high conductivity (Huang et al., 2016). At a current density of 0.5 A g^{-1}, a specific capacitance of 482 F g^{-1} was achieved by the graphene and PPy composite in a supercapacitor. The specific capacitance was reduced by less than 5% after 1000 cycles. In the study, the graphene and PPy composite material demonstrated its good performance such as high specific capacitance, shows higher specific capacitance, improved rate capability, and better cycling stability, when compared to the electrode with pure PPy.

2.2.2 Electrolyte Materials

The choice electrolyte used in an EDLC affects the capacitance of the EDLC and also affects the choice of electrode materials. The charge storage ability is depending whether the ions are accessible to the porous electrode surface. Both electrolyte and electrode must be compatible to each other in a way that the size of ion from electrolyte and the size of pore of electrode surface are optimum. Thus, the pore size distribution of electrode should enable the accessibility of the particular size of ions in electrolyte. The electrolyte also affects the power density of the device since the attainable voltage of EDLC is depending on the breakdown voltage of electrolyte.

Electrolytes applied in EDLC can be classified into organic electrolytes and aqueous electrolytes. Organic electrolytes are commonly used in the commercial EDLCs. The

devices using organic electrolytes enable to tackle the voltage ranging from 2 to 2.5 V. However, the power of the device is limiting due to the relatively high of the resistivity in organic electrolytes. Conversely, the aqueous electrolytes possess a lower breakdown voltage around 1 V and thus having higher conductivity compared to organic electrolytes.

2.2.2.1 Introduction of Polymer Electrolytes

Polymer electrolyte (PE) is a membrane containing a broad class of materials with main components of long polymeric backbone chain and relatively high concentration ions of dissolutions salt (Ramesh & Lu, 2012; Bocharova & Sokolov, 2020). PE is a solid solvent or sometimes also referred as solid solvent-free system which do not contain corrosive and toxic liquid electrolyte but possesses ionic transport and conduction properties which similar to the liquid ionic solution. PEs are more preferably used as ionic conductors compared to liquid electrolytes because they merge the advantages of solid-state electrochemistry with easier to inherently process plastic materials. (Javaid, 2017).

2.2.2.2 Advantages of Polymer Electrolytes

The discovery and use of PEs since they have characteristics which supercede liquid electrolyte and possess some improved features or properties. Thus, the PEs serve several advantages over the conventional liquid electrolytes. Enhancement of ionic conductivity is one of the most promising properties for PEs. Besides, PEs possess other interesting features such as transparency, light in weight, flexible, solvent-free, able to form thin film, easy to process, and able to configure into various shapes (MacCallum & Vincent, 1987; Susan et al., 2005). The application of the PE in the devices have better safety features compared to the utilization of liquid electrolytes, such as no internal shorting, prevent electrolyte leaking, prevent use of corrosive solvent, no production of harmful gases (Gray, 1991; Gray, 1997; MacCallum & Vincent, 1987; Scrosati, 1993).

2.2.2.3 Applications of Polymer Electrolytes

Development of novel PE material has become important research area during last few decades. PEs have received much attention because there are using as building blocks for a wide variety of applications in electrical/electrochemical power generation, energy storage and conversion for electronic, electrochromic and electrochemical devices. The devices and products with the application of PE are rechargeable batteries like lithium-ion batteries, nickel-metal hydride, dye-sensitized solar cells, fuel cells, supercapacitors, electrochemical sensors and electrochromic windows (Bruce 1995; Kim et al., 2004; (MacCallum & Vincent, 1987; Scrosati, 1993; Vincent, 1987). Table 2.2 compiles the general properties, advantages and applications of the PEs. Among PE technologies, much interest is focus on the electrolyte materials with excellent ionic conduction properties since they are related to their applications and performance of the products/devices.

2.2.2.4 History of Polymer Electrolytes Development

Work on PE was initialled in the 1970s and first launched by Fenton, et al. in 1973 (Fenton et al., 1973). In the study the ionic conductivity was discovered in the poly(ethylene oxide) (PEO) with addition of salt. However, the first generation of PEO-based PEs demonstrated a very low ionic conductivity at ambient temperature which is in the order of 10^{-8} S cm^{-1}. Since then, PEO was used as a benchmark of the study of PEs (Fenton et al., 1973; Wright, 1975). The technology importance of PEs was recognized and appreciated in early 1980s (Scrosati, 1993). The main direction of the PE development in the initial stage is to enhance the ionic conductivity since the specification to be included in the practical application should be at least 10^{-3} S cm^{-1} (Ye & Feng, 2010).

Table 2.2: A summary of the properties, advantages, and applications of the polymer electrolytes.

Properties of PEs	Advantages of PEs	Application of PEs
Transparency Light in weight Solvent-free Flexible Easy to process Able to form thin film Able to configure into various shapes	High ionic conductivity Wide electrochemical windows Enhance safety feature No leakage of electrolytes No internal shorting No production of harmful gases	Lithium-ion batteries Nickel-metal hydride Dye-sensitized solar cells Fuel cells Supercapacitors, Electrochemical sensors Electrochromic window Electric vehicles Electrocapacitors Actuators Analog memory devices Thermoelectric generator

2.2.2.5 Three Types of Polymer Electrolytes

The research and development of PEs has gone through and up to today's date the development processes produced three different categories of PE systems: dry/solid-state polymer electrolyte (SPE), gel/plasticized polymer electrolyte (GPE), and composite polymer electrolyte (CPE) (Bloise et al., 2001; Stephan, 2006). Wright invented the first sample of PEO-based dry/solid PE. The novelty in the invention was there is no organic liquid contained in the system whereas the polymer host is used as the solid solvent. This PE possessed a very low ionic conductivity but the mechanical strength and flexible geometry, and safety features were good (Ye & Feng, 2010).

GPE was first launched by Feuillade and Perche in 1975 (Feuillade & Perche, 1975). It is a gelled or plasticized polymer matrix produced by the addition of plasticizer causing the polymer matrix expand in a liquid electrolyte (Saikia et al., 2008). GPE is not liquid or solid, but a combination of both liquid and solid (Gray, 1991). It possesses both cohesive property of a solid and the diffusive property of a liquid.

2.2.2.6 Approaches to Improve Polymer Electrolytes

Many efforts have done across the years to improve the ionic and mechanical properties of PEs. The approaches which proposed in previous literature to overcome the disadvantages and limitations of SPE are via blending (Hu et al., 2011; Hu et al., 2009; Itoh et al., 2003; Ramesh et al., 2010; Liew et al., 2012a), cross-linking of polymer matrices (Walls et al., 2000; Wen et al., 2003), introduction of plasticizers (Ramesh & Bing, 2012), addition of fillers and dopant (Capiglia et al., 1999; Dai et al., 1998; Golodnitsky et al., 1997; Katsaros et al., 2002; Kim et al., 2008), application of ionic liquid (Hao et al., 2015; Liew et al., 2012a; Luo et al., 2013; Yin et al., 2019). Incorporation of fillers or dopants into the PE matrix result in the formation of CPEs.

Blending mix at least two polymer matrices with or without any chemical bonding between the polymers. It is a conventional technique to enhance the ionic conductivity via the reduction of crystallinity of the component polymer electrolytes. Thus, the blend polymer electrolytes can complement the limitations and disadvantages of the component polymer electrolytes. The resulting blend-based polymers exhibited higher conductivities and improved the physical and electrical properties compared to the individual polymer electrolytes (Ahmad et al., 2007). A PMMA/PVdF blend-based PE reported by Nicotera and co-workers reported a remarkable improve in lithium conduction property (Nicotera et al., 2006). Rajendran and co-workers had reported the enhancement in the performance of lithium polymer battery via the blending of PMMA and PVdF polymers (Rajendran et al., 2001).

2.2.2.7 Composite Polymer Electrolytes

Composite polymer electrolytes (CPEs) are formed upon incorporation of fillers or dopants into the PE matrices. The attempt of doping the PE with fillers/dopants is to

overcome the limitations and disadvantages of solid PE. The purposes of incorporating fillers into PE matrices is to increase the ionic conductivity at low temperature by enhance ion mobility; improve the mechanical stability at the interface with electrodes; high thermal stability, to increase the interfacial contact and transport properties of its polymer matrices (Chung et al., 2001; Croce et al., 1998; Gray 1997; Kam et al., 2014; Kim et al., 2003; Quartarone et al., 1998; Rajendran et al., 2002; Walls et al., 2000; Yang et al., 2020). The improved electrochemical and mechanical, thermal properties of CPEs are crucial for the technology enhancement to meet the requirements in electrochemical applications.

Literature show that several CPEs were prepared and characterized which demonstrated the improved electrochemical and mechanical properties. α-Al_2O_3 was added as a filler into PEO-$LiClO_4$ complex displayed an excellence improvement in the mechanical stability even in a high temperature (Weston & Steele, 1983). A better ionic conductivity and higher interfacial contact stability were achieved when fumed silica particulates were dispersed in a poly(ethylene glycol) (PEG) based polyment electrolytes (Raghavan et al., 1998). CPE which composed by PEO-NaSCN electrolyte and doped with γ-Al_2O_3 was reported to demonstrate an enhanced ionic conductivity and mechanical stability (Liquan et al., 1988). A study was conducted by Croce and co-authors shown that when $(PEO)_8LiClO_4$ complex added with γ-$LiAlO_2$ ceramic powders in granular-sized, the ionic conductivity is much better compared to the $PEO)_8LiClO_4$ complex without the dispersion of the ceramic powders (Croce et al., 1992). A CPE which prepared by Capiglia and co-workers was composed by nanosized silica (SiO_2) which embedded into PEO-$LiClO_4$ electrolyte systems (Capiglia et al., 1999). Madhurjya and co-authors demonstrated that the mechanical properties of a hydrotalcite-doped CPE was improved (Madhurjya et al., 2010). The natural source of polymer hosts such as starch was doped

with nanosized silica showed improvement in the mechanical strength and lower the level of crystallinity (Xiong et al., 2008). A biopolymer incorporated with TiO_2 nanoparticles was reported to show an improvement in ionic conductivity (Xiong et al., 2008; Khanmirzaei & Ramesh, 2014).

2.2.2.8 Polymer Hosts

PE is composed by at least one polymer host with addition of other material(s). The polymer host is a long chain polymer which acts a base matrix for the preparing PE system. The resulting PE should have better characteristic and properties compared to the parent polymer host. The crystalline structure of the polymer host is significantly disorder after addition of other material. This reduces the crystallinity in the PE than in the parent polymer host. Other improvement such as lower the glass transition temperature, and enhancement in ionic conductivity. Polymer host also acts as a solid solvent when the PE system does not contain any organic liquid or solvent. In the addition of filler, dopant of other nanosized particle, the ionic conductivity and mechanical strength of the parent polymer host could be enhanced. There are many polymer hosts had been using in the research and development of PEs. As reported from the previous literature, the polymer hosts which broadly use by the researchers are poly(ethylene oxide) (PEO) (Croce et al., 2001; Weston & Steele, 1983) , poly(vinylidene fluoride) (PVdF) (Tsunemi et al., 1983; Choe et al., 1995), poly(vinylidenefluoride-hexafluoro propylene) (PVdF-HFP), poly(methyl methacrylate) (PMMA) (Rhoo et al., 1997; Vondrak et al., 2001), poly(ethyl methacrylate) (PEMA), poly(acrylic acid) (PAA) (Kam et al., 2014; Arslan et al., 2006), poly(vinyl chloride) (PVC) (Alamgir & Abraham, 1993; Sukeshini et al., 1996), poly(vinyl alcohol) (PVA), poly(acrylonitrile) (PAN), Poly(ε-caprolactone) (PCL) and chitosan.

2.2.2.9 Fillers

The idea of incorporating fillers into PE matrices was first introduced by Weston and Steele (Weston & Steele, 1983). The fillers are electrochemically inert small particulate with the dispersion of these small particulates or fillers the matrices are known as composite polymer electrolyte (CPE) (Itoh et al., 2003). The particle size, surface area morphology and characteristics of the filler used such as porosity, concentration and the interaction between filler and polymer are greatly affect the nature and extent of the interaction, and the ionic/electronic conduction of the CPE (Capuano et al., 1991; Choi & Shin, 1996; Stevens & Wieczorek, 1996; Zhang et al., 2011b).

Fillers with smaller size possess high ratio of surface area over the volume which are more effective in reducing the crystallinity. The fine particle size also allows a better penetration of the fillers in the polymer matrix, The incorporation of fillers could deform the lattice structure of PE matrices and prevent recrystallization (Croce et al., 1992). Fillers provide alternative conduction pathways on the filler surfaces (Scrosati et al., 2000). The decrease in the crystallinity of CPE resulting in the improvement in ionic conduction and the alteration in the vitreous transition temperature. Example of particulate fillers with high surface area are hydrophobic fumed silica, zeolites, magnesium oxide (MgO), silicon oxide (SiO_2), zirconium oxide (ZrO_2), titanium oxide (TiO_2), aluminium oxide (Al_2O_3) which introduced into polymer matrix could support in making dimensionally stable PE systems for various applications ((Dai el al., 1998; Golodnitsky et al., 1997; Raghavan et la., 1998; Chung et al., 2001). Nanocomposite polymer electrolyte is formed when nanofillers are used as dopants. Factors which determine the workability, flexibility and conductivity of the nanocomposite polymer electrolytes are the size, structure and concentration of the nanofillers (Ahn et al., 2003). The advantages of the nanofillers with large surface area is to increase the amorphous

ratio of the nano-CPE and thus improve the material features such as breaking elongation, water resistance and tensile strength (Xiong et al., 2008).

2.2.3 Separator Materials

The separator is part of the EDLC which acting as mechanical barrier to avoid the diffusion of unwanted materials or impurities in the electrolyte. It prevents the electric contact between two carbon electrodes. Besides, the separator is ion-permeable and should have good electrolytic ion transport property to allow the transfer of ionic charges in taking place. The separator should possess the properties such as high ionic conductance, low thickness and high electrical resistance to facilitate it functions and thus to improve the performance of EDLC. Paper, polymer, ceramic and glass fiber are examples of material that can be used as separator. Paper and polymer separators are the choice when organic electrolytes are in used; whereas glass fiber and ceramic separators can be used with aqueous electrolytes. PE which possesses desired characteristics such as good mechanical property, good thermal stability and wide electrochemical window also can be used as a separator in electrochemical system.

2.3 Storage Technology and Basic Principle of Electrical Double Layer Capacitors

The storage technologies are approaching maturity in the recent decades. Numerous storing devices are launched to the market due to their desired storing capacities and also possessing reversibility in charge storing and releasing capabilities. Another desired characteristics are the devices whether can withstand a huge number of charge/discharge cycles besides having a considerable charge/discharge speed.

Electrostatic and electrolytic capacitors exhibit am ionic conducting solution between the electrodes. In batteries, energy storage in the form of chemical and convert via redox reactions. Electrochemical capacitors exhibit different storage mechanism which is differ from electrostatic capacitors as well as electrolytic capacitors. Activated carbons, micro porous materials are use as active electrode materials which offer a large surface area.

In EDLC, the energy stores through a physical process, i.e. the electrostatic interactions. With a working principle based on the double layer formation which occurs between the carbon electrodes and the ions from electrolytes. The electric charges from carbon are accumulated on the electrode surfaces; hence the opposite charge ions from the electrolyte solution are arranged approaching the electrode surface. The capacitance is charging at the electrode/electrolyte interface based on the reversible adsorption of opposite charge ions from the electrolyte solutions on carbon electrode surface.

The formation of double layer is a very fast process which take place in a short timeframe down to msec. The charging and discharging of EDLC occur in very short time. Thus, EDLC demonstrates extremely high power density. The working mechanism of EDLC is a physical storage process which do not imply any structural damage or change in the material integrity. Therefore, the EDLC enable an extremely long cycle life. These unique characteristics of EDLC make it potentially applicable to variety of electric and electrochemical devices.

The energy of EDLCs can be increased by increasing the operative voltage. The operative voltage is directly related to the electrode and electrolyte stabilities. The electrode materials which are typically composed of carbonaceous materials are chemically and electrochemically more stable than electrolyte. Therefore, the performance of EDLC is

mainly affected by the chemical and electrochemical stability of electrolyte. Nowadays, the sourcing and introduction of new electrolyte materials become one of the key factors of the high performance EDLCs.

2.4 Factors Affecting the Performance of Electrical Double Layer Capacitors

Typical EDLCs use porous carbon as electrode materials. When a voltage is applied to one of the carbon electrodes, the ions of opposite charge from the electrolyte solution accumulate on the electrode surface with a quantity is proportional to the potential applied. This leads to the formation of electric double layer. The electric double layer at the electrode/electrolyte interface is consisting of a layer of electric charge from the electrode and a layer of ions from the electrolyte.

The structural properties of electrode material affect some of the critical properties of EDLC Those critical structural properties including the particle size, pore size, electrode thickness, electrode surface structure and surface functional groups. The pore size is crucial to determine the accessibility of the electrolyte to the pores. Different type of electrolyte ions required different pore size as it affects the mobility of the electrolyte ions in the pores. The activated carbon materials usually undergo treatment to influence the structure and size of the pores on electrode surface; and thus facilitate the access of the electrolyte ions to the pores. The pore size chosen must be suitable to the electrolyte ions, and the distribution of pores should be optimal. The double layer capacitance will form when the electrolyte ions have good accessibility in entering the pores.

A few factors affected the energy density and power density in EDLC. Those factors are the specific surface area (SSA), pore size distribution (PSD), electrical conductivity, and wettability. A large specific surface area which available for ion electro-adsorption; and an optimized pore size distribution are required to achieve high energy and high power

density. Both pore size and surface area are significant to the charge capacity. Maximum capacitance will reach when the mean pore size of carbon electrode is similar to the size of ion. Thus, it's also important to do the measurements of specific surface area and pore size distribution. A large SSA and an optimized PSD of the electrode material will offer a high energy and high power density to the EDLC.

2.5 Desired Characteristics of Electrolyte Materials

Due to the fact that electrolyte ions are directly involved in the formation of double layer, thus the characteristics of electrolyte ions are essential not only to guarantee the process realization but also to ensure a longer life cycle. The choice of electrode materials should ultimately affect the characteristics and performance of EDLC. There are some factors which the device fabricator should considered in order to produce a device with excellence performance and good features. Electrolyte materials which offer a large electrochemical stability window (ESW), high conductivity and low viscosity are definitely desirable which affect the energy and power density of EDLCs. The large ESW is desired since a high cycle life is granted with an electrochemically stable electrolyte material.

A high conductivity and low viscosity of electrolyte resulting a fast double layer formation. The faster the formation of double layer, the higher the resulting power. A high chemical stability is achieved when both electrolyte ions and solvent do not react or decompose even when they are in contact with electrodes or other electrochemical capacitor components. The electrolyte ions are directly participating in the formation of double later, thus the integrity and stability are significant to ensure the realization of the process and also the reaching of long-life cycle. From the working mechanism we can see that the formation of double layer will not affect the structural and chemical properties of

both electrolyte and electrodes. This made the electrochemical capacitors different from other electrochemical devices in which the electrochemical processes have implied changes within the components of the device.

Electrolyte materials with good chemical stability, high boiling points, high flash point and low melting point are affecting on other features of the device such as safety and cycle life. Safety feature is one of the important characteristics of all kinds of energy storing and converting devices. The leaking of electrolyte liquid is frequently happened for primary batteries and some energy storing devices such as power bank also encountered over-heated and explosion. Thus, the materials used in the fabrication of EDLC should not imply any chemical reactions among the device components and also no chemical changes on the integrity of electrode and electrolyte materials.

The solvent used in the device ideally to have high flash point to ensure the safe use of EDLC, and reduce the risk of fire and explosion. Besides, the components of the device should be compatible in their chemical stability where not chemical reaction should be occurred when the electrolyte in contact with the solvent or with components in the EDLC. However, an ideal electrolyte should be a solvent free medium due to the involvement of ions from electrolyte in the formation of double layer. For the safety concern, the solvents could be not flammable.

The electrolyte should have a usable range from 60 to 100 ^{o}C and should stable over a wide range of temperature. The devices are able to tackle for many applications if the electrolytes are stable over s broad temperature range. Apart of these, the cost of the electrolyte materials also considerable since the low in cost raw materials are most easily

to be introduced to the commercial systems and also for the competitiveness of the products.

2.6 Selection Criteria of Polymer Host, Inorganic Salt and Dopant

2.6.1 Selection Criteria and the Choice of Polymer Host

The material is known as polymer host if it is remains intact as a polymer and without addition of any inorganic salt, dopant, etc. Some of the polymer such as poly(ethylene oxide) (PEO) (Croce et al., 2001; Weston & Steele, 1983) , poly(vinylidene fluoride) (PVdF) (Tsunemi et al., 1983; Choe et al., 1995), poly(methyl methacrylate) (PMMA) (Rhoo et al., 1997; Vondrak et al., 2001) are widely used as polymer host in the preparation of PEs. Polymer host can be conductive or non-conductive. For the conductive polymer, there are still some limitations in the dry solid polymer performance. When the conductive polymer host is subject to various characterization studies, the outcomes could be not satisfactory. The poor application performance of the polymer host could attribute to the poor ionic conductivity. However, most of the polymer hosts are ionic or electrical non-conductive, electrochemical instabilities, and have less desired properties for the electrical and electrochemical applications.

The basic function of the polymer host is to create the solid matrix of the PEs. Polymer with high molecular weight and high crystallinity among the main criteria to be selected as the polymer host in the preparation of PEs. Among the polymer hosts which widely used in polymer electrolyte research studies, PAA offers a potentially high ionic conductivity. There are considerable amount of literature reported on the PEs making from PAA (Kam et al., 2014; Arslan et al., 2006; Wu et al., 2006). The reason for choosing PAA is due to its promising characteristics, such as low cost, flexible, biodegradable, good processability and mechanical strength (Kam et al., 2014; Stamenkovic et al., 1997).

The use of green materials as polymer hosts minimizes potential environmental hazards. Acrylic acid is a weak acid with the presence of a carboxylic group. PAA is hydrophilic and behaves like an electrolyte when dissolved in water (Stamenkovic et al., 1997).

Like most solid polymers, PAA is electrically inactive which does not offer any ionic conducting characteristics. The molecular structure of the PAA also indicating a high potential with desired characteristics. The functional groups found on the PAA could offer a good molecular dispersion and thus resulting to a homogenous and hybrid electrolyte film. The interesting features of PAA make it a vital and promising material to be used as a polymer host in a new PE system.

2.6.2 Selection Criteria and the Choice of Inorganic Salt

A PE composed by at least two components, polymer host and inorganic salt with favourable electrical properties. In the PE, polymer host is acting like an encapsulating matrix but the inorganic salt contributes to the charge carriers. The addition of inorganic salt could alter the generic characteristics of the polymer. Synergistic interaction between different types of polymer host and inorganic salt could exert different extend of inorganic salt dissociation which affect the conductive properties of the materials. Thus, the key is to find the best pairing system between polymer host and inorganic salt in such a way that the most cations are available and the ion mobility is least hindered.

Due to the present of electrostatic interactions between polymer host and inorganic salt, the conductivity is mainly affected by the type and concentration of cation and also temperature. The incorporation of inorganic salt into polymer host should allow a greater dissociation of the inorganic salt in the polymer matrix; thus increase the cation mobility and ionic conductivity even under ambient temperature. The characterization of the PEs

should include the study on the effect of various temperatures and the effect of different inorganic salt content on the conductivity of the PEs.

The dissociation of salt trapped in the polymer system allows conductivity through the mobile ions also effected by the concentration of cation when different types of inorganic salt are applied. The present of inorganic salt in the polymer matrix establish a good mechanical strength and stability windows to the PE systems. The dissolution of inorganic salt in polymer host should make changes on the electrical and electrochemical properties of the PE systems.

In my study, PAA complexed with lithium salts is to improvement ambient temperature ionic conductivity. Concentration of different lithium salts in PE establish own unique trend in the plot of ionic conductivity vs lithium salt content plot. In application, the performance of the electrochemical devices such as EDLC could affected by the increasing of lithium salt content. However, there is a limit in the salt content which the further increase of salt concentration led to the reducing of device performance. The main criteria of choosing the lithium salt against a selected polymer host is the complexation of both could form a complex with improve mechanical stability and ionic conductivity. When the inorganic salt such as lithium salt is added to the PAA, it's expecting the formation of complexes between PAA and lithium salt.

Considerable research has been performed to investigate the properties of various lithium salt used in the polymer electrolytes preparation, including lithium bis(trifluoromethane) sulfonimide (LiTFSI) ($LiN(CF_3SO_2)_2$) (Wen et al., 2003; Li et al., 2001), and lithium triflate ($LiCF_3SO_3$) (Shin et al., 2002; Stephan et al., 2000), lithium perchlorate ($LiClO_4$) (Saikia et al., 2004; Saikia et al., 2008; Watanabe et al., 1983; Bloise et al., 2001; Chen-

Yang et al., 2002; Chung et al., 2001; Li et al., 2001; Rajendran et al., 2002) and lithium tetrafluoroborate ($LiBF_4$) (Rajendran & Uma, 2000; Shin et al., 2002; Stephan et al., 2000; Appetecchi et al., 2000).

Optimization of the ionic conductivities of selected PE can be done when choosing the polymer host and selective complexing salt with appropriate salt concentration. Polymer host of PAA containing polar group of O and hydroxyl group of OH in the polymer chain which are found to dissolve lithium salt. PAA based PEs possess strong electron-withdrawing functional group and thus leading to a high anodically stable PE.

Previous literature reported that PEs complexed with $LiClO_4$ exhibit good electrochemical properties (Chen-Yang et al., 2002; Watanabe et al., 1983; Choi & Shin, 1996). Several literatures have reported the use of $LiBF_4$ as an inorganic salt in PE preparation which demonstrated a high ionic conductivity (Shin et al., 2002; Stephan et al., 2000). Complexation between PAA and $LiBF_4$ could ease the dissociation of lithium salt to tetrafluoroborate ion. Also, the tetrahedral molecular geometry of both tetrafluoroborate ion and perchlorate ion will not hinder the segmental motion of polymer chain which could reduce the conductivity. The presence of fluorinated or chlorinated compound in the lithium salt are potential offer good conductivity and electrochemical properties to the polymer complexes.

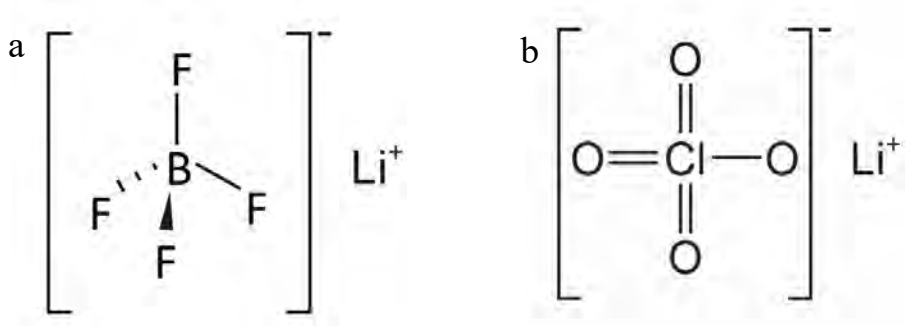

Figure 2.2: The chemical structure of the lithium salts used in the study: (a) $LiBF_4$ and (b) $LiClO_4$.

2.6.3 Selection Criteria and the Choice of Dopant

Impurities such as fillers or dopants could be introduced into the PE system to form a material known as composite polymer electrolyte (CPE). Dopant should be inert. Many types of materials been used dopants such as silica, metal oxide such as magnesium oxide (MgO), titanium oxide (TiO_2), aluminium oxide (Al_2O_3), zirconium oxide (ZrO_2) (Zhang et al., 2011b; Ramesh & Liew, 2010; Kim et al., 2003; Raghavan et al., 1998; Croce et al., 1998).

The purpose of the incorporation of dopant is to reduce the crystallinity of the polymer complex, increase the ionic conductivity, improve mechanical strength, thermal stability and interfacial stability (Chung et al., 2001; Croce et al., 1998; Kim et al., 2003; Walls et al., 2000; Rajendran & Uma, 2000). Doping exert the impurities into the system, thus could significantly disorder the crystalline structure of the polymer-lithium salt complexes. When the dopants are highly dispersed and immobilized in the polymer matrix, it could deform lattice structure of the PE systems and thus reduce the crystallization by preventing the agglomeration of the polymer chains. The degree of enhance in amorphous nature of the polymer matrix affect the increase in ionic conductivity. The dopant could provide more conductive pathways on the polymer system. The increase in conductivity is affected by the type of dopant, concentration and size of dopants in the CPE materials (Zhang et al., 2011b). Apart of the reduction in crystallinity, the addition of dopant should improve the mechanical strength of the PE system. The type and amount of dopant incorporation into PE system which affect the improve of mechanical strength in polymer host. Therefore, the criteria for the selection of dopant are affected by the types, amount and size of dopant. In general, smaller size dopant are more effective due to the higher ratio of surface area over the volume.

Barium titanate, $BaTiO_3$ is among the most widely used dopant in the electrochemical study (Yoon & Lee, 2002). It had been used as dopant or filler in many previous literature (Itoh et al., 2003; Li et al., 2001; Wen et al., 2003). In the previous research work presented by Croce and co-workers, TiO_2, Al_2O_3 and g-$LiAlO_2$ were used as the dopants in the CPE materials formed by PEO and $LiBF_4$ or $LiClO_4$ (Croce et al., 2000). A study also demonstrated that incorporation of $BaTiO_3$ in the PE prepared by PEO and $LiN(CF_3SO_2)_2$ offered a wide ESW of 4.0 V (Itoh et al., 2003). However, the doping effect of $BaTiO_3$ in the PE formed by PAA and $LiBF_4$ or $LiClO_4$ were not reported previously.

$BaTiO_3$ was reported to increase the conductivity and reduce interfacial resistance between the lithium anode and PEO (Sun et al., 2000). Therefore, $BaTiO_3$ was selected as the dopant in my study of the polymer materials prepared by PAA and $LiBF_4$ or $LiClO_4$. $BaTiO_3$ was used as a dopant in this study to deform the lattice structure of the PE systems. The addition of $BaTiO_3$ expected not only lead to better ionic conductivity but also provide better mechanical strength to the polymer matrix.

2.7 The Stand of Polymer Electrolytes in the Past, Recent and Future Developments of Electrical Double Layer Capacitors

2.7.1 In the Previous Development of Electrical Double Layer Capacitors

In the early stages of PE development, the EDLC is considered as an improved version of capacitor as energy storage solution and also as a good alternative for battery. However, EDLC only useful and applicable for a selected range of power and energy requirements. Regardless of these limitations, the EDLC technology has been widely used for many decades.

Previous development efforts have been dedicated to develop various energy storage technologies to tackle the various applications in market. The previous strategies are to develop the innovative and advanced especially electrolyte materials which considered to be one of the keys towards the current state of the technology. It is evident that the choice of electrolyte materials could increase the operative voltage of EDLCs. In the last few decades many alternative electrode and electrolyte materials have been studied and proposed for the realization of high energy, high power EDLCs. Besides, considerable efforts have been made toward the alternatives of solvent, inorganic salt, charge carrier, dopant. The earlier development had led to a high conductivity and wide electrochemical stability of these electrolytes which causing the realization of high power and high energy EDLCs. The EDLC technology offers many advantages such as long life cycle, wider operating temperature range, better charging efficiency and fast response. Nevertheless, the space and room of improvements are always there.

2.7.2 In the Recent Development of Electrical Double Layer Capacitors

Many lab-scale investigations and studies in private companies, research institutes and Universities nowadays are still dedicated towards innovative electrolyte materials to replace the current electrolytes. The focus is on novel composites, new solvents, new salts, new dopants, ionic liquid new carbon materials and hybrid systems. This is considered as one of the most significant approaches for the realization of high energy and high voltage EDLCs. In the industries, the focuses are mainly on the carbon technology to fulfil the requirements of existing markets and applications.

2.7.3 In the Future Development of Electrical Double Layer Capacitors

The future research directions are to allow the EDLCs achieve a well-balanced set of properties such as reasonable cost and highly safety features, apart from the high voltage

and high energy in device performance. The identification of new and novel PE materials with high conductivity, wide ESW and low viscosity are still on-going. Special tools such as computation screening are used to search, identify and investigate the chemical & physical properties of the new materials within a reasonable timeframe. When the research incorporation with computation simulations, these tools which facilitates with advanced techniques enable to provide guidance in designing new porous carbon structure with improved features such as high energy density; and provide new insights of the charge storage mechanism. Besides, the study to investigate the interaction between new electrolytes and both active and inactive materials should be carried on apart from the study with other EDLCs components. Other attention is the thermal stability and the interaction between ion-ion and ion-solvent to understand of the thermal and chemical properties of the device. Another important aspect of the future study is the strengths and limitations of new EDLCs, applicability and effectiveness on the intended uses. The trends for the future EDLC developments also highlighted by the recent proposed redox-active moieties into anions or cations of electrolyte. The bi-redox electrolytes with a combined redox contributed to double capacitance. The approach offers new field of bi-redox electrolytes and also opens up new directions to develop high energy EDLCs.

CHAPTER 3: MATERIAL AND METHODOLOGY

3.1 Introduction

The whole study is divided into two parts: preparation of polymer electrolytes (PEs) and composite polymer electrolytes (CPEs); and characterization of the prepared PEs and CPEs. In the preparation of PEs and CPEs, different chemicals are used. Thus, Subchapter 3.2 lists down all the chemicals including polymer, conducting salts, dopant and solvent used in the preparation of PEs and CPEs. In Subchapter 3.3, two major Subsubchapters cover the methodology for PEs/CPEs preparation and characterization methods.

3.2 Material

The chemicals used for the preparation of PEs and CPEs are listed in this Subchapter.

3.2.1 Poly(acrylic acid)

Poly(acrylic acid), PAA with an average molecular weight of 450,000 was obtained from Sigma-Aldrich Co., St. Louis, MO, USA.

3.2.2 Lithium Tetrafluoroborate

Lithium tetrafluoroborate, $LiBF_4$ (98% in purity) was purchased from Sigma-Aldrich and employed as conducting salt.

3.2.3 Lithium Perchlorate

Lithium perchlorate, $LiClO_4$ (99.99% in purity) was also obtained from Sigma-Aldrich Co.

3.2.4 Barium Titanate

Barium titanate oxide, $BaTiO_3$ (99% in purity) with the particle size < 3 μm was obtained from Sigma-Aldrich Co.

3.2.5 Deionized Water

Deionized water was used as the solvent.

3.3 Methodology

In this Section, two major scopes are covered: the methodology for PEs/CPEs preparation and methodology for PEs/CPEs characterization. In Subsubchapter 3.3.1, detailed methodology of the preparation of PEs and CPEs used in this study is discussed. In Subsubchapter 3.3.2, information about the measuring and analytical instruments used for the measuring and analysis are clearly provided, this including specification of the instrument, operating and testing conditions. The relevant formulae and equations are given, including the step-by-step procedure to derive the formula and calculation of the test results.

3.3.1 Preparation of Polymer Electrolytes

PE is prepared by using at least one polymer as a polymer host and at least one type of conducting salt, which is usually an inorganic salt. Throughout this study, poly(acrylic acid) (PAA) was employed as a polymer host. Two different types of conducting salts are used for the preparation of PEs: lithium tetrafluoroborate ($LiBF_4$) and lithium perchlorate ($LiClO_4$). Thus two types of PEs are prepared: PAA-$LiBF_4$ namely poly(acrylic acid)/lithium tetrafluoroborate and PAA-$LiClO_4$ namely poly(acrylic acid)/lithium perchlorate. Only one type of filles or dopant is used in the preparation of CPEs, which is barium titanate, $BaTiO_3$. The incorporation of this dopant into two different types of

PE led to the preparation of two CPEs, which are PAA-$LiBF_4$-$BaTiO_3$ namely poly(acrylic acid)/lithium tetrafluoroborate/barium titanate and PAA-$LiClO_4$-$BaTiO_3$ namely poly(acrylic acid)/lithium perchlorate/barium titanate.

In the preparation of PEs and CPEs, all chemicals are used as received without further purification. Any physical pre-treatments are as per stated in the relevant section. In case a solvent is required for the chemical preparation, deionized water was used as a solvent to dissolve all starting chemicals.

3.3.1.1 Preparation of PAA-$LiBF_4$

PAA-$LiBF_4$ electrolytes were prepared using solvent casting method. In the beginning of the preparation, $LiBF_4$ was dried at 100 ºC in the conventional air oven for 1 h. This is to eliminate any trace amounts of water in the material since $LiBF_4$ is a hydroscopic material. Several PAA-$LiBF_4$ electrolytes were weighed according to the ratio of polymer to lithium salt, ranging from 95/5 to 60/40 as shown in Table 3.1. The weighed amounts of PAA and $LiBF_4$ were added into a 250 mL conical flask and 25 mL of deionized water was added to dissolve all the starting materials. The mixtures were continuously stirred for 12 h using magnetic stirring hotplate at 100 ºC to obtain homogeneous mixtures. The mixtures were then poured onto a flat glass wrapped with the Teflon paper and dried in an oven at a 50 ºC for at least 12 h. This is to evaporate the solvent and to produce a dried, mechanically stable and free-standing PE film. The ready films were placed inside clean and dried plastic bags with air-tight seal and stored in a desiccator to avoid moisture contamination.

Ionic-conductivity measurements at ambient temperature indicated that PAA-$LiBF_4$ with a weight percent ratio of 70/30 yielded the highest conductivity. Thus, this composition

was used for the electrochemical study. Composition which offers the top three highest ionic conductivity are used for electrical, thermal and structural studies.

Table 3.1: Chemical composition for PAA-$LiBF_4$ electrolyte systems with different weight percentage of $LiBF_4$ at ambient temperature.

PE Sample Notation	Sample weight (g)	Weight of PAA (g)	Weight of $LiBF_4$ (g)	Composition of PAA-$LiBF_4$ (wt.%)
P95-LB5	1.0	0.95	0.05	(95:5)
P90-LB10	1.0	0.90	0.10	(90:10)
P85-LB15	1.0	0.85	0.15	(85:15)
P80-LB20	1.0	0.80	0.20	(80:20)
P75-LB25	1.0	0.75	0.25	(75:25)
P70-LB30	1.0	0.70	0.30	(70:30)
P65-LB35	1.0	0.65	0.35	(65:35)
P60-LB40	1.0	0.60	0.40	(60:40)

3.3.1.2 Preparation of PAA-$LiClO_4$

PAA-$LiClO_4$ electrolytes were prepared using exactly the same method as described in 3.3.1.1 except that $LiClO_4$ is used as conducting salt instead of $LiBF_4$. Table 3.2 presented the composition of PAA-$LiClO_4$ and the respective notation used in the remaining Chapter.

Table 3.2: Chemical composition for PAA-$LiClO_4$ electrolyte systems with different weight percentage of $LiClO_4$ at ambient temperature.

PE Sample Notation	Sample weight (g)	Weight of PAA (g)	Weight of $LiClO_4$ (g)	Composition of PAA-$LiClO_4$ (wt.%)
P95-LC5	1.0	0.95	0.05	(95:5)
P90-LC10	1.0	0.90	0.10	(90:10)
P85-LC15	1.0	0.85	0.15	(85:15)
P80-LC20	1.0	0.80	0.20	(80:20)
P75-LC25	1.0	0.75	0.25	(75:25)
P70-LC30	1.0	0.70	0.30	(70:30)
P65-LC35	1.0	0.65	0.35	(65:35)
P60-LC40	1.0	0.60	0.40	(60:40)

3.3.2 Preparation of Composite Polymer Electrolytes

3.3.2.1 Preparation of PAA-$LiBF_4$-$BaTiO_3$

PAA-$LiBF_4$-$BaTiO_3$, a CPE was prepared using solvent casting method. The process is started with the preparation of PAA-$LiBF_4$ electrolyte first, then followed by the addition of $BaTiO_3$, a dopant. $LiBF_4$ was dried at 100 °C for 1 h to remove the moisture in the material prior to the preparation of the CPE. Firstly, PAA and $LiBF_4$ were measured and mixed together in a conical flask containing 25 mL of deionized water, followed by the addition of 2 wt.% of $BaTiO_3$. Then the mixture was mixed well and treated with ultrasonicate for 30 minutes to allow the dopant to disperse well in the mixture solution. After the ultrasonication, the mixture solution is heated at 100 °C for 12 h with stirring. The homogeneous solution is then cast on petri dish wrapped with Teflon foil and dry in an oven at 50 °C for 12 h to dry the content. A mechanically stable, dry and stand-alone of PAA-$LiBF_4$-$BaTiO_3$ thin film is produced. It is stored in a sealed plastic bag and kept

inside desiccator prior to the characterization analyses. Most of the previous literature prepared the CPE using dopant content up to 10 wt.% (Croce et al., 2001; Chen-Yang et al., 2002). A lower dopant content is not significant in altering the lattice structure of the polymer matrix. However, higher dopant concentration could lead to uneven distribution of the particles due to the dispersive nature of the material used.

Table 3.3: Chemical composition for PAA-$LiBF_4$-$BaTiO_3$ electrolyte systems with different $BaTiO_3$ weight percentages at ambient temperature.

CPE Sample Notation	Sample weight (g)	Weight of PAA (g)	Weight of $LiBF_4$ (g)	Weight of $BaTiO_3$ (g)	Weight Percent of $BaTiO_3$ (wt.%)
CPE2B	1.0	0.686	0.294	0.02	2.0
CPE4B	1.0	0.672	0.288	0.04	4.0
CPE6B	1.0	0.658	0.282	0.06	6.0
CPE8B	1.0	0.644	0.276	0.08	8.0
CPE10B	1.0	0.630	0.270	0.10	10.0

3.3.2.2 Preparation of PAA-$LiClO_4$-$BaTiO_3$

PAA-$LiClO_4$-$BaTiO_3$ electrolytes were prepared using exactly the same method as described in 3.3.2.1 except that PAA-$LiClO_4$ is used as conducting salt instead of PAA-$LiBF_4$ and the composition of the PAA-$LiClO_4$-$BaTiO_3$ is varied, which is presented as in Table 3.4.

The mechanically stable membranes obtained an average thickness of about 0.234 mm, as determined by Mitutoyo digital gauge. In the preparation of PAA-$LiClO_4$ with 2 wt.% $BaTiO_3$, the PAA-$LiClO_4$ electrolyte is prepared according to the weights as stated in Table 3.4. 0.02 g (2 wt.%) of the $BaTiO_3$ is then blended with the mixture and dry via

heating in oven until a free-standing film is obtained. CPEs with different $BaTiO_3$ weight percentages were prepared by referring to the composition as stated in Table 3.4. The $BaTiO_3$ doped PAA-$LiClO_4$ electrolytes were then used for characterization studies.

Table 3.4: Chemical composition for PAA-$LiClO_4$-$BaTiO_3$ electrolyte systems with different $BaTiO_3$ weight percentages at ambient temperature.

CPE Sample Notation	Sample weight (g)	Weight of PAA (g)	Weight of $LiClO_4$ (g)	Weight of $BaTiO_3$ (g)	Weight Percent Of $BaTiO_3$ (wt.%)
CPE2C	1.0	0.882	0.098	0.02	2.0
CPE4C	1.0	0.864	0.096	0.04	4.0
CPE6C	1.0	0.846	0.094	0.06	6.0
CPE8C	1.0	0.828	0.092	0.08	8.0
CPE10C	1.0	0.810	0.090	0.10	10.0

3.4 Characterization

3.4.1 Effect of Conducting Salt and Dopant Concentration Studies

3.4.1.1 Effect of Conducting Salt Concentration Studies

Ionic conductivity measurement was carried out at ambient temperature on both PAA-$LiBF_4$ and PAA-$LiClO_4$ samples. From Subsubchapter 3.3.1, both PEs samples are comprising of different concentration with measured in weight percent, ranging from 5 to 40 wt.% of salt as shown in Tables 3.1 and 3.2. Both tables list down the chemical composition for the PAA-hosted electrolyte systems with various $LiBF_4$ and $LiClO_4$ content. The PE films are labelled as PX-LY, where P refers to the polymer used which is poly(acrylic acid) and L refers to the conducting salt, either lithium tetrafluoroborate (LB) or lithium perchlorate (LC). X and Y refer to the PAA and $LiBF_4$/$LiClO_4$ weight

percent, respectively. For example, P70-LB30 refers to 70 wt.% of PAA and 30 wt.% of lithium tetrafluoroborate, prepared with 0.70 g of PAA powder mixed with 0.30 g $LiBF_4$.

3.4.1.2 Effect of Dopant Concentration Studies

Ionic conductivity measurement was carried out at ambient temperature on both PAA-$LiBF_4$-$BaTiO_3$ and PAA-$LiClO_4$-$BaTiO_3$ samples prepared. From Subsubchapter 3.3.2, both CPEs samples are comprising of different $BaTiO_3$ concentration with measured in weight percent, ranging from 2 to 10 wt.% as shown in Tables 3.3 and 3.4 which list the chemical composition for the PAA-hosted electrolyte systems with various $LiBF_4$ or $LiClO_4$, and $BaTiO_3$ content. The CPE films are labelled as CPEX, where CPE refers to the composite polymer electrolyte which X is the weight percent of $BaTiO_3$ in the composition. CPEXB is the notation given to CPE using $LiBF_4$ as conducting salt; whereas CPEXC is the notation given to CPE using $LiClO_4$ as conducting salt.

3.4.2 Ambient Temperature-Ionic Conductivity Studies

All the prepared PEs and CPEs films are subjected to the AC-impedance spectroscopy for the determination of ionic conductivity at ambient temperature. Initially the PE/CPE samples were removed from the plastic bags and the thickness of the samples was measured by the aid of a micrometer screw gauge. The samples were cut to resemble the shape of the stainless steel (SS) blocking electrodes which were used to sandwich them. Then the cut samples were mounted between two parallel SS blocking electrodes under the pressure of springs with a configuration of SS/Film/SS. The bulk resistance of the PE/CPE films is measured using electrochemical impedance spectroscopy (EIS) HIOKI Model 3532–50 LCR HiTESTER which connected to a computer for data acquisition within a frequency range of 50 Hz – 5 MHz at ambient temperature, 25 °C. The bulk ionic conductivity is calculated by using the equation below:

$$\sigma = \frac{L}{R_b \times A} \tag{3.1}$$

where σ (S cm^{-1}) is the ionic conductivity, L (cm) is the thickness of a thin film, R_b (Ω) is the bulk resistance obtained from Cole–Cole impedance plot, and A (cm^2) is the surface area of stainless-steel blocking electrodes. The semicircle fitting was accomplished to obtain R_b value.

3.4.3 Temperature Dependent-Ionic Conductivity Studies

In the temperature dependent–ionic conductivity study, freshly prepared PE/CPE samples were subjected to EIS for ionic conductivity measurement over the frequency range of 50 Hz to 5 MHz with the elevation of temperature ranging from or 30 ºC to 120 ºC (303 K to 393 K) with an interval of 10 ºC. The temperature of the samples is maintained using a convection oven and samples were kept for 30 minutes to attain the thermal equilibrium for each temperature tested. This is to ensure the stability in the measured temperature and also avoid the temperature fluctuation during data collection. Prior to the spectroscopy measurement, the thicknesses of the sample films were measured using micrometer screw gauge.

When the Arrhenius rule is obeyed by the PEs/CPEs system, the relationship between the ionic conductivity and the temperature is expressed as follows:

$$\sigma = A \exp\left(\frac{-E_a}{kT}\right) \tag{3.2}$$

where σ (S cm^{-1}) is the ionic conductivity, A is the pre-exponential factor, E_a (kJ mol^{-1}) is the activation energy, k is the Boltzmann constant and T (K) is the absolute temperature.

3.4.4 Dielectric Studies

The dielectric behaviour of a dielectric material is composed by two components, the real and imaginary parts of a dielectric constant, which is expressed by:

$$\varepsilon^* = \varepsilon' - i\varepsilon'' \tag{3.3}$$

where ε' denotes the real part of dielectric constant and ε'' denotes the imaginary part of dielectric constant (also known as dielectric loss) of the PE system.

The real part of the dielectric constant is the measurement of charge storage in a dielectric material. It is illustrated by:

$$\varepsilon' = \frac{-Z''}{\omega C_0 (Z'^2 + Z''^2)} \tag{3.4}$$

The imaginary part of the dielectric constant (dielectric loss) is a measurement of energy dissipated from the polarization effect and transport of charge carriers. It is illustrated by:

$$\varepsilon'' = \frac{Z'}{\omega C_0 (Z'^2 + Z''^2)} \tag{3.5}$$

where Z' is the real parts of complex impedance and Z'' is imaginary part of complex impedance. Angular frequency, ω (in Hertz, Hz) is equal to $2\pi f$. C_0 is calculated by the following formula:

$$C_0 = \frac{\varepsilon_o A}{l} \tag{3.6}$$

where ε_o is the vacuum permittivity or the permittivity of free space (equal to 8.854×10^{-12} F m^{-1}), A refers to the electrolyte–electrode contact area, l (cm) denotes the thickness of the dielectric sample.

The relative permittivity, ε_r (or dielectric constant, K) is expressed by:

$$\varepsilon_r = \frac{\varepsilon}{\varepsilon_o} \tag{7}$$

Dielectric loss can be expressed by means of loss tangent, and it is defined by:

$$\tan \delta = \varepsilon''/\varepsilon' \tag{8}$$

The real part of dielectric moduli is expressed by:

$$M' = \frac{\varepsilon'}{[(\varepsilon')^2 + (\varepsilon'')^2)]} \tag{9}$$

The imaginary part of dielectric moduli is expressed by:

$$M'' = \frac{\varepsilon''}{[(\varepsilon')^2 + (\varepsilon'')^2)]} \tag{10}$$

3.4.5 Electrochemical Stability Studies

Linear sweep voltammetry (LSV) was employed to study the ESW of the all the PE and CPE samples with the highest ionic conductivity. A GAMRY electrochemical interface was used for the measurement with the configuration of stainless steel (SS)/PE film/SS. The applied potential range is different for the different type of PEs/CPEs. The analysis was performed at a scan rate of 5 mV s^{-1} with a sample interval of 0.001 V with 2 s as the rest time prior to the measurement. The applied potential range was tested at a wide potential range but eventual the result is reported based on the stable ESW. Thus, the final applied potential range is varied accordance to the types of electrolyte systems as shown in Table 3.5. The potential range applied for PAA-$LiBF_4$, PAA-$LiClO_4$, PAA-$LiBF_4$-$BaTiO_3$ and PAA-$LiClO_4$-$BaTiO_3$ are -2.5 to +2.5 V, -3.0 to +3.0 V, -9.0 to +4.0 V and -10.0 to +3.0 V, respectively. The LSV responses of the samples were accomplished using GAMRY electrochemical interface at ambient temperature.

Table 3.5: The applied potential range for various types of PE/CPE system in the LSV analysis.

PE/CPE	Potential range (V)
PAA-$LiBF_4$	-2.5 to +2.5
PAA-$LiClO_4$	-3.0 to +3.0
PAA-$LiBF_4$-$BaTiO_3$	-9.0 to +4.0
PAA-$LiClO_4$-$BaTiO_3$	-10.0 to +3.0

3.4.6 Thermogravimetric Analysis

The thermal stability of all PE and CPE electrolyte systems prepared were investigated using a thermogravimetry analyzer (TGA). TGA consisting of STA 6000 main unit and Pyris software, version 11 to determine the residual mass of electrolytes. The electrolyte samples were heated from 30 °C to a maximum temperature of 600 °C with a flow rate of 20 mL min^{-1} under inert nitrogen condition.

3.4.7 X-ray Diffraction Studies

The amorphous nature of all the PE and CPE samples prepared were investigated using X-ray diffraction (XRD) study. with Cu Kα radiation of wavelength 1.5406 Å, scattering over the range of 2θ between 5º – 90º. The XRD patterns were recorded on an EMPYREAN X-ray Diffractometer with Cu-Kα radiation (λ=1.54060 Å) scatters over the range of 2θ = 5–90° at ambient temperature.

3.4.8 ATR-FTIR Analysis

Attenuated total reflectance-fourier transform infrared (ATR-FTIR) analysis was carried out using Perkin-Elmer FTIR Spectrometer Spectrum 400. The spectra of the PE and CPE

films prepared were recorded in the transmittance mode at the wave regime between 4000 and 450 cm^{-1} with a resolution of 4 cm^{-1} at room temperature.

CHAPTER 4: PAA-$LiBF_4$ ELECTROLYTES CHARACTERIZATION

4.1 Introduction

Acrylic acid, a monomer of poly(acrylic acid), is an unsaturated compound of vinyl and able to undergo polymerization to form polymer (Stamenkovic et al., 1997). The acrylic acid monomer molecules which build-up a polymer chain as illustrated in Figure 4.1.

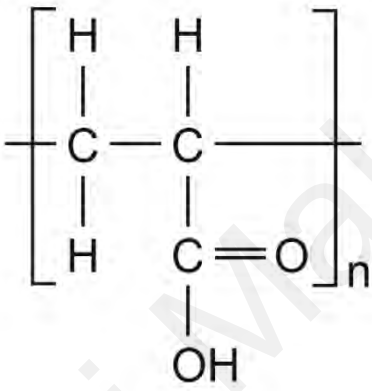

Figure 4.1: Repeat unit of poly(acrylic acid), the polymer host used in this research study.

A pure product of poly(acrylic acid), PAA is a powder precipitate which is insoluble in its own monomer but it is soluble in aqueous at neutral pH. PAA is broadly used as a material for electrolyte due to its properties which containing many carboxylic groups along the polymer chain (Kam et al., 2014). Polymer electrolyte, PE is typical synthesis by dissolving the polymer(s) with an ionic salt in a polar solvent follow by the evaporation of the solvent, either partial or complete evaporation. PAA not only a promising material for PE materials, it is also used as a binder on solid electrode interphase in silicon anode (Parikh et al., 2019) and also used as a copolymer to improve the electrical conductivity of poly(ethylene oxide) (Saikia et al., 2008).

In the preparation of PAA-based electrolyte, deionized water is used as a solvent. PAA behaves as hydrophilic and thus can be easily dissolved in water due to the ionization of

the pendent carboxyl side chains. Like most polymers, pure PAA is electrically inactive and also does not offer any ionic conducting property. PAA could form a stable complex with metals (Dasenbrock et al., 1998). A few previous literature reported the application of PAA as polymer host in PE preparation, which complexed with poly(vinyl alcohol) (Dasenbrock et al., 1998), chitosan (Smitha et al., 2004), lithium bis(trifluoromethane) sulfonimide, LiTFSI (Kam et al., 2014), and carboxy methyl cellulose (Parikh et al., 2019). The PE dissociates in solvent become complex ions which are electrochemically stable and enable to support the current transport in the solution.

In this study, PAA was selected and used as the polymer host due to its good characteristics such as superior mechanical strength, biodegradability, good processability, flexibility, and being inexpensive (Kam et al., 2014). Application of PAA as an electrolyte material definitely serve minimal harmful effect to the environment. The characteristics of PEs much dependent on its composition such as conducting salt, filler or dopant; and the interaction between these compositions which could alter the properties of the PE.

Conducting salt such as inorganic salt is the most important component for the preparation of PE, apart from the polymer host. In case of application in the EDLC, the ions of the conducting salt are directly involved in the formation of double layer. Thus, the selection of the conducting salts is important in order to prepare a PE which desired characteristics (Ramesh et al., 2012). In the last few decades, there are a few conducting salts are been considered for the preparation of PE such as lithium hexafluorophosphate ($LiPF_6$) (Liew & Ramesh, 2014; Liew et al., 2012b), lithium triflate ($LiCF_3SO_3$) (Ramesh & Liew, 2010), lithium tetraborate ($Li_2B_4O_7$) (Ramesh & Bing, 2012; Ramesh et al., 2011), lithium bis(trifluoromethane) sulfonimide (LiTFSI) ($LiN(CF_3SO_2)_2$) (Li et al., 2001; Ramesh &

Liew, 2013; Ramesh et al., 2013; Wen et al., 2003), and ammonium acetate (CH_3COONH_4) as an non-metal salt (Liew et al., 2014b). In this study, the chemical, electrical, electrochemical, thermal and structural properties of PAA-based electrolytes with different $LiBF_4$ and $LiClO_4$ conducting salts with and without the doping of $BaTiO_3$ have been investigated.

4.2. Results and Discussion

4.2.1 Electrical Properties

4.2.1.1 Ambient Temperature-Ionic Conductivity Studies of PAA-$LiBF_4$

Impedance spectroscopy is a typical method used to measure the ionic conductivity of the electrolyte film. Analysis of the impedance spectra yields some information about the electrolytes' properties, such as bulk resistance. Figure 4.2 presents the Impedance plot of PAA-$LiBF_4$ solid electrolytes. The bulk resistance (R_b) of 5 Ω was measured from the intercept on the real axis at high frequency region of the plot. The thickness of the PAA-$LiBF_4$ films was determined using Mitutoyo digital gauge. The average thickness was found to be 0.095 mm. The highest ionic conductivity of 6.61 $\times 10^{-4}$ S cm^{-1} of the film was reached and calculated using the equation described in the Chapter 3 Material & Methodology.

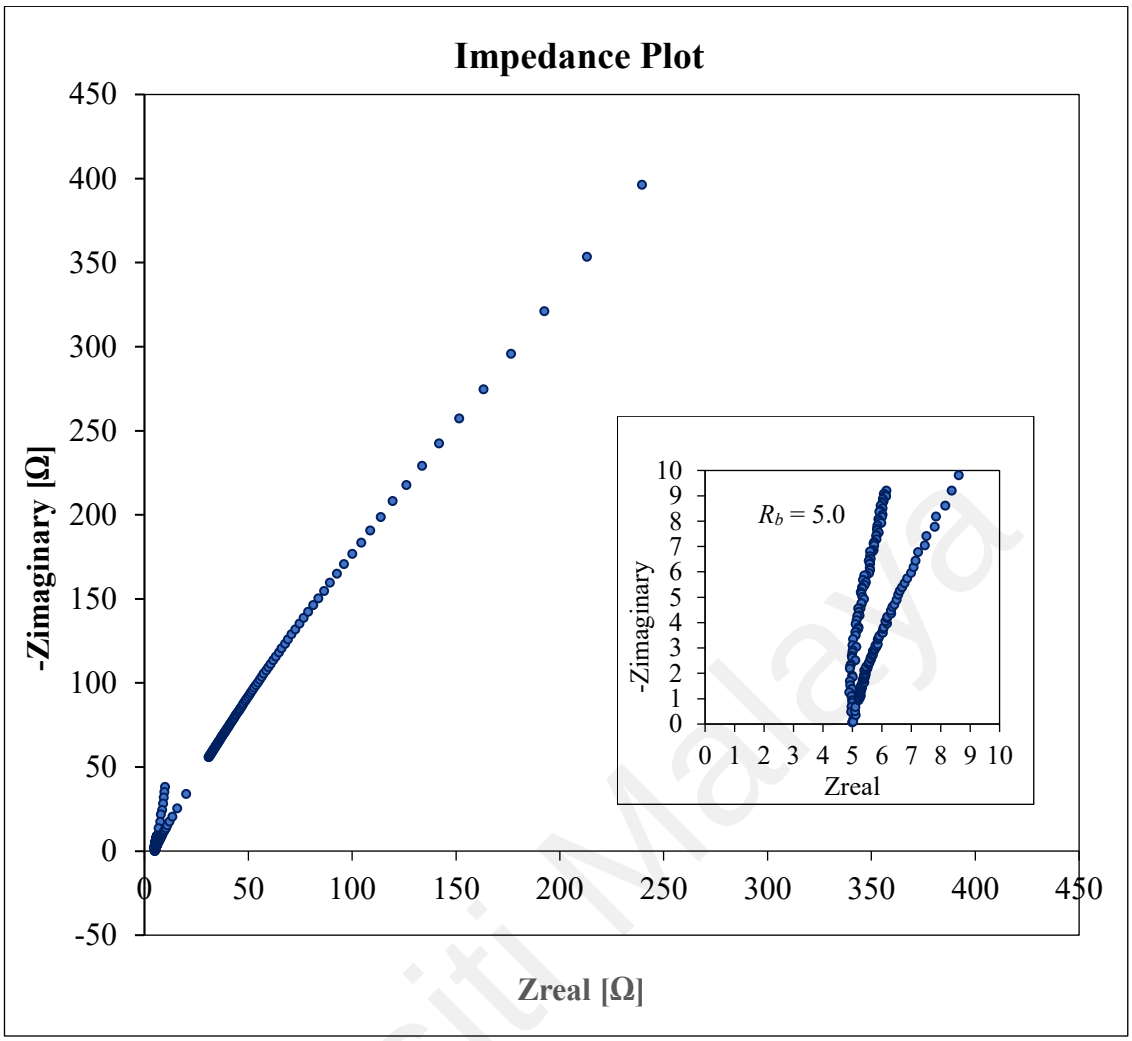

Figure 4.2: Impedance plot of PAA-$LiBF_4$ electrolyte film at ambient temperature. The inset: Magnified axis in a higher frequency region of the real part of complex impedance (x-axis). The imaginary part of complex impedance is the y-axis.

The optimum composition of PE is very crucial in determining the suitability of electrolyte systems for practical application in electrochemical devices. Figure 4.3 depicts the ionic conductivity of PAA-based electrolytes with different $LiBF_4$ weight percent (wt.%) at ambient temperature. As shown in Figure 4.3, ionic conductivity increases instantaneously with the loading of $LiBF_4$. As shown in the figure, PAA-hosted sample with 5 wt.% of $LiBF_4$ (P95-LB5) demonstrated the ionic conductivity of 2.32×10^{-7} S cm^{-1} which is the lowest among all samples prepared. PAA-hosted sample with 30 wt.% of $LiBF_4$ (P70-LB30) achieved the highest ionic conductivity of 6.61×10^{-4} S cm^{-1}. The

casting films for PAA with more than 35 wt.% of $LiBF_4$ are not appropriate for the experiment due to the soft and viscous texture and thus difficult to handle.

The mobile lithium ions in the $LiBF_4$ salt acts as charge carriers. When the weight percent of the $LiBF_4$ increases, the number of mobile lithium ions increases. The initial addition of $LiBF_4$ led to the increase of mobile ions available in the PAA electrolytes system. However, from 30 wt.% onwards, the ionic conductivity was continued to decrease until 40 wt.% of $LiBF_4$. At the higher concentration of $LiBF_4$, the number of dissolved ions in the PAA-$LiBF_4$ matrix increases but the effective number of the free mobile ions which available for migration is reduced. This is due to the replacement of re-dissociation of solvated ion pairs by the short-range ion-solvent interaction. The excessive lithium ions may be re-associate and obstructs the conduction pathway of the mobile lithium ions.

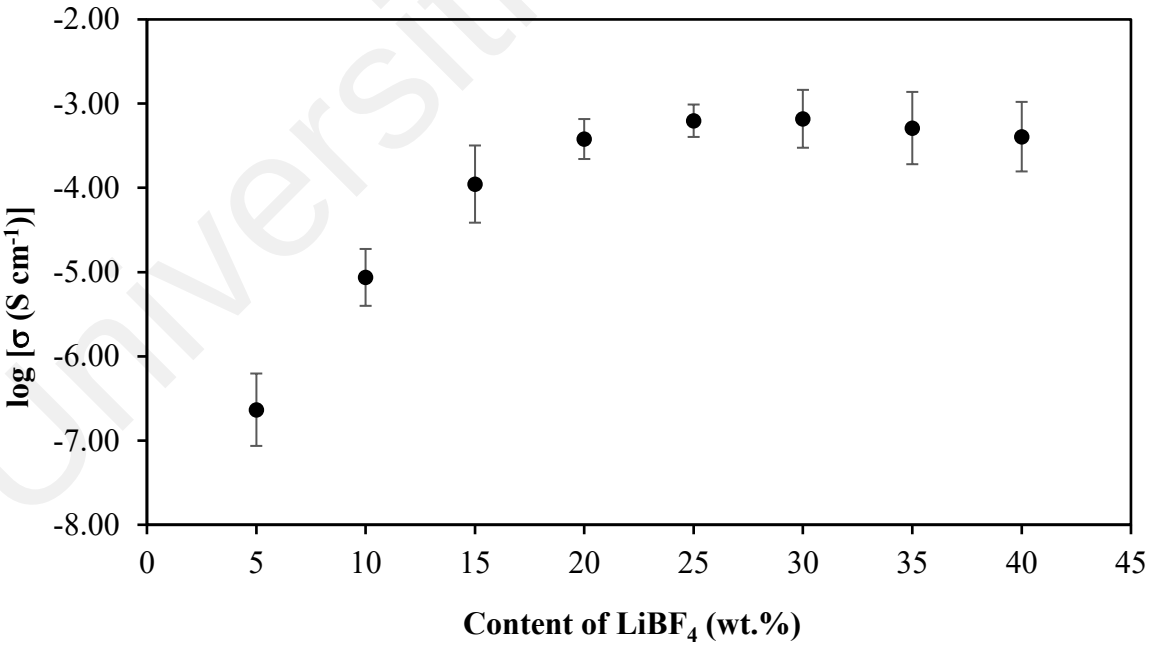

Figure 4.3: Effect of $LiBF_4$ salt content on the ionic conductivity of PAA-based electrolytes at ambient temperature.

4.2.1.2 Ambient Temperature-Ionic Conductivity Studies of PAA-$LiBF_4$-$BaTiO_3$

In this study, AC-electrochemical impedance spectroscopy is used to examine the ionic conductivity of PAA-$LiBF_4$-$BaTiO_3$ electrolytes by sandwiched the thin film between two stainless steel blocking electrodes. The Impedance plot of PAA-$LiBF_4$-$BaTiO_3$ electrolyte thin film at ambient temperature is demonstrated in Figure 4.4. Impedance is measured as a function of frequency. The plot portrays a straight line inclined towards the real-axis which intercept at a higher frequency. This indicates a low bulk resistance of (R_b) where a reading of 7 Ω was determined from the plot. The thickness of 0.177 mm was measured using Mitutoyo digital gauge.

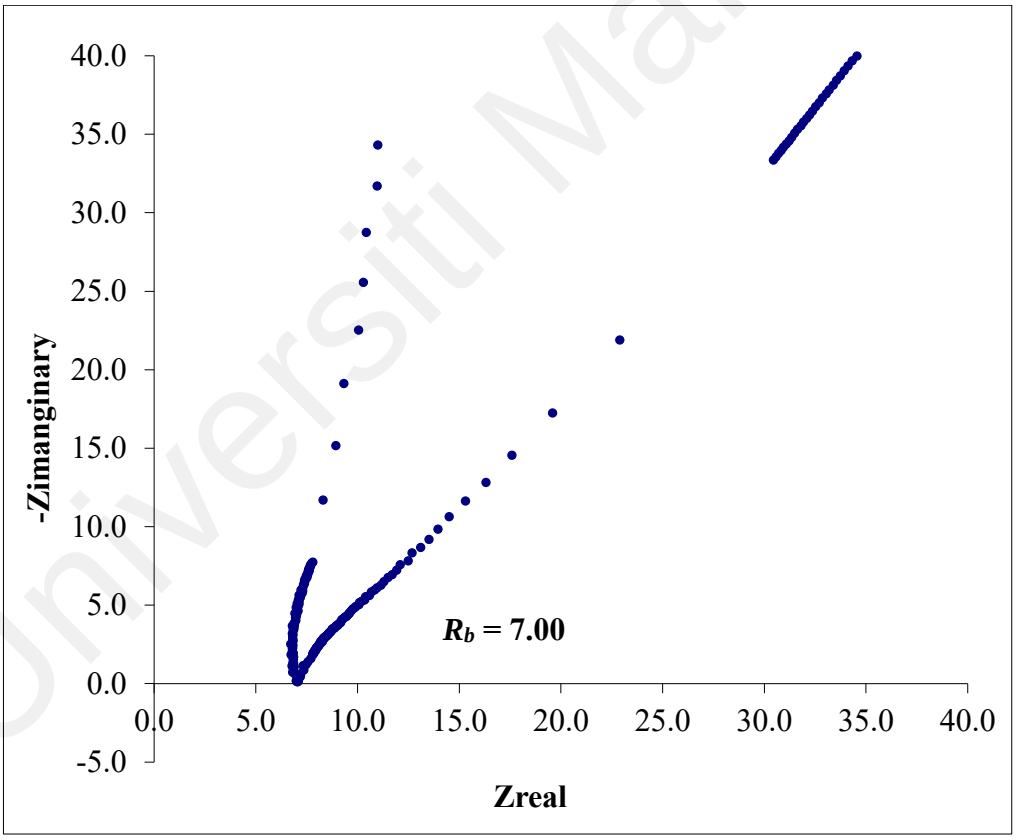

Figure 4.4: Impedance plot of PAA-$LiBF_4$-$BaTiO_3$ electrolyte film at ambient temperature.

In this work, the ionic conductivity dependence on the chemical composition of PAA-$LiBF_4$ reveals the effect of $BaTiO_3$ on ionic conduction after the PAA-$LiBF_4$ electrolyte

system incorporated with the dopant. Table 3.3 (Chapter 3) depicts the chemical composition of composite polymer matrix when different weight percent of $BaTiO_3$ are embedded into PAA-$LiBF_4$ complex. The logarithm of ionic conductivity of PAA-$LiBF_4$-$BaTiO_3$ electrolytes against different weight percent of $BaTiO_3$ is shown in Figure 4.5.

The ionic conductivity was expected to be enhanced with the inclusion of dopant like $BaTiO_3$. As can be seen in the Figure 4.5, the ionic conductivity increases with the $BaTiO_3$ loading. The ionic conductivity of CPE is at lowest when only 2 wt.% of $BaTiO_3$ was added to the system. The ionic conductivity of CPE increased when another 2 wt.% of $BaTiO_3$ was added to the system. The ionic conductivity continuous to increase with the further addition of $BaTiO_3$.

The highest ionic conductivity of 8.95×10^{-4} S cm^{-1} is obtained with the $BaTiO_3$ loadings up to a maximum level. At 2 wt.% of $BaTiO_3$, the low mass fraction of dopant cannot be distributed uniformly throughout the polymer matrix. Thus, the $BaTiO_3$ are far apart so couldn't play a significant role in generating a conducting path for ionic migration. When more $BaTiO_3$ are added to the PAA-$LiBF_4$ electrolyte matrix, the dopant starts to involve in the dissociation of lithium salts into lithium ions. When the weight percentage of the dopant increases further, the presence of excessive $BaTiO_3$ further disrupts the amorphous phase of the CPE. The changing of the morphology in polymer matrix increases the amorphous nature of the system, which have a significant effect on the ionic conduction in the electrolyte.

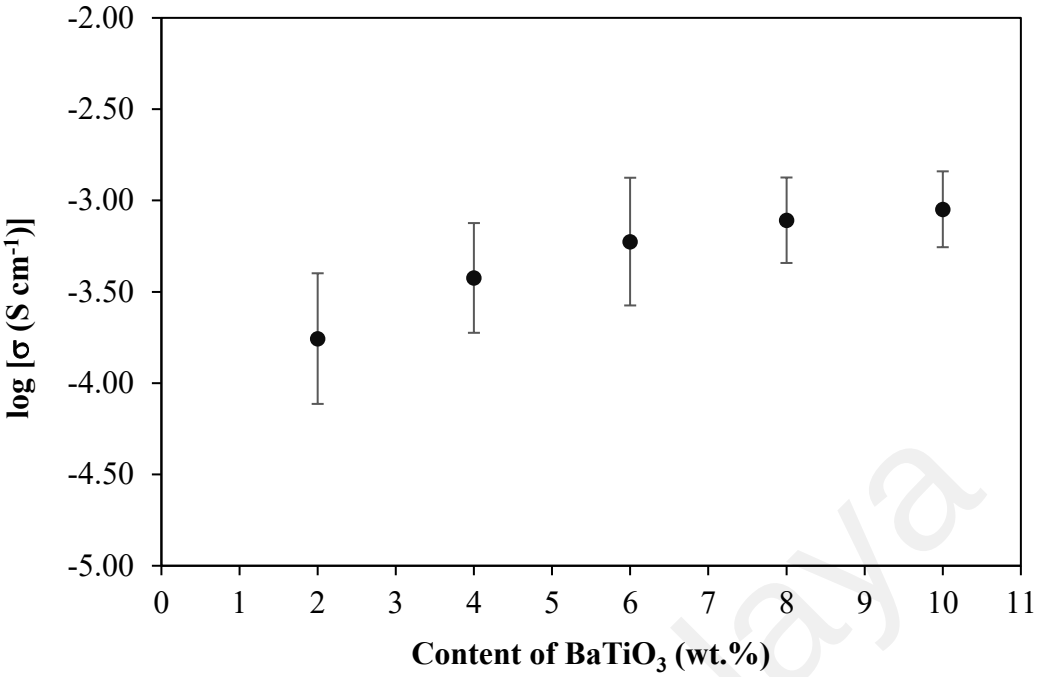

Figure 4.5: Effect of $BaTiO_3$ content on the ionic conductivity of PAA- $LiBF_4$ electrolytes at ambient temperature.

4.2.1.3 Temperature Dependent-Ionic Conductivity Studies of PAA-$LiBF_4$

Ionic conductivity is one of the major aspects in PE research for determining the ability of the electrolyte systems in generating current. The information of the charge carrier generation processes, carrier mobility, and mechanism of ionic conduction can be acquired through impedance analyses. Ionic conductivity is determined at different temperatures in order to evaluate the ionic conduction mechanism for the tested PEs. The activation energy borne by the tested PE films can be obtained using Arrhenius plot.

The temperature dependent ionic conductivities for PAA-$LiBF_4$ electrolytes were examined using impedance spectra. Ionic conductivity was measured at temperatures higher than ambient, from 30 °C to 120 °C. Figure 4.6 presents the logarithm of ionic conductivity against reciprocal of absolute temperature for PAA-$LiBF_4$ electrolytes. The

linearity of the plots which close to unity suggest that pattern follows Arrhenius relationship.

The impedance spectra confirmed the increase of ionic conductivity with the increase in temperature. When the temperature increases, both ion and segmental mobility increase. The faster movement of the ions is due to the increased of bond rotations which resulted from the absorption of heat energy from the elevated temperature. This weakens the interaction between lithium ion and the polar groups of the polymer chain; and induces the formation of vacant sites. When the neighbouring ions tend to occupy the vacant sites, the ionic hopping mechanism is generated. As can be seen from the figure, the ionic conductivity of the PE is directly proportional to the reciprocal of temperature. The highest ionic conductivity is achieved when PAA-$LiBF_4$ electrolyte system is subjected to the highest temperature of the range used in the experiment.

Table 4.1 presented the activation energy (E_a) of various PAA-$LiBF_4$ electrolyte systems. The activation energy (E_a) for the P70-LB30 electrolyte system is 3.4×10^{-4} eV. The decrease in activation energy is attributed to the increase of amorphous nature of the PAA-$LiBF_4$ electrolyte which increase the mobility of lithium ions inside the polymer matrix. The activation energy of P70-LB30 was lower than P80-LB20 which needed lesser energy for the mobility of charge carriers thus resulting a higher ionic conductivity. Different PE systems coupled with own characteristic E_a value as one of the intrinsic properties. When the heat applied to the electrolyte systems between the range 303 K to 393 K, the heat absorbed converted to kinetic energy and led to the increment of the charge carriers' mobility. When the heat absorbed exceed the E_a of the respective electrolyte system, the charge carriers migrate. Lower E_a implies an increase rate of ionic conductivity where higher charge carrier mobility at a characteristic time when an

absolute temperature is applied. The linear behaviour of the plot indicates there is only one ionic conduction mechanism. Both real and imagination axes of impedance plot are function of frequency. Since the frequency is inversely proportional to time, the impedance plot presents the impedance spectra and the dielectric relaxation of the PE at a graphical approach.

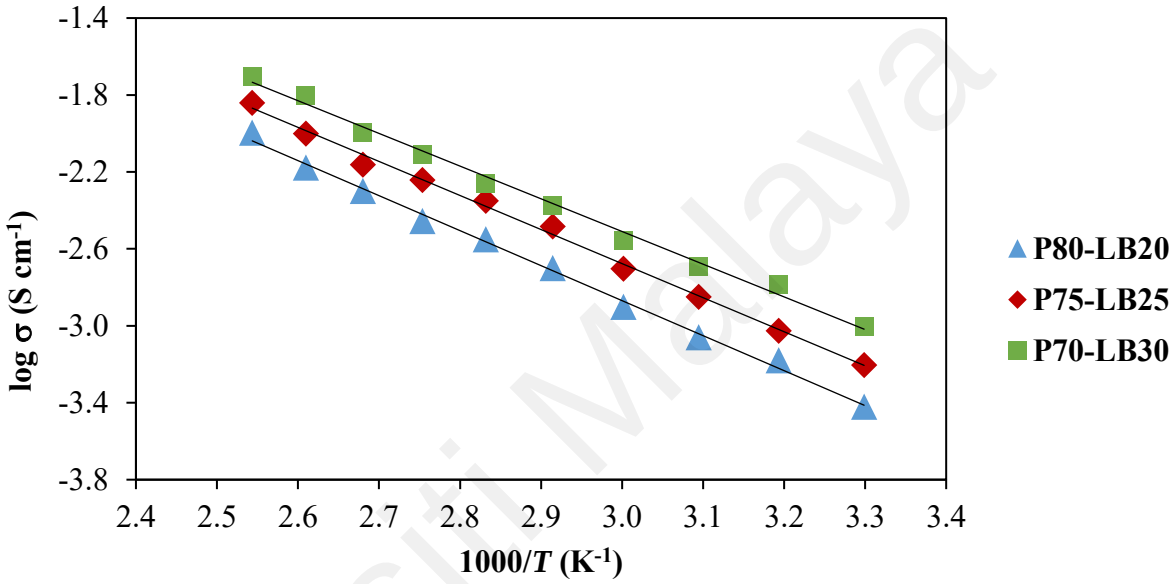

Figure 4.6: Arrhenius plot of ionic conductivity for P80-LB20, P75-LB25, and P70-LB30 with frequency ranging from 50 Hz to 5 MHz at temperatures from 303 K to 393 K.

Table 4.1: The activation energy of the PAA-$LiBF_4$ electrolyte systems.

Polymer Electrolyte Systems	Activation Energy (eV)
P80-LB20	3.61×10^{-4}
P75-LB25	3.51×10^{-4}
P70-LB30	3.37×10^{-4}

4.2.1.4 Temperature Dependent-Ionic Conductivity Studies of PAA-$LiBF_4$-$BaTiO_3$

The activation energy (E_a) and the effect of temperature on the PAA-$LiBF_4$-$BaTiO_4$ electrolytes' ionic conductivity can be validated by the Arrhenius plot. In this study, different wt.% of $BaTiO_3$ with fixed ratio of PAA-$LiBF_4$ electrolyte system were chosen for investigation. Figure 4.7 depicts the log σ versus reciprocal of absolute temperature for various $BaTiO_3$ wt.% in PAA-$LiBF_4$ at temperature ranging from 303 K to 393 K. According to the Arrhenius relationship, ionic conductivity varies with temperature. Based on Figure 4.7, the ionic conductivities of the PAA-$LiBF_4$-$BaTiO_4$ electrolyte systems increase steadily with increasing temperature without any break. The ionic conductivity of CPE10B reaches up to 8×10^{-3} S cm^{-1} when temperature exceeded 60 °C. Incorporation of dopant creates more sites for ionic transport. Thus, the number of mobile ions increased. When the neighbouring lithium ions occupy the vacant sites, hopping mechanism is created.

From Figure 4.7, the Arrhenius plot shows a straight line confirmed the increase of temperature leads to the increase in ionic conductivity. The ionic conductivities of the PAA-$LiBF_4$-$BaTiO_3$ electrolytes increase gradually with the elevation of temperature, from 30 °C to 120 °C. As the temperature increases, the heat energy was absorbed and lead to the faster mobility of ions. The CPE matrices expand which created more volume and spaces for the ions' migration. The movement of the polymer segments also increases with the increases of temperature. This enable the polymer segments to overcome the hydrostatic pressure which is imposed by the neighbouring atoms. Eventually the ionic conductivity increases due to the formation of voids which facilitates the transportation of charge carriers (Rajendran et al., 2004). Table 4.2 presented the activation energy (E_a) of various PAA-$LiBF_4$-$BaTiO_3$ electrolyte systems. The activation energy of CPE10B electrolyte system was less than that of CPE6B. It can be confirmed that the ion

movement in the former was faster than in the latter. A lower E_a value suggests that ionic conduction is facile in the optimum composition of CPE.

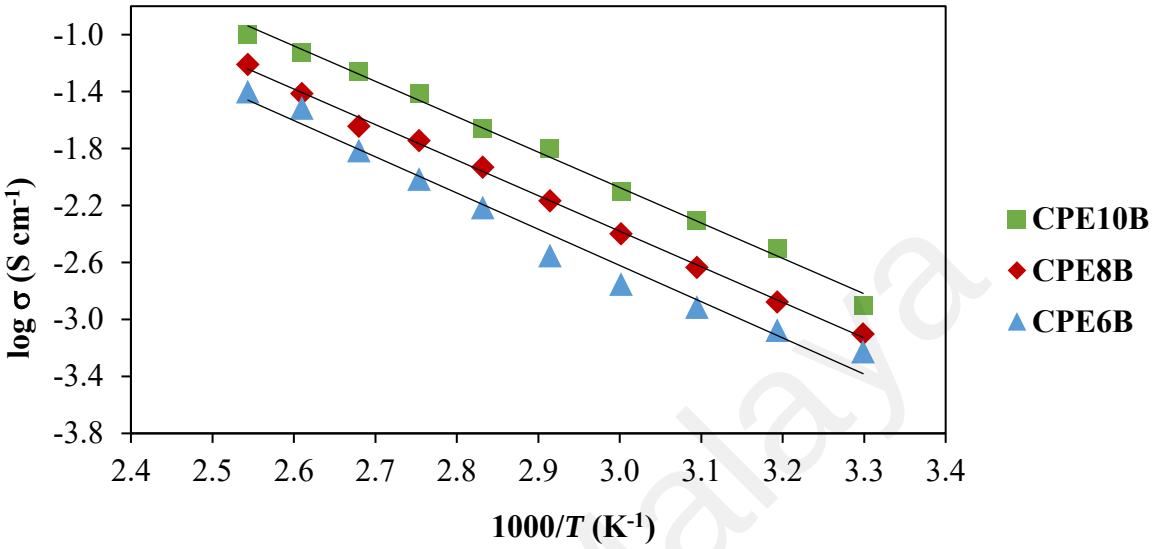

Figure 4.7: Arrhenius plot of ionic conductivity for PAA-LiBF$_4$-BaTiO$_3$ CPE6B, CPE8B, and CPE10B with frequency ranging from 50 Hz to 5 MHz at temperatures from 303 K to 393 K.

Table 4.2: The activation energy of the PAA-LiBF$_4$-BaTiO$_3$ electrolyte systems.

PAA-LiBF$_4$-BaTiO$_3$ Electrolyte Systems	Activation Energy (eV)
CPE6B	5.05×10^{-4}
CPE8B	4.95×10^{-4}
CPE10B	4.94×10^{-4}

4.2.1.5 Dielectric Permittivity Studies of PAA-LiBF$_4$

Dielectric material is an insulator which can be polarized under an electric filed. The dielectric properties of a dielectric material can be characterized through dielectric study. The important measurement parameter in dielectric study including dielectric

permittivity, dielectric loss, loss tangent, dielectric constant, relaxation time and dielectric modulus. Dielectric study can be performed using AC-impedance spectroscopy.

Figures 4.8(a) and 4.8(b) illustrate the variation of dielectric permittivity and dielectric loss for sample (a) P90-LB10, (b) P80-LB20, and (c) P70-LB30 as a function of frequency. P70-LB30 indicated the highest dielectric permittivity and P90-LB10 indicated the lowest dielectric permittivity at a selected frequency. As what displayed in figures, all three PEs exhibit similar patterns. There is a rapid fall in the lower frequency range which is due to the electrode polarization and space charge effect at the electrode-electrolyte interface which resulting the fall of dielectric permittivity. It affirms the non-Debye response in which the direction is affected by electrical fields. When the electrical field is applied across the PE, the polarization of electrode causing the free charge carriers accumulate at the electrode-electrolyte interface (Liew et al., 2012a). The readings decreased at higher frequency region and then saturated. This feature is commonly observed in the dielectric permittivity plots for PE systems. Figures 4.8(a) and 4.8(b) portray that dielectric permittivity increases when the content of inorganic salts in the PE matrices is increased. High inorganic salt content is associated to the number of charge carriers. When the inorganic salt content increases, the charge carrier density is also increased which resulting to the increase in charges storage in the PE sample (Buraidah et al., 2009).

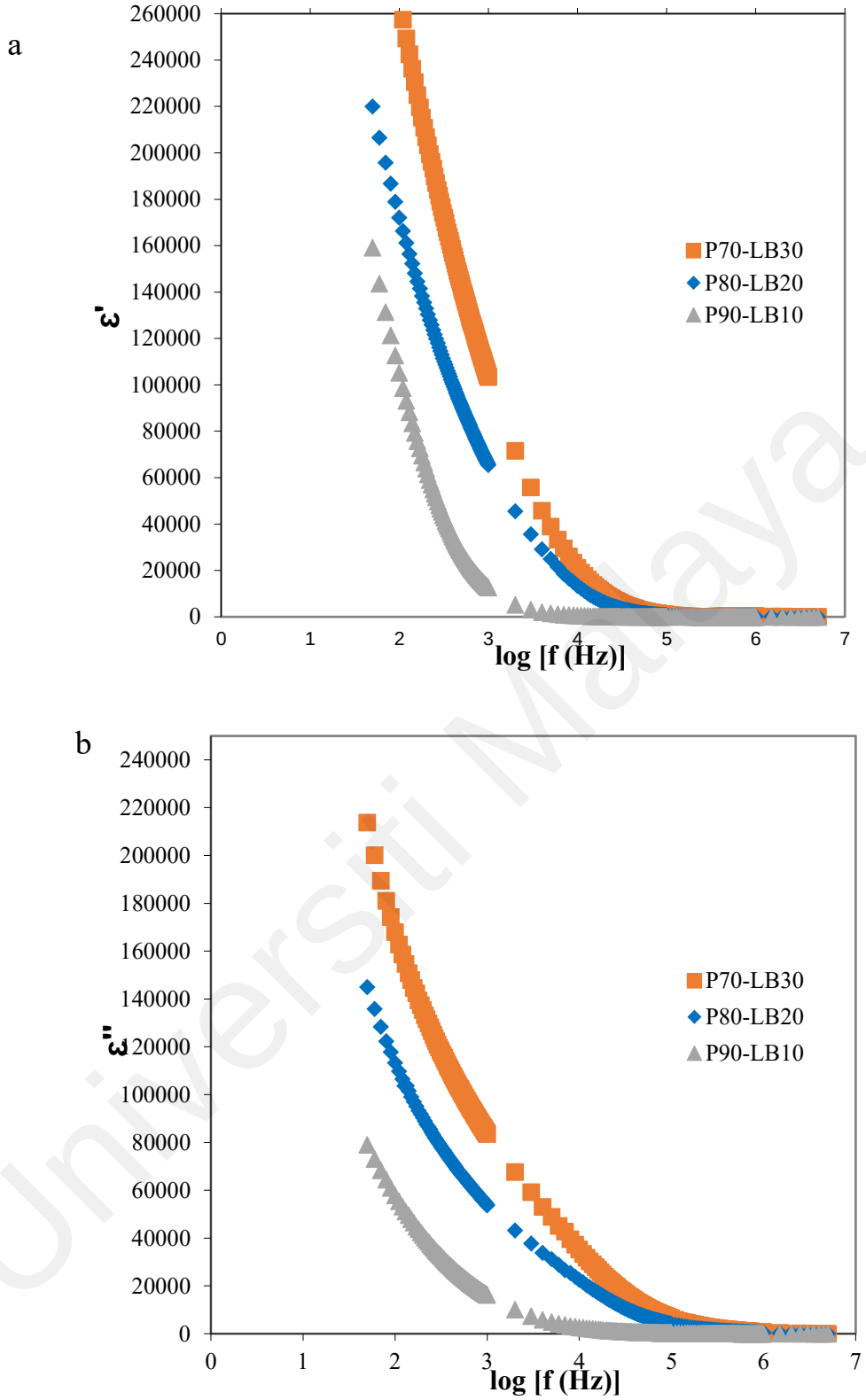

Figure 4.8: Variation of (a) dielectric permittivity and (b) dielectric loss for P90-LB10, P80-LB20, and P70-LB30 as a function of frequency at ambient temperature.

4.2.1.6 Dielectric Permittivity Studies of PAA-$LiBF_4$-$BaTiO_3$

Figures 4.9(a) and 4.9(b) display the frequency dependence variation of (a) real and (b) imaginary parts of the dielectric constant for PAA-$LiBF_4$-$BaTiO_3$. CPE2B, CPE6B and CPE10B which represent the CPE with $BaTiO_3$ content in low, medium and high level, respectively. The plots illustrate a typical pattern observed in CPE matrices. The pattern shown a rapid fall of the permittivity curve at lower frequency region. The plots decreased slowly and getting saturated at the higher frequency region. At lower frequency, a sharp decrease in both real and imaginary parts of dielectric constant and dielectric loss is due to both electrode polarization and space charge effect which led to charge carrier localization. This confirms the non-Debye behaviour in the PAA-$LiBF_4$-$BaTiO_3$ matrix. By this behaviour, the charge region with frequency dependence is explained by ion diffusion. Free mobile ions initiate the polarization after built up at the electrode-electrolyte interface, form the space charge region and follow by the shift of direction in applied electric field (Li et al., 2006; Wen et al., 2003; Khiar et al., 2006). At a higher frequency range, both dielectric permittivity and dielectric loss shown a much lower value. It is mainly due to the fast periodic reversal of electric field which results the absence of ion diffusion in the direction of electric field. Consequently, the ionic polarization decreases and thus causing the reduction of dielectric constant at a higher frequency (Venkateswarlu et al., 2000; Li et al., 2006).

The difference between PAA-$LiBF_4$-$BaTiO_3$ samples with higher conductivity and other features can be observed clearly at high frequency region. As shown from the Y-axis with logarithm scale, CPE10B indicates a subtle fall at both ε' and ε'' at a high frequency range. ε' appears as a sharp fall but ε'' demonstrates a delayed effect. This could be attributed to the existence of excessive charge carriers which carrying a lower polarization tolerance and resulting a lower storage and a higher energy loss.

As demonstrated in Figure 4.9, a higher dielectric constant was found for CPE10B. $BaTiO_3$ is a tiny and fine particle that possess high ratio of surface area over the volume. Doping of $BaTiO_3$ not only dissociate the lithium salt, but also reduce the crystallinity of PAA-$LiBF_4$-$BaTiO_3$ and increase the degree of amorphous nature. $BaTiO_3$ deform the lattice structure of PAA-$LiBF_4$-$BaTiO_3$ matrices and promote polarization. The amorphous nature hinder the PAA-$LiBF_4$-$BaTiO_3$ from recrystallization and led to a higher ionic conductivity.

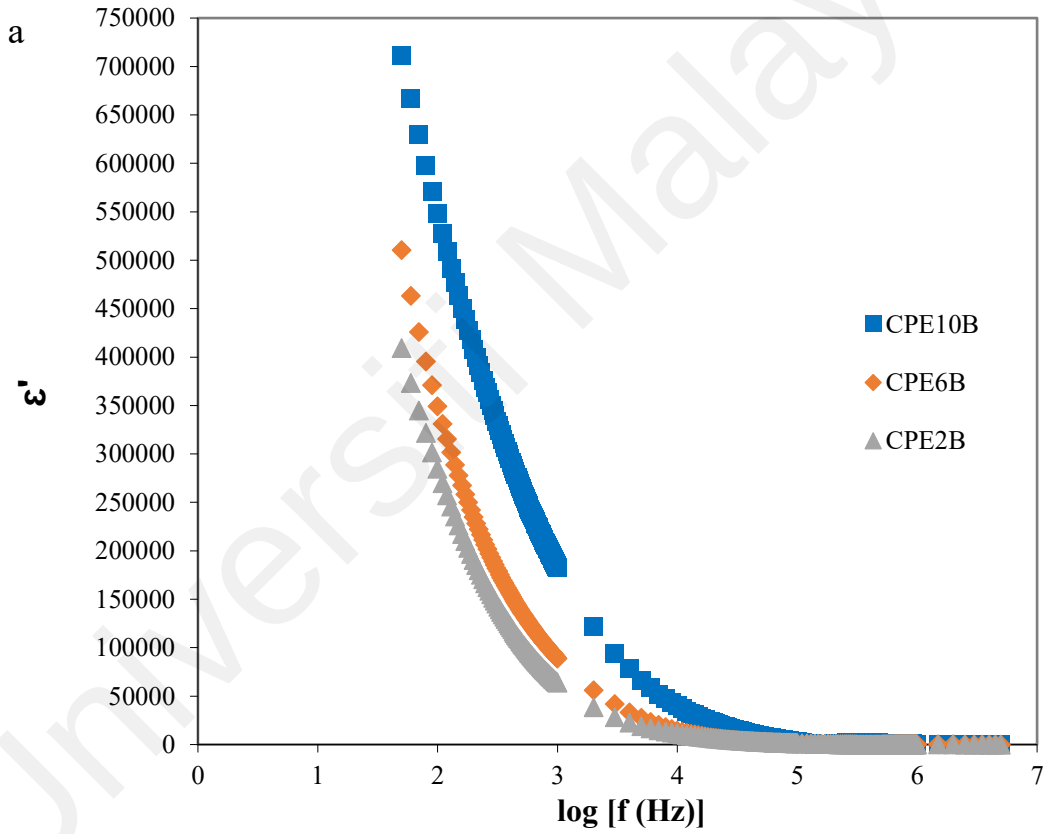

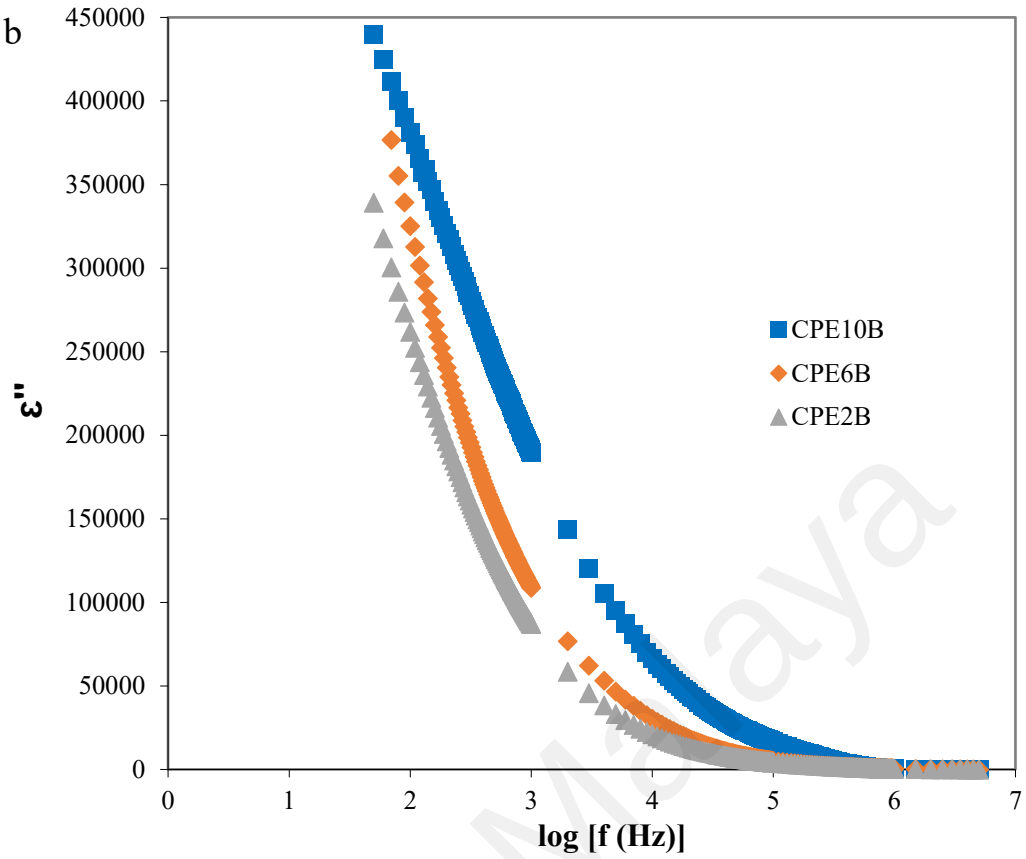

Figure 4.9: Variation of (a) dielectric permittivity and (b) dielectric loss for PAA-$LiBF_4$-$BaTiO_3$ CPE2B (low), CPE6B (medium), and CPE10B (high) as a function of frequency at ambient temperature.

4.2.1.7 Modulus Studies of PAA-$LiBF_4$

Dielectric modulus is an analysis to investigate the dielectric relaxation behaviour of dielectric materials (Dionisio et al., 2000). The dielectric modulus study is conducted by suppressing the polarization effect of the electrodes (Almond and West, 1983). Figures 4.10(a) and 4.10(b) depict the real part and imaginary part of dielectric moduli as a function of frequency for different PEs. As can be seen from the figures that the relaxation peaks are absent in the plots. Another observation from the plots is the abrupt increments are found in the higher frequency end. Both P80-LB20 and P70-LB30 plots shown a long tail prior leading to the zero end at a lower frequency regime. The long tail correlates to the suppression of the electrical double layer effect at the contact of electrode-electrolyte

area (Shastry & Rao, 1991). This implies that the contribution of electrode polarization is insignificant and the suppression of electrical double layer is associated with a large capacitance value associated with the electrodes in the polymer electrolyte systems (Gogulamurali et al., 1992; Suthanthiraraj, et al., 2009).

a

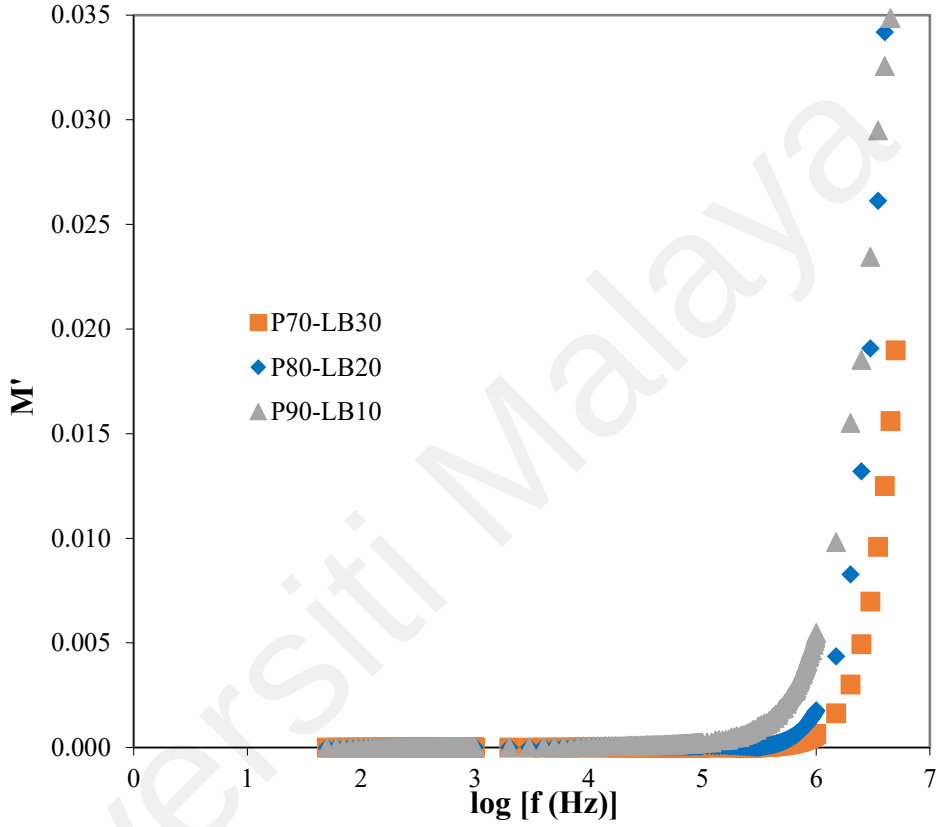

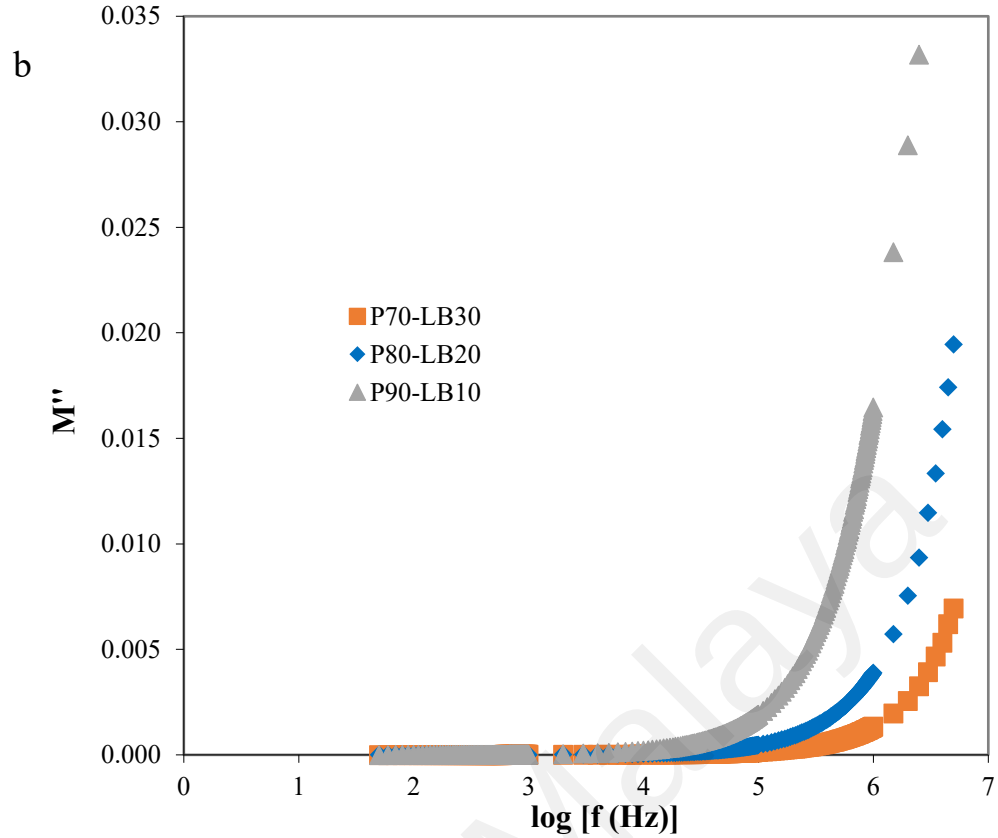

Figure 4.10: The (a) real part and (b) imaginary part of dielectric moduli as a function of logarithmic frequency for P90-LB10, P80-LB20, and P70-LB30 in the frequency range of 50 Hz – 5 MHz at ambient temperature.

4.2.1.8 Modulus Studies of PAA-$LiBF_4$-$BaTiO_3$

The variation of real part and imaginary part of dielectric moduli as a function of frequency for CPE2B, CPE6B and CPE10B are exemplified in Figures 4.11(a) and 4.11(b). The figures illustrate an abrupt increase is observed at a higher frequency end and the relaxation peaks are unseen. However, all CPE plots demonstrate long tail which tends to move towards zero at a lower frequency regime. The long tail indicates the suppression of electrical double layer effect at the interface of electrode-electrolyte (Shastry & Rao, 1991) which attributed to the high capacitance value in the electrode (Suthanthiraraj, et al., 2009). This ascribes that the doping of $BaTiO_3$ could assist in the dissociation of $LiBF_4$ salt into ions which accumulate at the electrode-electrolyte interface in lower frequency range (Osman et al., 2001).

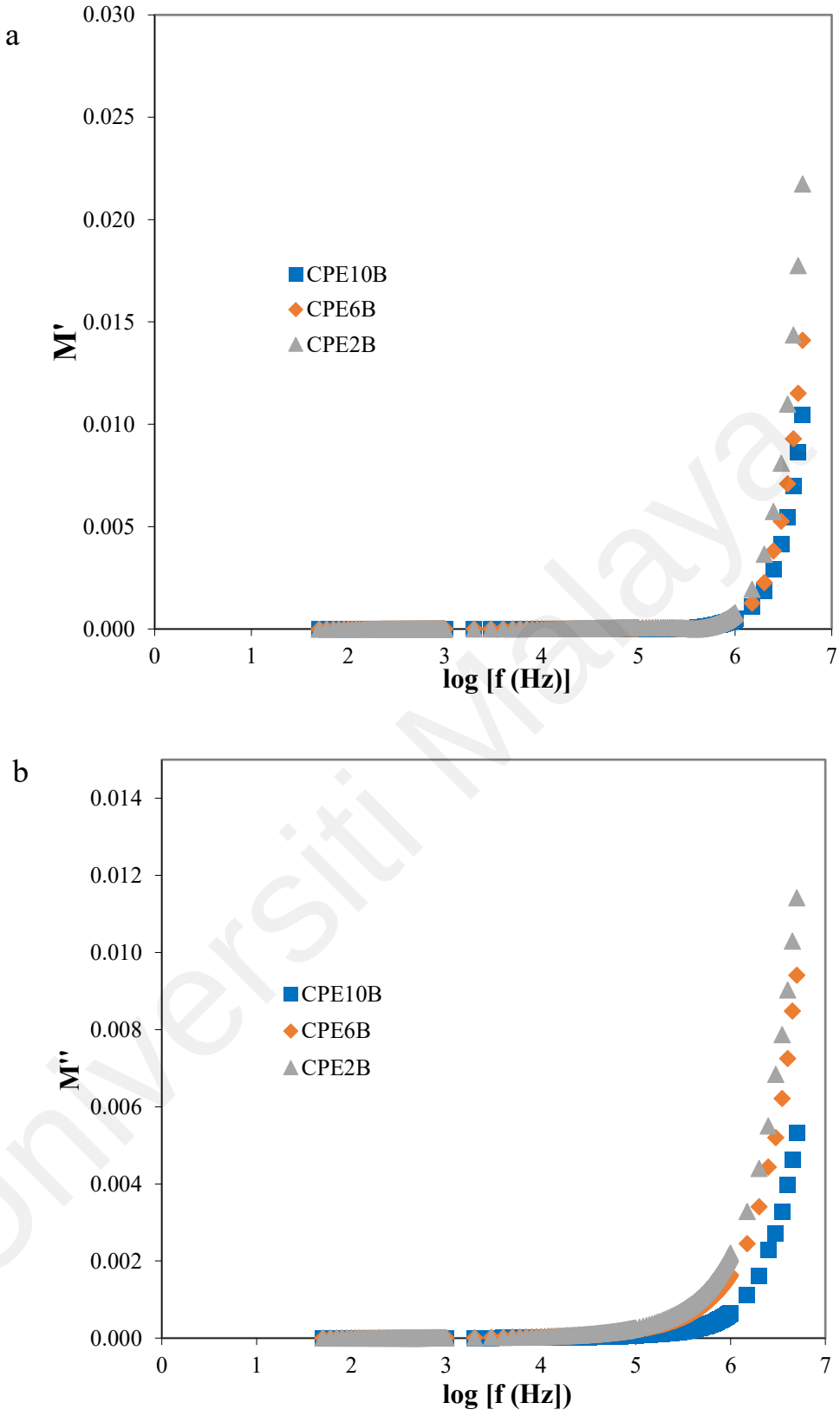

Figure 4.11: The (a) real part and (b) imaginary part of dielectric moduli as a function of logarithmic frequency for PAA-$LiBF_4$-$BaTiO_3$: CPE2B, CPE6B and CPE10B in the frequency range of 50 Hz – 5 MHz at ambient temperature.

4.2.2 Electrochemical Properties

4.2.2.1 Electrochemical Stability Window of PAA-$LiBF_4$

The electrochemical property of the PAA-$LiBF_4$ electrolyte matrix was evaluated by linear sweep voltammetry (LSV) measurements at ambient temperature. The measurement was performed at a potential range between -2.5 to +2.5 V with a scan rate of 5 mV s^{-1}. LSV response of PAA-$LiBF_4$ is illustrated in Figure 4.12. It was found that PAA-$LiBF_4$ demonstrated a wide electrochemical stability window at about 3.2 V within the selected potential range from -1.5 to +1.7 V.

Optimized electrode and electrolyte materials should allow at least 3 V in electrochemical potential window (Kot and Carlen, 2000). These demonstrated that PAA-$LiBF_4$ possesses better electrochemical stability than that of conventional electrolyte materials which expected to be stable within the operating voltage of electrochemical devices. The suitability of PAA-$LiBF_4$ in electrochemical devices application is supported since the oxidation occurring at potentials higher than 3.2 V. A wider electrochemical stability window indicated by PAA-$LiBF_4$ could be due to the electron delocalization of tetrafluoroborate anions. The tetrafluoroborate anions undergo electron delocalization process is induced by the strong electron withdrawing group to form resonance structures (Liew & Ramesh, 2014). When the tetrafluoroborate anions reach a stable state, the electrochemical stability is improved.

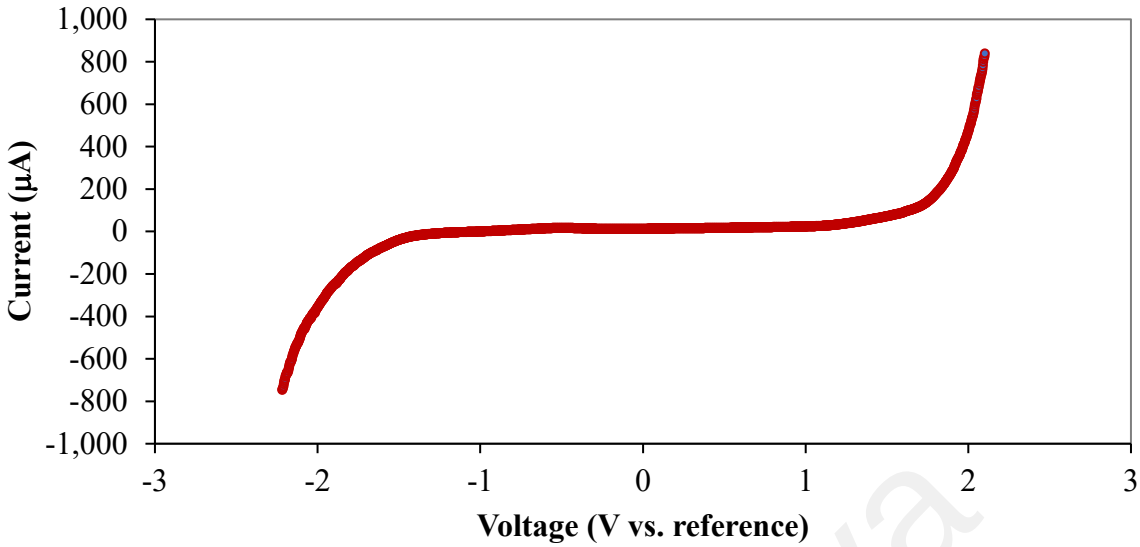

Figure 4.12: Linear Sweep voltammogram of PAA-$LiBF_4$ (30 wt.% $LiBF_4$) electrolyte system at ambient temperature. Scan rate: 5 mV s^{-1}.

4.2.2.2 Electrochemical Stability Window of PAA-$LiBF_4$-$BaTiO_3$

The electrochemical stability range of the PAA-$LiBF_4$-$BaTiO_3$ electrolyte with 10 wt.% $BaTiO_3$ was determined using linear sweep voltammetry (LSV) at ambient temperature and at a scan rate of 5 mV s^{-1} in the potential range from -3 to +3 V. The CPE film was tested with LSV and the electrochemical stability window is demonstrated in Figure 4.13. PAA-$LiBF_4$-$BaTiO_3$ electrolyte portrays a wide electrochemical stability of 4.0 V, in the potential range from -2.5 to +1.5 V. Beyond this potential range, the composite polymer electrolyte starts to degrade. The wider in electrochemical stability for CPE may be due to the combined presence of $LiBF_4$ and $BaTiO_3$ in the composite matrix. Figure 4.13 shown the absence of additional peaks at lower voltage and low residual current. This infers that PAA-$LiBF_4$-$BaTiO_3$ electrolytes are highly pure. The wider electrochemical stability range infers that PAA-$LiBF_4$-$BaTiO_3$ suitable for lithium-ion battery application.

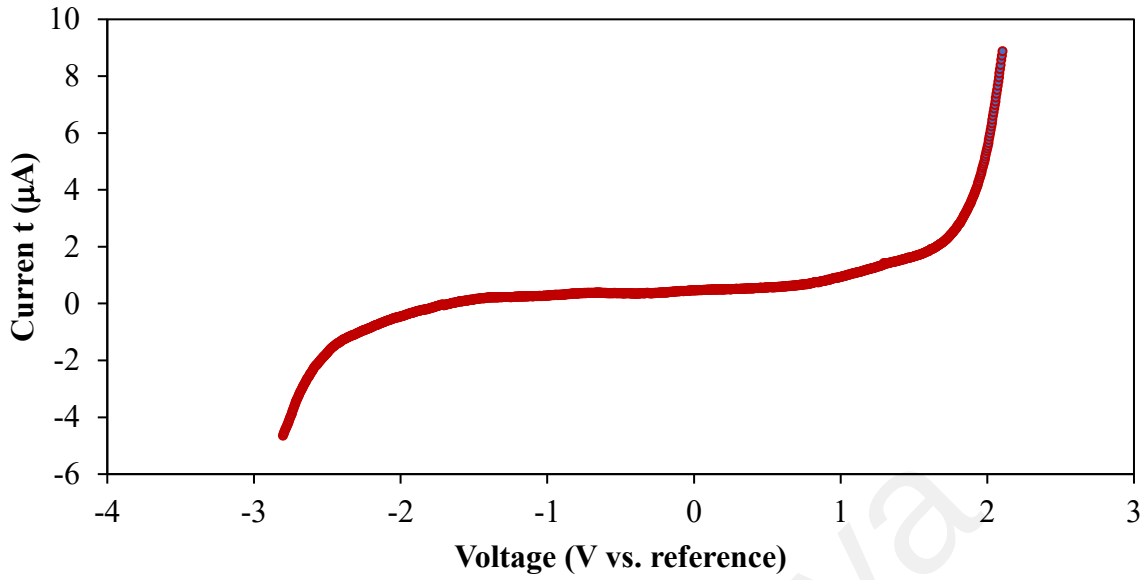

Figure 4.13: Linear Sweep voltammogram of PAA-$LiBF_4$-$BaTiO_3$ electrolyte (with 10 wt.% $BaTiO_3$) at ambient temperature. Scan rate: 5 mV s^{-1}.

4.2.3 Thermal Properties

4.2.3.1 Thermal Studies of PAA-$LiBF_4$

Thermogravimetric analysis (TGA) is thermal technique to study the thermal stability of a material under inert condition. Thermal stability can be determined by monitoring the weight loss of the sample in an inert condition over a temperature range at a controlled and uniform heating rate. Figure 4.14 describes the TGA curves of pure PAA, P80-LB20, P75-LB25, and P70-LB30 in the temperature range of 30–600 °C. For the TGA curves of PEs, the initial weight loss of 5% in the region of 30-144 °C is observed which is due to the dehydration of PEs. Water is the solvent used in the preparation of PEs. The initial heating causing the evaporation of water molecules which trapped within PE film or small cavities formed in the polymer matrices upon solidification. It is hard to diffuse the water molecules out of the polymer matrices under room temperature. As can be seen from the figure, P70-LB30 subjected to an initial weight loss of 5% up to 110 °C. The prolonger heating between 110-200 °C resulting the gradual removal of water molecules from the

PEs. Besides, the decarboxylation that occurs in PAA after prolonged heating also contributed to the initial weight loss (Kam et al., 2014).

PAA as a standard was prepared and examined by TGA. From the Figure 4.14, it was observed that there are four distinct degradation processes occurred at different temperature regions: 20 – 150 °C, 150 – 270 °C, 270 – 320 °C, and above 320 °C (Kam et al., 2014). In the first region (20–150 °C) both dehydration and formation of anhydride group occur. The major reaction which takes place below 150 ºC is the formation of intramolecular anhydride. In the second region (150–270 °C), an overall reduction of acrylic acid content was found as 11.4% while the concentration of anhydride is reduced (McGaugh & Kottle, 1967). In this region, the anhydride concentration decreased due to the overall reduction in acrylic acid content (McGaugh & Kottle, 1967). In the third region (270–320 °C), a significant reduction in weight is observed which could attributed to the formation of cyclic ketone in the decarboxylated PAA chain at higher temperatures (Gurkaynak et al., 1996). Above 320 °C, the polymer chain is breakdown completely due to the excessive heat. It is evidently shown from Figure 4.14, the pure PAA decomposes at a temperature of 270 °C until a residual mass of 15.5% was achieved.

Moisture absorption is increased upon the addition of hydrophilic $LiBF_4$ into the polymer electrolyte systems. As can be seen in Figure 4.14, P70–LB30 has the highest initial weight loss and P80–LB20 shown the relatively lower initial weight loss among the three tested PEs. The TGA curve of P70–LB30 indicated 13% weight loss at 200 ºC could be attributed to the hydrophilicity of $LiBF_4$. TGA curve of P80–LB20 shown a weight loss of 8% at 200 ºC evidently proven that P80–LB20 has a better thermal stability compared to P70–LB30. The second weight loss between 100–150 ºC implies the occurrence of decarboxylation process. In this region, P70–LB30, P75–LB25 and P80–LB20 shown a

small weight loss between 2–5%. The PE samples continue to encounter some weight lost when subjected to prolong heating between 150–300 °C. A maximum weight loss was observed as the third weight loss with a sharp reduction in weight percentage at 244 °C. This could be attributed to the elimination of ketone compound (Kam et al., 2014). Above 300 °C, $LiBF_4$ degraded to form boron trifluoride. In the last stage of weight loss, the decomposition of main polymer chain taken place at temperature range of 300–450 °C. Incorporation of $LiBF_4$ improved the weight loss of polymer electrolytes where the total weight loss of pure PAA is 84.5% but reduced to 73.7% upon addition of 30 wt.% of $LiBF_4$. The higher residual mass of polymer electrolytes at 600 °C is ascribed to the improvement of thermal stability of PAA-$LiBF_4$.

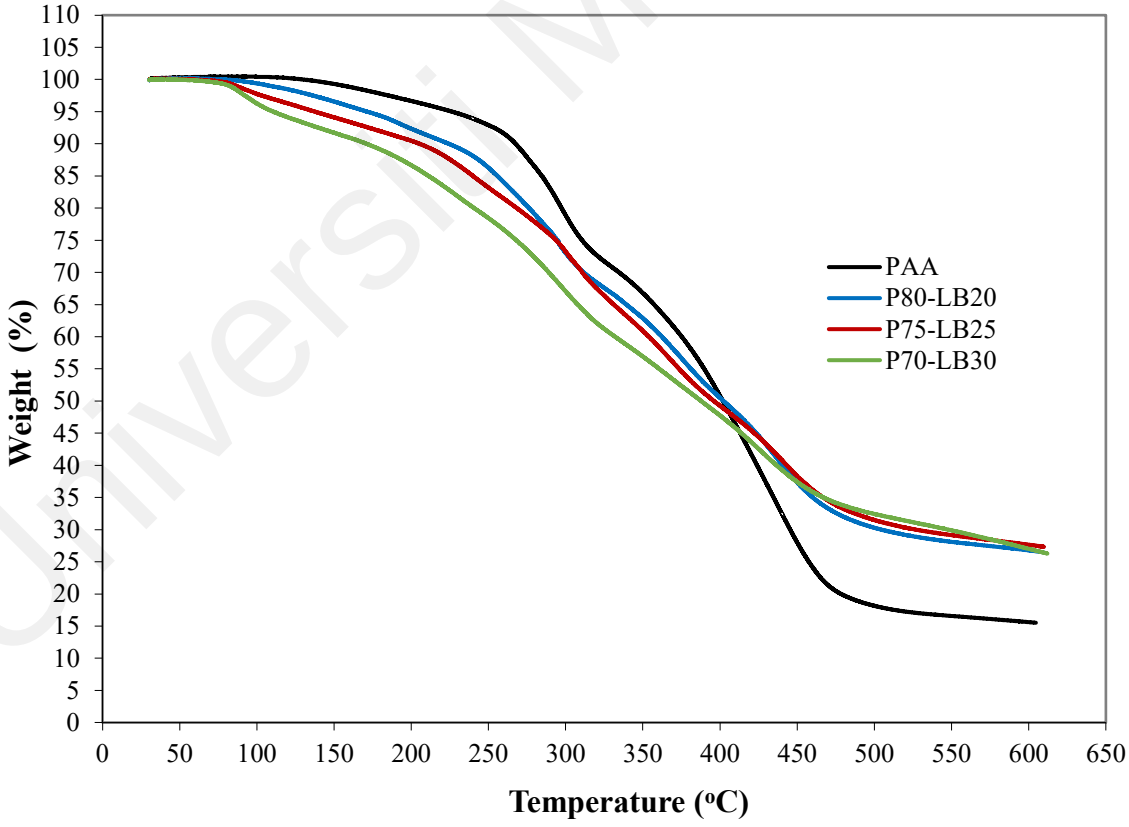

Figure 4.14: TGA thermograms of pure PAA, P70-LB30, P75-LB25, and P80-LB20 in the temperature range of 30–600 °C under inert condition.

4.2.3.2 Thermal Studies of PAA-$LiBF_4$-$BaTiO_3$

Figure 4.15 depicts the TGA curves of pure PAA, CPE6B, CPE8B and CPE10B of PAA-$LiBF_4$-$BaTiO_3$. From the TGA curves of CPE samples, the removal of water molecules led to the initial weight loss about 13-15% from 30-240 °C. With the doping of $BaTiO_3$ in PAA-$LiBF_4$ system, the PAA-$LiBF_4$ with 10 wt.% $BaTiO_3$ shown a relatively smaller initial weight loss compared to PAA-$LiBF_4$ doped with 8 wt.% and 6 wt.% of $BaTiO_3$. The presence of $BaTiO_3$ in the polymer matrices could reduce the absorption of moisture. The prolonged of this process could be attributed to the evaporation of the entrapped of water molecules in PAA matrix since the polymer is water soluble. Therefore, it is hard for the water to diffuse out from the polymer matrix. The decomposition of polymer chain contributed to the second stage of weight loss which starts at 240 °C. However, no significant difference in the decomposition temperature is observed for PAA-$LiBF_4$ doped with 6 wt.%, 8 wt.% and 10 wt.% $BaTiO_3$ within the temperature range of 250-520 °C. The residual weight of CPE10B, CPE8B and CPE6B are 20%, 25%, and 37%, respectively at 600 °C which is definitely higher than PAA (16%). The high residue weight of the CPEs could be due to the thermal stability of the composite matrices after the incorporation of $BaTiO_3$ as dopant.

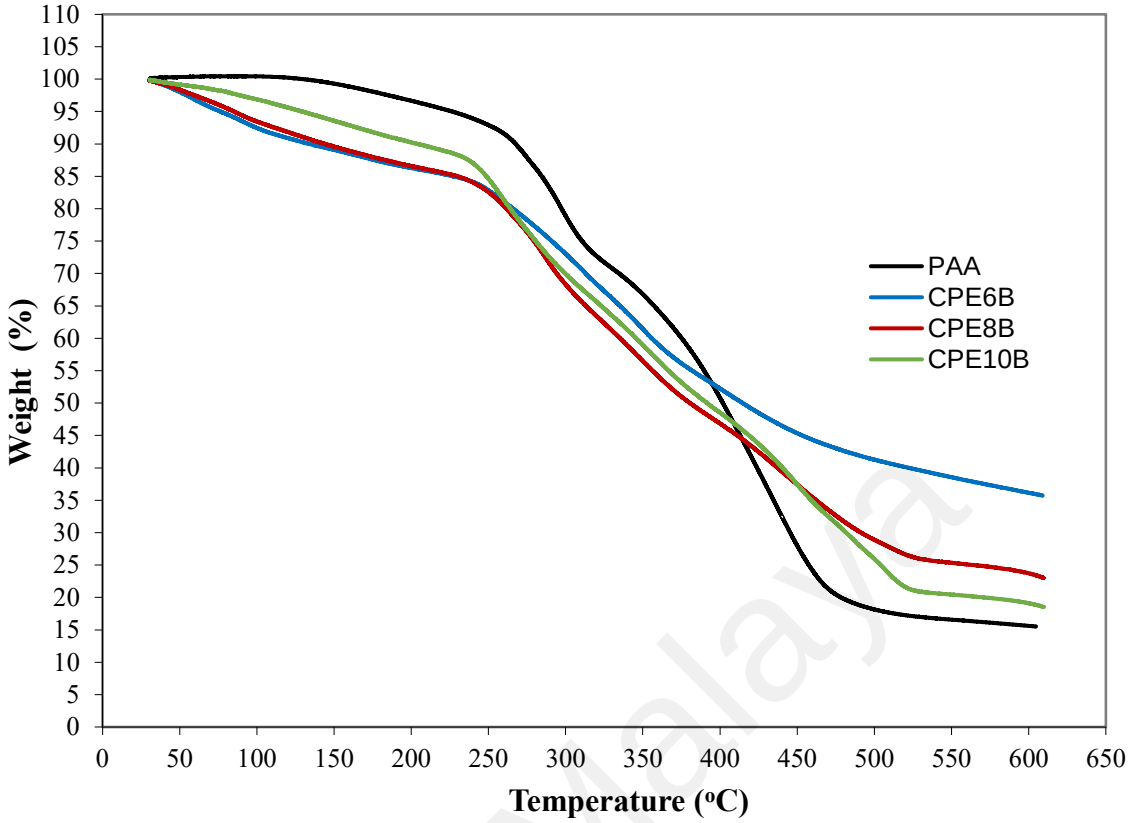

Figure 4.15: TGA thermograms of pure PAA, PAA-$LiBF_4$-$BaTiO_3$ in 6 wt.% (CPE6B), 8 wt% (CPE8B) and 10 wt.% (CPE10B) in the temperature range of 20–600 °C under inert condition.

4.2.4 Structural Properties

4.2.4.1 X-ray Diffraction Studies of PAA-$LiBF_4$

X-ray diffraction (XRD) is a physical analysis which employed to examine crystallinity of the PEs and also to provide the crystallographic data. The complexation of PEs can also be verified by XRD. Figure 4.16 illustrated the diffraction patterns of PEs and its constituents of pure PAA and pure $LiBF_4$. As can be seen in Figure 4.16, XRD pattern (a) showing nine sharp intense peaks are detected at $2\theta = 21.2^o$, 23.6^o, 26.7^o, 28.2^o 31.9^o, 32.7^o, 36.3^o, 40.1^o, and 53.7^o for pure $LiBF_4$. XRD pattern (b) indicated four sharp peaks at $2\theta = 13.5^o$, 17.0^o, 18.6^o, and 30.2^o for pure PAA. The results demonstrated the crystallinity of pure PAA and pure $LiBF_4$. The PAA crystalline peaks at $2\theta = 13.5^o$, 17.0^o, 18.6^o, and 30.2^o were absent in PAA-$LiBF_4$ electrolytes. The disappearance of the peaks

shown that $LiBF_4$ complexed with PAA while PAA has effectively solvated the lithium cations to reach complete dissolution. Additional two peaks at $2\theta = 22.0^o$ and 23.0^o of P80-LB20, L75-LB25 and L70-LB30 indicated the $LiBF_4$ crystalline peaks were absent in pure PAA. As can be seen in XRD patterns (c)-(e), the diffraction peaks corresponding to $LiBF_4$ decreases. The occurrence of complexation is confirmed by the reduction in peak intensity upon inclusion of $LiBF_4$. Addition of $LiBF_4$ resulting in the shift of the peaks which further confirms the complexation between PAA and $LiBF_4$.

Among the three polymer electrolyte samples, the peaks of P80-LB20 are slightly sharper than P70-LB30. This suggests that P70-LB30 exhibits higher degree of amorphous nature. P70-LB30 also indicates a broader peak between $2\theta = 21.5 – 22.0^o$ which reveals the increases in amorphous nature and thus resulting the higher ionic conductivity. The increase in amorphous nature in polymer electrolytes triggers the ionic hopping mechanism which resulting in the elevation of the ionic conductivity (Ramesh & Liew, 2013).

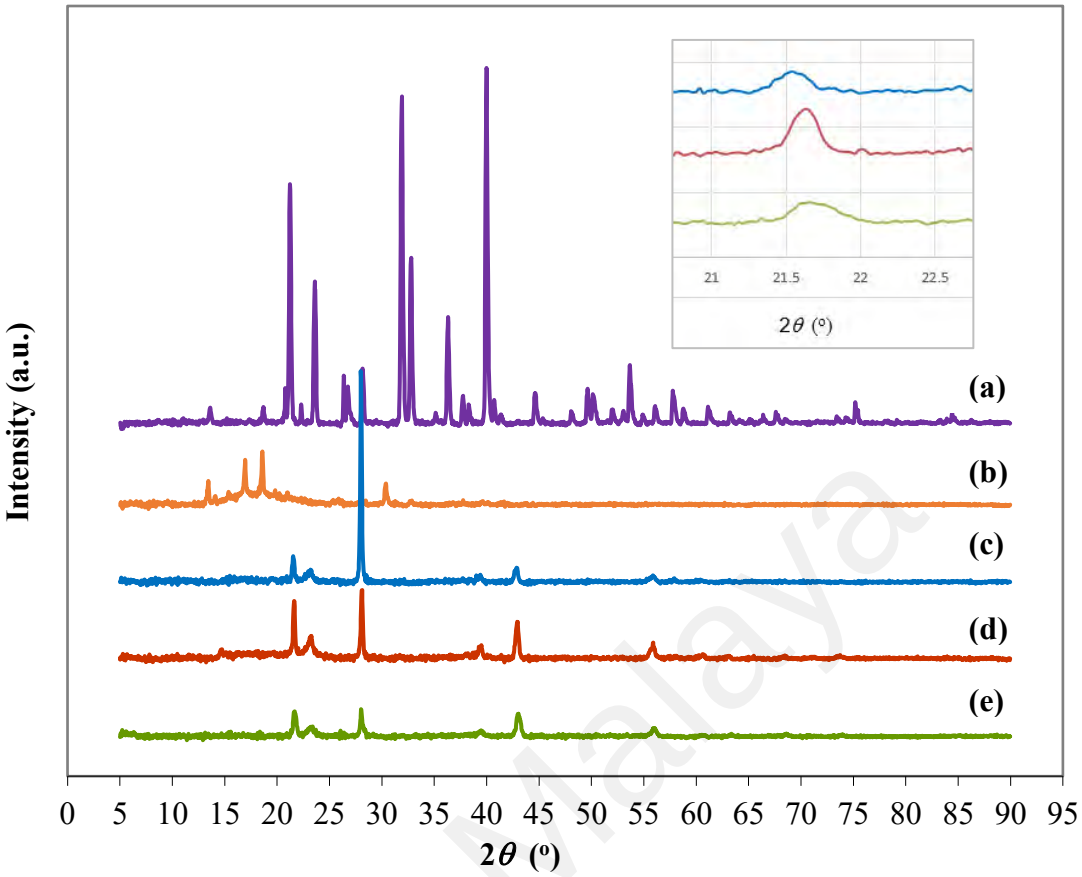

Figure 4.16: XRD pattern of (a) pure $LiBF_4$, (b) pure PAA, (c) P80-LB20, (d) P75-LB25, and (e) P70-LB30. The inset: Magnified axis between 2θ = 21.0– 22.5 °

4.2.4.2 X-ray Diffraction Studies of PAA-$LiBF_4$-$BaTiO_3$

Figure 4.17 exemplifies the X-ray diffractograms of pure PAA, $LiBF_4$, $BaTiO_3$, CPE6B, CPE8B, and CPE10B. The occurrence of interaction or complexation between the CPE's constituents can be detected via the shifting of the peaks or broadening of peaks (Ramesh & Lu, 2012). As can be seen from the XRD patterns, sharp and intense crystalline peaks at 2θ = 22.3°, 31.6°, 39.1°, 45.4°, 56.4° indicate a highly crystalline character of $BaTiO_3$. As shown in Fig 4.17, the sharp intense peaks are found at 2θ = 21.2°, 23.6°, 31.6°, 32.8°, 36.3°, 40° indicate the crystalline behaviour of $LiBF_4$.

The presence of interactions between constituents in the polymer systems led to the absence of these crystalline peaks in the diffractograms of CPEs. This resulting in the

complexation and thus the increase of the amorphous portion. CPE6B shows medium sharp peaks at 24.7, 46.3° and broad peak at 28.2° which further divulges the semicrystalline behaviour of the material. Another evidence is the decrease of peak intensity of CPE8B and CPE10B upon incorporation of additional percentage of $BaTiO_3$. The increase of the amorphous nature in the CPE matrices also implies by the reduction of peak intensity and broadening of peaks in CPE8B and CPE10B. All these results evidenced that complexation has taken placed in the PE matrix upon addition of $LiBF_4$ and $BaTiO_3$ (Khanmirzaei & Ramesh, 2014). Crystallinity calculation can be quantified based on full width at half maximum (FWHM) (Yu et al., 2020). The FWHM obtained of the sharp intense peaks between $2\theta = 27.5°$ to 29.0° were 0.2639°, 0.6014° and 0.7080° for CPE6B, CPE8B and CPE10B, respectively. Increases in FWHM of CPE10B indicates reduced in crystallinity degree and thus the amorphous character increases. The shifting of peaks implies a high amorphous degree of CPE. The orderly arrangement of polymer electrolyte matrix could disturb by the incorporated $BaTiO_3$. A high flexibility in polymer chains is induced by an irregular arrangement of constituents in CPE. This increases the ionic conductivity resulting from the enhancement of the amorphous nature of the polymer system.

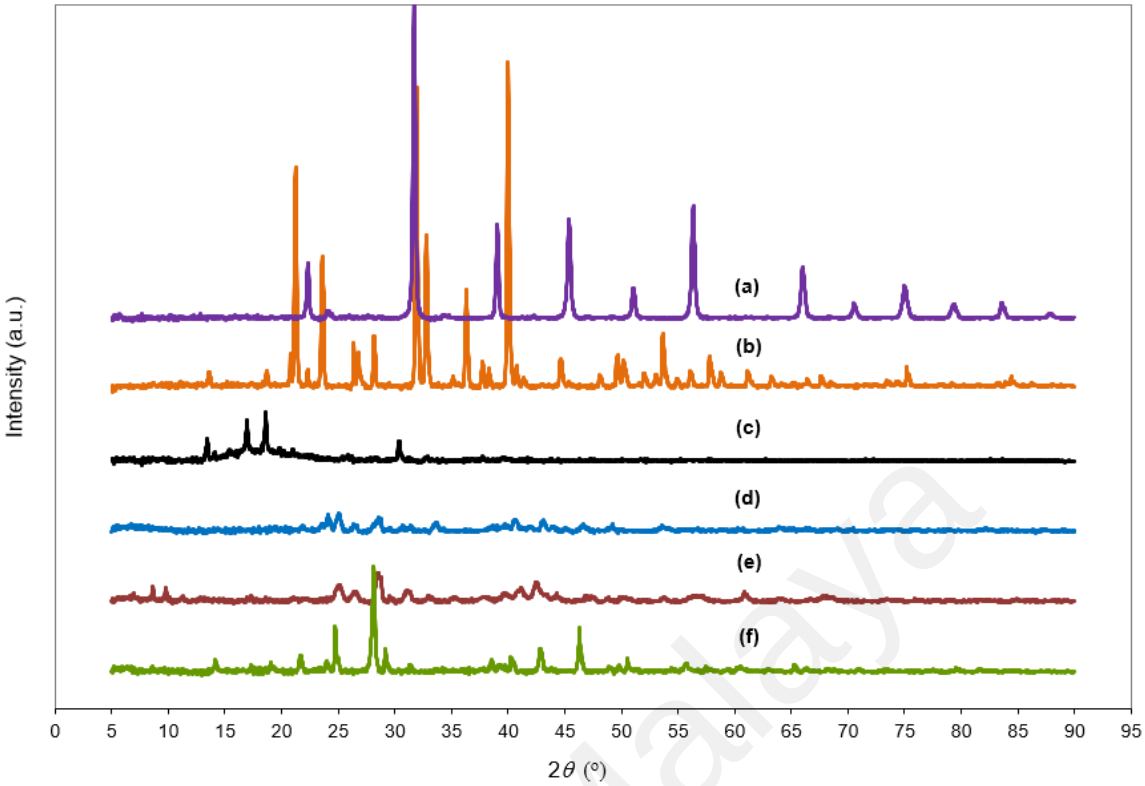

Figure 4.17: XRD patterns of (a) $BaTiO_3$, (b) $LiBF_4$, (c) PAA, (d) CPE10B, (e) CPE8B, and (f) CPE6B.

4.2.4.3 ATR-FTIR Studies of PAA-$LiBF_4$

The evidence of complexation of PAA molecule to the inorganic salt of $LiBF_4$ is confirmed by ATR-FTIR as shown in Figure 4.18. As report by Sankar and co-authors, there are five major peaks are observed for pure PAA near 3448, 2952, 1727, 1455 and 1407 cm^{-1} (Sankar et al., 2012). As can be seen in the FTIR spectra of pure PAA at Figure 4.18(a), stretching bands at 1451 cm^{-1} and 1415 cm^{-1} are due to the asymmetric and symmetric stretching vibrations of the C-O in COOH group of the PAA. The strong and intense stretching vibration band near 1721 cm^{-1} is due to the C=O group in the COOH group in PAA. However, the sharp and intense stretching vibration bands of OH in COOH group of PAA near 3448 cm^{-1} are not seen from the spectra. The vibration peaks near 2952 cm^{-1} which could attributed to the stretching vibrations of CH_2 group in the pure PAA also cannot be detected from the spectra. The broad band regions between 3500 and

2800 cm^{-1} indicates the presence of different OH group types (Sankar et al., 2012). However, the bands are getting more structured and a strong band found at 3185 cm^{-1} for all PAA-$LiBF_4$ electrolytes indicating the complexation of the lithium salt with the PAA chains. Besides, by comparing the stretching vibration band near 1721 cm^{-1} for C=O group between pure PAA and PEs prepared, the intensity of the band for PAA is reduced at PEs could be attributed to the attachment of the group to the Li^+ of $LiBF_4$ that incorporated into the electrolyte system.

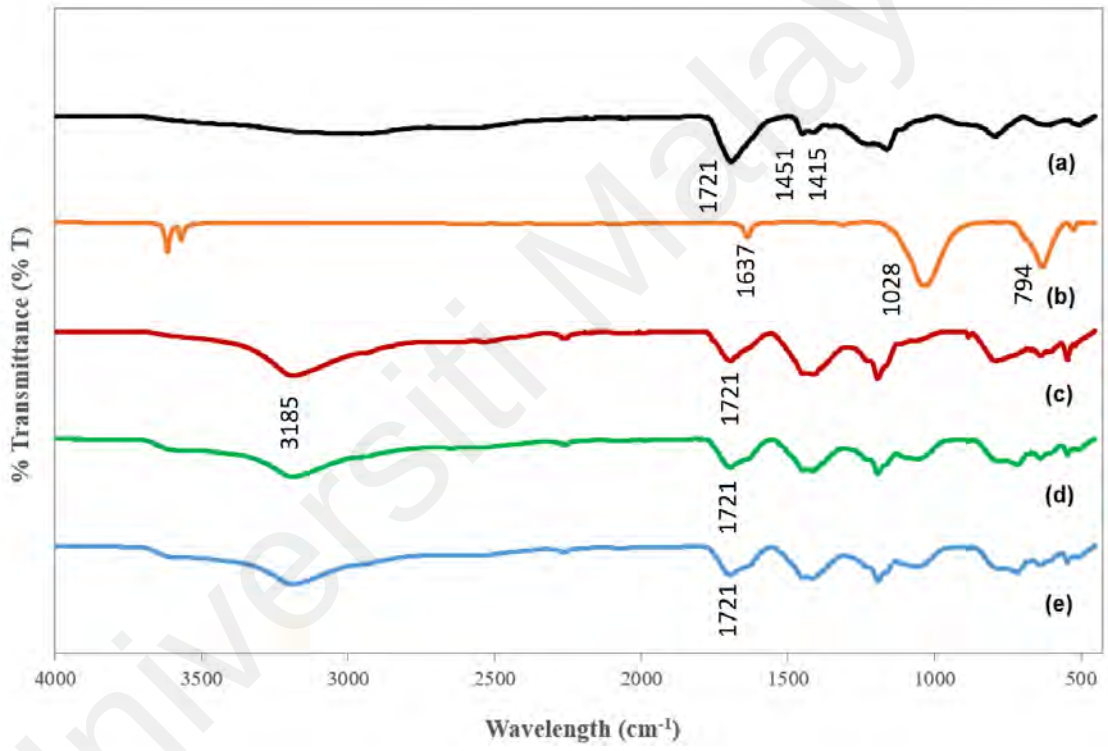

Figure 4.18: ATR-FTIR Spectra of (a) pure PAA, (b) pure $LiBF_4$, (c) P80-LB20, (d) P75-LB25, and (e) P70-LB30.

4.2.4.4 ATR-FTIR Studies of PAA-$LiBF_4$-$BaTiO_3$

In this study, ATR-FTIR is used to verify the complexation of the dopant and inorganic salt. Figures 4.19(a) and 4.19(c) show the ATR-FTIR spectra of pure PAA and $BaTiO_3$, respectively. Figures 4.19(d), (e), (f) shows the spectra of CPE films with 10, 8 and 6 wt.% loading with $BaTiO_3$, respectively. As we can be seen from the spectra 4.19(a), (d),

(e), (f), both PAA and CPEs shown similar peaks, indicating the PAA chain as a backbone matrix of the CPEs. The narrowing of the 3500 – 2800 cm^{-1} band region in PAA to form characteristic bands at 3195 cm^{-1} of all CPE as Figures 4.19(d), (e) and (f), implies that the lithium cations form complexation with the OH groups from the COOH of PAA chains. The reduce intensity of the vibration band near 1721 cm^{-1} implies that most of the COO^- groups of the PAA chain are attached to the Li^+ ions from the $LiBF_4$. As reported in the previous literature, the stretching vibration bands near to 3412, 1634, 1421, 860, 540 and 438 cm^{-1} are the bands of $BaTiO_3$ (Singh et al., 2017). However, as can be observed in Figure 4.19, only vibration band of 1435 cm^{-1} can be read from the FTIR spectra obtained. The strong peak 1435 cm^{-1} is due to the COO group bending vibrations.

As reported by Singh and co-authors, the stretching vibration bands of BF_4^- in $LiBF_4$ were observed near 1734 and 752 cm^{-1} (Singh et al., 2019). Figure 4.19(b) depicted the stretching vibration bands of BF_4^- near 1637, 1028 and 794 cm^{-1}. As shown in Figures 4.19(d), (e) and (f), two vibration bands near 1028 and 794 cm^{-1} were disappeared in PAA-$LiBF_4$-$BaTiO_3$. This suggests that the BF_4^- anions could dissolved in the solvent and complexed with polymer host thus leading to the disappear of the respective stretching vibration bands.

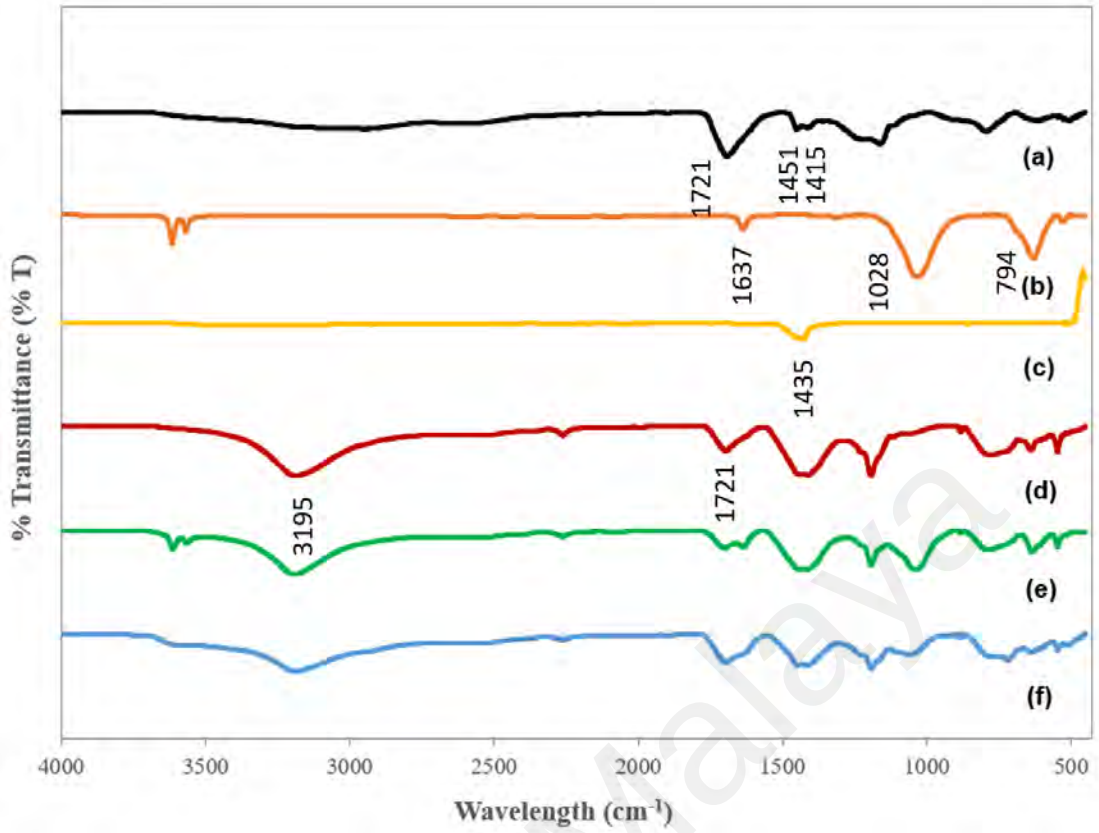

Figure 4.19: ATR-FTIR Spectra of (a) PAA, (b) $LiBF_4$, (c) $BaTiO_3$, (d) CPE10B, (e) CPE8B, and (f) CPE6B.

4.3 Conclusion

In summary, PEs which composed by PAA and $LiBF_4$ and CPEs composed by PAA-$LiBF_4$ electrolyte doped $BaTiO_3$ were prepared by solution casting method. The electrical properties of PAA-$LiBF_4$ and PAA-$LiBF_4$-$BaTiO_3$ electrolyte systems were determined by AC-impedance spectroscopy. The highest ionic conductivity of 6.61×10^{-4} S cm^{-1} and 8.95×10^{-4} S cm^{-1} were achieved by PAA-$LiBF_4$ with 30 wt.% $LiBF_4$, and PAA-$LiBF_4$-$BaTiO_3$ with 10% of $BaTiO_3$. The results indicated that ionic conductivity of the CPEs increased due to the decrease of the crystallinity of PAA-based matrices. The temperature dependence-ionic conductivity study demonstrated that both PAA-$LiBF_4$ and PAA-$LiBF_4$-$BaTiO_3$ systems follows Arrhenius equation by having low activation energy upon increases of temperature.

The dielectric permittivity studies showed that dielectric permittivity increased enormously with the decrease of frequency. When the lithium salt content in the polymer electrolytes increases, the number of charge carriers accumulated at the electrode-electrolyte interface increased. The dielectric modulus studies implied that both PAA-$LiBF_4$ and PAA-$LiBF_4$-$BaTiO_3$ systems were very capacitive. Electrochemical properties of all PE/CPE systems were conducted via LSV where the results are presents in ESW. The optimized PAA-$LiBF_4$ and PAA-$LiBF_4$-$BaTiO_3$ electrolytes demonstrated electrochemical stability window of 3.2 V and 4.0 V, respectively at ambient temperature. This infers that both systems offer a potential application in electrochemical devices.

From thermal analyses via TGA on PAA-$LiBF_4$ electrolytes, P80-LB20 exhibits better thermal stability compared to P70-LB30 and P85-LB25. When tested with CPEs, the residual weight of CPE10B, CPE8B and CPE6B are 19%, 23%, and 37%, respectively at 600 °C which is definitely higher than PAA (16%). The high residue weight of the CPEs implies the thermal stability of the composite matrices after the incorporation of $BaTiO_3$ as dopant. In the structural analyses via XRD, the disappearance of selected peaks and reduction in selected peak intensity also implied that there is an increase in amorphous nature in the PEs and CPEs, compared to their polymer host. The ATR-FTIR shows the evident of complexation between Li^+ and the polymer host. From the characterization study, it is suggested that PAA-$LiBF_4$ and PAA-$LiBF_4$-$BaTiO_3$ are very promising electrolyte materials for the next generation rechargeable electrochemical devices.

CHAPTER 5: PAA-$LiClO_4$ ELECTROLYTES CHARACTERIZATION

5.1 Introduction

$LiClO_4$ which comprised of a large-sized anion and a small-sized cation is another promising option of conducting salt. The advantages of $LiClO_4$ over other lithium salts is based on its low interfacial resistance, high dissociation energy, and good solubility in most solvents (Teoh et al., 2012). The coordination interaction between lithium ions and the polar group of polymer host causing it to be easily dissolved in the PE matrix. However, the dissociation of the conducting salts that trapped in the PE system allow the ionic conduction via the mobile ions. Previous literature reported that PEs complexed with $LiClO_4$ exhibit good properties (Capiglia et al., 1999; Chen-Yang et al., 2002; Rajendran et al., 2002; Teoh et al., 2012; Watanabe et al., 1983; Chung et al., 2001; Choi & Shin, 1996). When the PE is doped with the conducting salt, the resulting PE have a better stability and high conductivity since both polymer host and conducting salt having the low lattice energies.

In this Chapter, the studies of chemical, electrical, electrochemical, thermal and structural properties of PAA-$LiClO_4$ and PAA-$LiClO_4$-$BaTiO_3$ were studied. The addition of dopant such as $BaTiO_3$ is to prepare CPE which could exhibit higher ionic conductivity. The results of the dispersion of dopant in the PE matrix is considerable when an appropriate amount of the dopant is used. Therefore, the ionic conductivity of the CPE is influenced by the concentration of $BaTiO_3$. Filler or dopants should stabilize the PE system at high temperature and induces more mechanical strength to the film, apart from the improvement in ionic conductivity and wider ESW. $BaTiO_3$ has been reported in previous studies which could enhanced some features of the CPE (Itoh et al., 2003).

5.2. Results and Discussion

5.2.1 Electrical Properties

5.2.1.1 Ambient Temperature-Ionic Conductivity Studies of PAA-$LiClO_4$

The AC-impedance spectroscopy analysis is a typical method used to measure the ionic conductivity of the PE films. Figure 5.1 illustrates the complex impedance spectrum of PAA-$LiClO_4$ electrolyte film at ambient temperature. It is observed from the figure that complex impedance plot for PAA/$LiClO_4$ electrolyte film is composed of a semicircle at a high frequency region and a slanted spike at a low frequency region. Figure 5.1 depicts the impedance spectrum of the respective electrolyte matrix at a low bulk resistance. The bulk resistance, R_b is determined by reading the intercept point of the slanted line on the real axis. The parallel combination of R_b and bulk capacitance of the electrolyte matrix is representing by the semicircle. The slanted line at the low frequency region represents the capacitance behaviour of the electrode/electrolyte double layer.

The ionic conductivity, σ is calculated by the equation (1), as described in the Chapter 3 Material & Methodology. As illustrated in Figure 5.1, R_b of the thin electrolyte films is determined as 4010 Ω from the interception of the semicircle and the spike. The thickness of the electrolyte film in the experiment is measured by Mitutoyo digital gauge which an average thickness of 0.273 mm was obtained. The highest ionic conductivity of 2.4×10^{-6} S cm^{-1} was achieved for 10 wt.% $LiClO_4$ in the PAA/$LiClO_4$ electrolyte system.

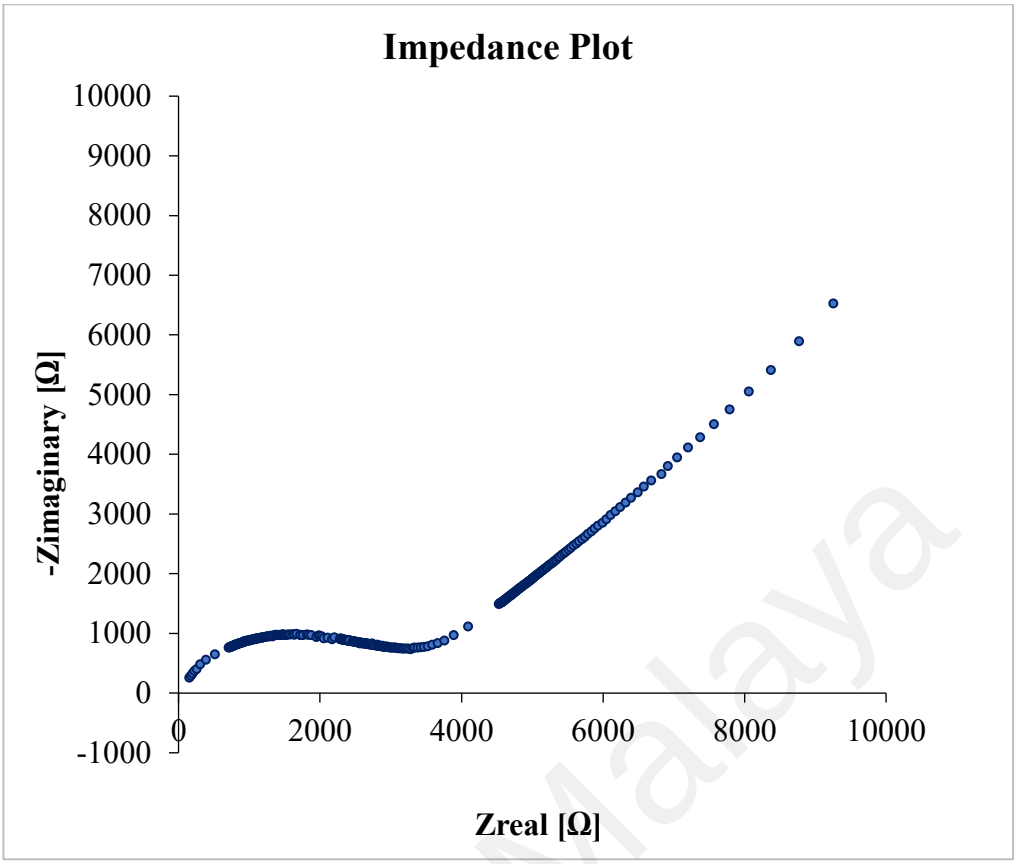

Figure 5.1: Impedance plot of PAA-$LiClO_4$ electrolytes at ambient temperature.

The technological applicability of the PE in various electrochemical applications are dependent on the optimum composition of PAA-based solid electrolyte. In this study, the dependence of ionic conductivity with different $LiClO_4$ content in PAA is investigated. Figure 5.2 reveals the effect of $LiClO_4$ concentration on the ionic conductivity of the PAA-based electrolyte systems. The ionic conductivity of PAA with the addition of 5 wt.% $LiClO_4$ is found to be 2.7×10^{-7} S cm^{-1}. The incorporation of 10 wt.% $LiClO_4$ demonstrated a highest ionic conductivity, which is 2.40×10^{-6} S cm^{-1}. After addition of more than 10 wt.% of $LiClO_4$, ionic conductivity decreases until 40 wt.% of the $LiClO_4$ content is achieved.

Lithium ions in $LiClO_4$ salt act as charge carriers. However, the negative species of perchlorate ion, ClO_4^- also contributed to the ionic conductivity (Watanabe et al., 1986).

When the $LiClO_4$ concentration increases, the number of mobile lithium ions also increased which led to the increased of ionic conductivity in the initial stage. When the lithium salt content increased from 5 wt.% until 15 wt.%, the presence of lithium salt starts to disrupt the crystallinity of PAA matrix. The increase in the amorphous nature in the polymer matrices lead to the increases in ionic conductivity. The ionic conductivity starts to reduce from 15 wt.% of $LiClO_4$ and onwards. This could be attributed to the formation of neutral ion pairs with the excessive lithium salt. The tendency of the re-association of lithium salts consequently reduces the availability of freely mobile lithium ions which could contributed to the decreasing of ionic conductivity.

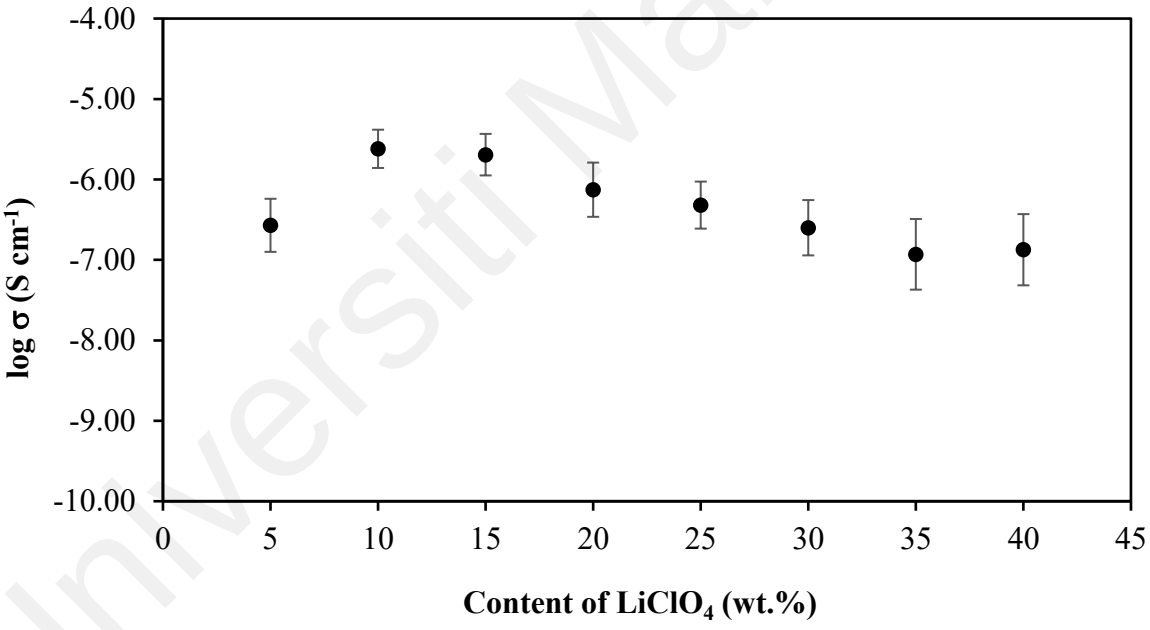

Figure 5.2: Effect of $LiClO_4$ content on the ionic conductivity of PAA-based electrolytes at ambient temperature.

5.2.1.2 Ambient Temperature-Ionic Conductivity Studies of PAA-$LiClO_4$-$BaTiO_3$

AC-impedance spectroscopy was used to determine the ionic conductivities of the PEs by placing thin films between two SS blocking electrodes. The Impedance plot was obtained from the AC-impedance of the PE system with 10 wt.% $BaTiO_3$. Two well

defined regions can be obtained from the impedance plot as in Figure 5.3: the low frequency region and the high frequency region, with a slanted spike and a semicircle in the regions, respectively. At the high frequency region, R_b values are determined from the intercept on the real-axis. The semicircle reveals the characteristic of the parallel combination of both bulk resistance and bulk capacitance of the CPE matrix. The slanted line which inclined towards the real axis at an angle less than 90° ascribed the capacitance behaviour of electrode/electrolyte double layer.

The ionic conductivity of PAA-$LiClO_4$-$BaTiO_3$ electrolytes is calculated from the equation 1, as described in the Chapter 3 Material & Methodology. From the impedance spectra, R_b of PAA-$LiClO_4$-$BaTiO_3$ electrolyte was measured as 825 Ω at ambient temperature. The thickness of the CPE film was measured using Mitutoyo digital gauge and found to be 0.234 mm. The highest ionic conductivity of 1.00×10^{-5} S cm^{-1} was obtained for 10 wt.% of $BaTiO_3$ in PAA-$LiClO_4$-$BaTiO_3$ electrolyte system.

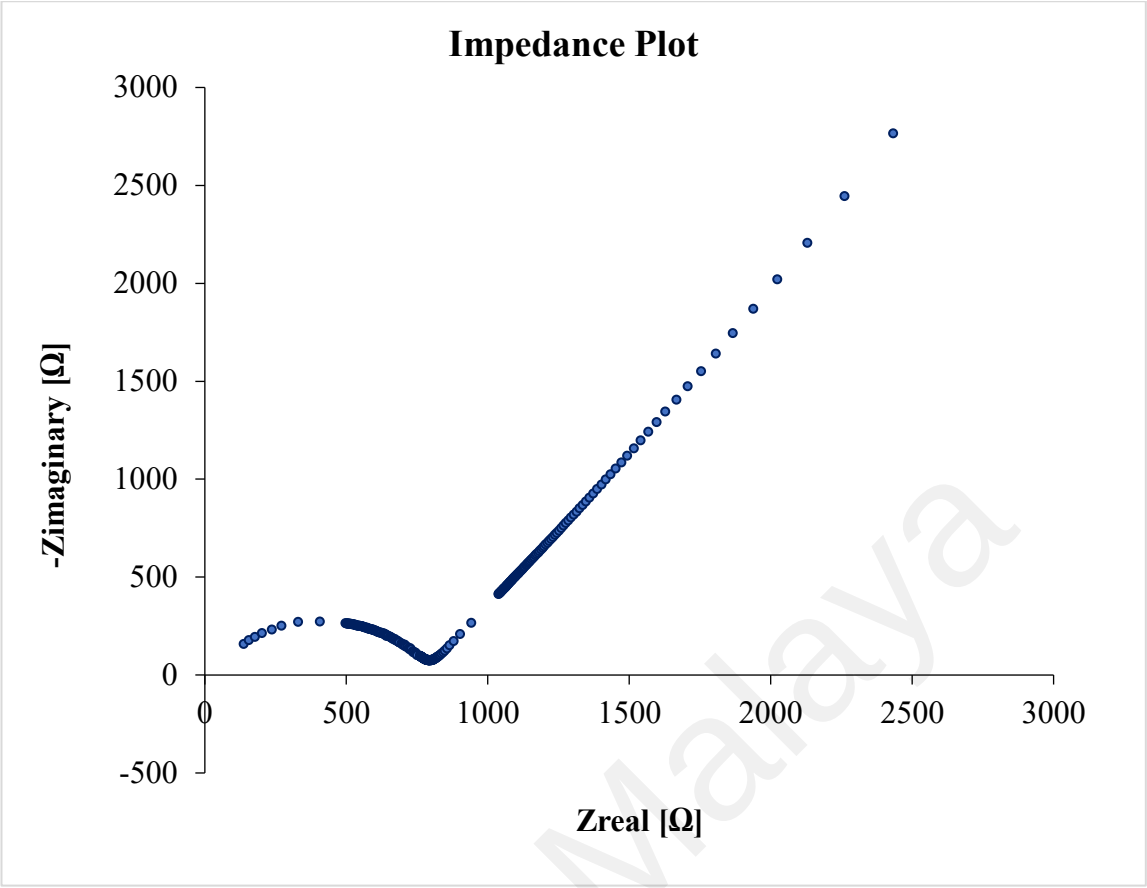

Figure 5.3: Impedance plot of PAA-$LiClO_4$-$BaTiO_3$ electrolyte at ambient temperature using AC-impedance spectroscopy.

The optimum amount of dopant in CPEs is very important to ensure the polymer matrices are suitable for electrochemical device applications. In this study, we investigated the dependence of ionic conductivity on $BaTiO_3$ concentration doped into the PEs. Figure 5.4 shows the variation of ionic conductivity as a function of $BaTiO_3$ content doped into the PAA-$LiClO_4$ electrolyte systems. Ionic conductivity showed a slight increase when 2 wt.% of $BaTiO_3$ was added into a PAA-$LiClO_4$ electrolyte system. Ionic conductivity increases with the amount of $BaTiO_3$ up to the maximum level in the experiment. The highest ionic conductivity was achieved at ambient temperature by doping 10 wt.% of $BaTiO_3$ which is 1.00×10^{-5} S cm^{-1}. The chemical composition study demonstrated that dopant content has a direct effect on ionic conductivity, which dramatically increases ionic conductivity in CPE systems with higher dopant contents.

Doping of $BaTiO_3$ helps in dissociating lithium salts into lithium ions. In general, there are two main factors affecting the ionic conductivity, i.e. mobility and concentration of charge carriers. At a low $BaTiO_3$ concentration, the dopant particles are low in mass fraction and are far apart. The dopant distribution is also uniform throughout the polymer matrix, which makes it hard to build a conducting pathway to allow ionic migration. When more $BaTiO_3$ is doped into the polymer matrix, the dopant could be distributed more evenly throughout the membrane. As the dopants are closer to each other, more conducting paths are available for ionic transport around the surface of the dopant. Furthermore, the mobile charge carriers have greater mobility within the vicinity of grains. At 10 wt.% of $BaTiO_3$, mobile charge carriers could migrate more efficiently due to the large surface area of the dopant. The higher charge carriers' mobility increases the ionic conductivity. In addition, the incorporation of dopant further disrupts the ordered structure of the polymer matrix. The doping effect increases the amorphous nature of the structure of macromolecules.

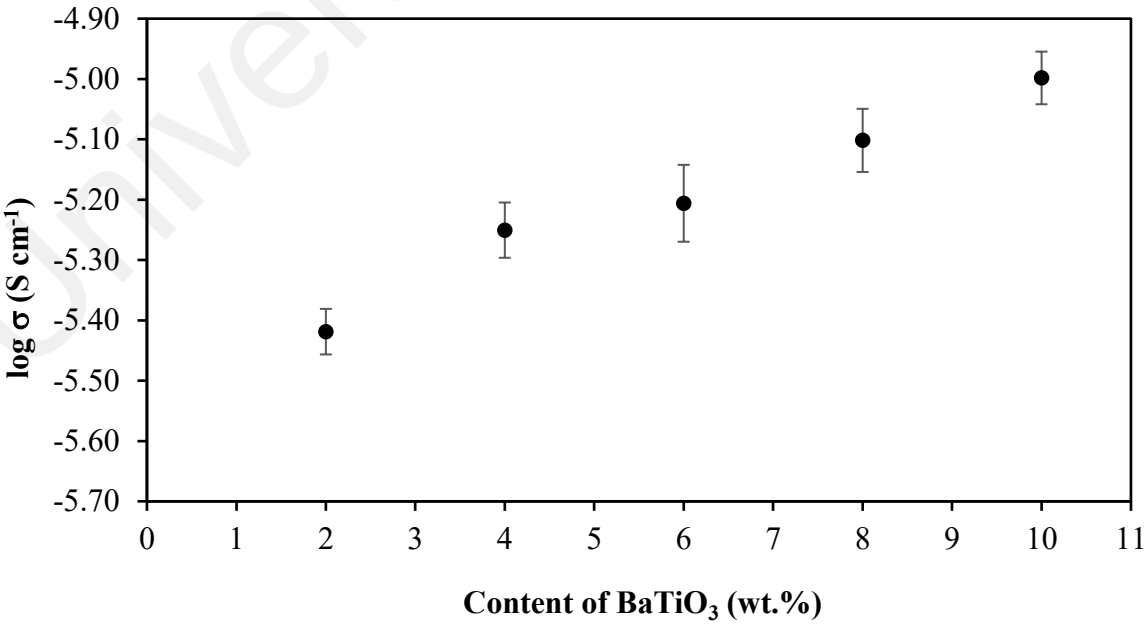

Figure 5.4: Effect of $BaTiO_3$ content on the ionic conductivity of PAA-$LiClO_4$ electrolytes at ambient temperature.

5.2.1.3 Temperature Dependent-Ionic Conductivity Studies of PAA-$LiClO_4$

In this study, the temperature-dependent conductivity measurement was carried out in the temperature ranging of 303 to 393 K in order to analyze the ionic conduction mechanism in the PAA-$LiClO_4$ electrolyte systems. 0.9898, 0.9894 and 0.9838 of regression (R_2) values are determined for P90-LC10, P85-LC15, and P80-LC20, respectively. The ionic conductivity of the tested PEs complies with Arrhenius equation which is expressed as equation 1 in Chapter 3. Table 5.1 presented the activation energy (E_a) of various PAA-$LiClO_4$ electrolyte systems. Activation energy (E_a) was calculated by using the slope value and equation 2. The results showed that the E_a of PEs calculated are in the range between 0.00043 and 0.00049 eV. The higher ionic conductivity of the PEs is attributed to the lower activation energy.

When 10 wt.% of lithium salt was incorporated into the PE, the highest ionic conductivity was achieved at ambient temperature, as illustrated in Figure 5.5, Arrhenius plot confirms the increase of ionic conductivity with the increase in temperature. It was observed that all the tested polymer electrolyte films obey the Arrhenius theory which reveal that ion conduction mechanism is thermally assisted. When the temperature of the polymer matrices is elevated, the freely moving ions acquire more energy thus allows faster movement. The freely moving ions jump into neighbouring vacant sites. The faster motion of lithium ions in the polymer network is attributed to the reducing in crystallinity of PAA-$LiClO_4$ electrolyte system.

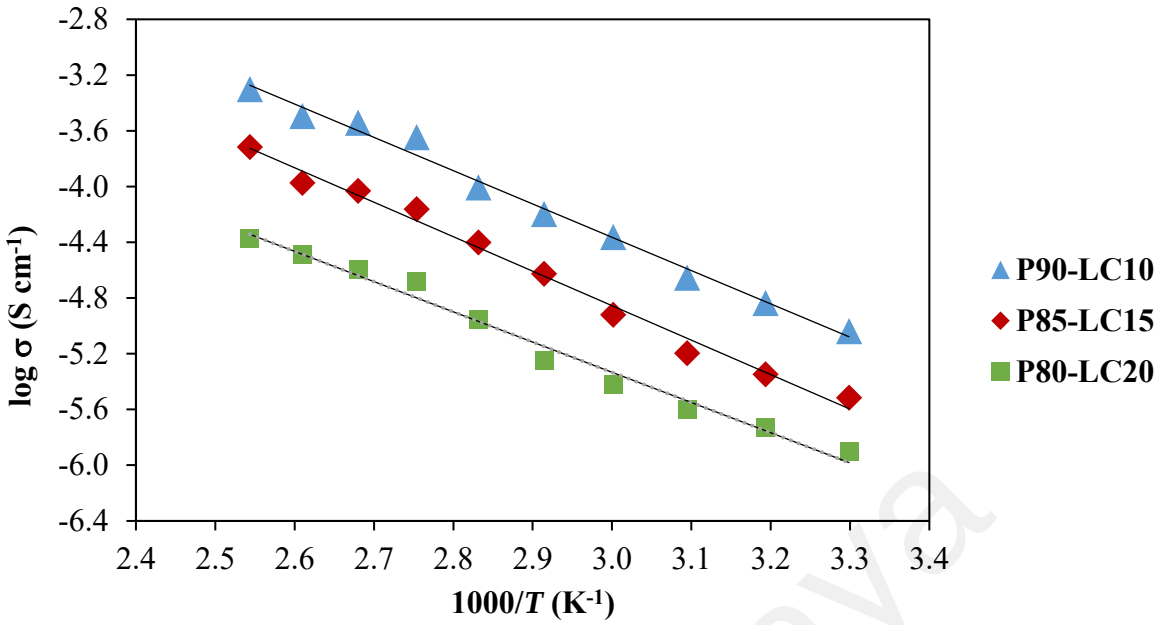

Figure 5.5: Arrhenius plot of ionic conductivity for P90-LC10, P85-LC15 and P80-LC20 with frequency ranging from 50 Hz to 5 MHz at temperatures from 303 K to 393 K.

Table 5.1: The activation energy of the PAA-$LiClO_4$ electrolyte systems.

Polymer Electrolyte Systems	Activation Energy (eV)
P90-LC10	4.31×10^{-4}
P85-LC15	4.74×10^{-4}
P80-LC20	4.90×10^{-4}

5.2.1.4 Temperature Dependent-Ionic Conductivity Studies of PAA-$LiClO_4$-$BaTiO_3$

In this work, ionic conductivity of PAA-$LiClO_4$-$BaTiO_3$ electrolytes with different compositions of $BaTiO_3$ was measured at different temperatures, ranging from 30 °C to 120 °C using impedance spectroscopy. The temperature-dependent ionic conductivity

measurements were carried out to study the mechanism of ionic conduction of PAA-$LiClO_4$-$BaTiO_3$ electrolyte system.

The highest ionic conductivity is achieved as 5.0×10^{-4} S cm^{-1} at 120 °C by CPE10C sample. As shown in Figure 5.6, all the tested PE samples obey Arrhenius theory in the temperatures studied. Arrhenius plot reveals that the ion conduction mechanism was thermally assisted. CPE10C has the highest ionic conductivity compared to CPE8C and CPE6C as the degree of amorphous nature is the highest in CPE10C.

Activation energy (E_a) is inversely proportional to ionic conductivity. Lower E_a implies a higher ionic conductivity this is because less energy is required for the transformation between transit sites (Khanmirzaei & Ramesh, 2013). Table 5.2 presented the activation energy (E_a) of various PAA-$LiClO_4$-$BaTiO_3$ electrolyte systems. E_a values which acquired from equation 2 from Chapter 3 for the three CPEs are ranging between 0.00030-0.00036 eV. Figure 5.6 indicated an average regression of 0.98 implies a good linearity of the thermal behaviour of CPEs. The incorporation of $BaTiO_3$ disrupt the interaction between the polymer system and lithium ions. This causes less energy is required for the charge carriers hopping mechanism. Thus, the CPE with the lower activation energy value exhibits a higher ionic conductivity due to the easier and greater migration of lithium ions.

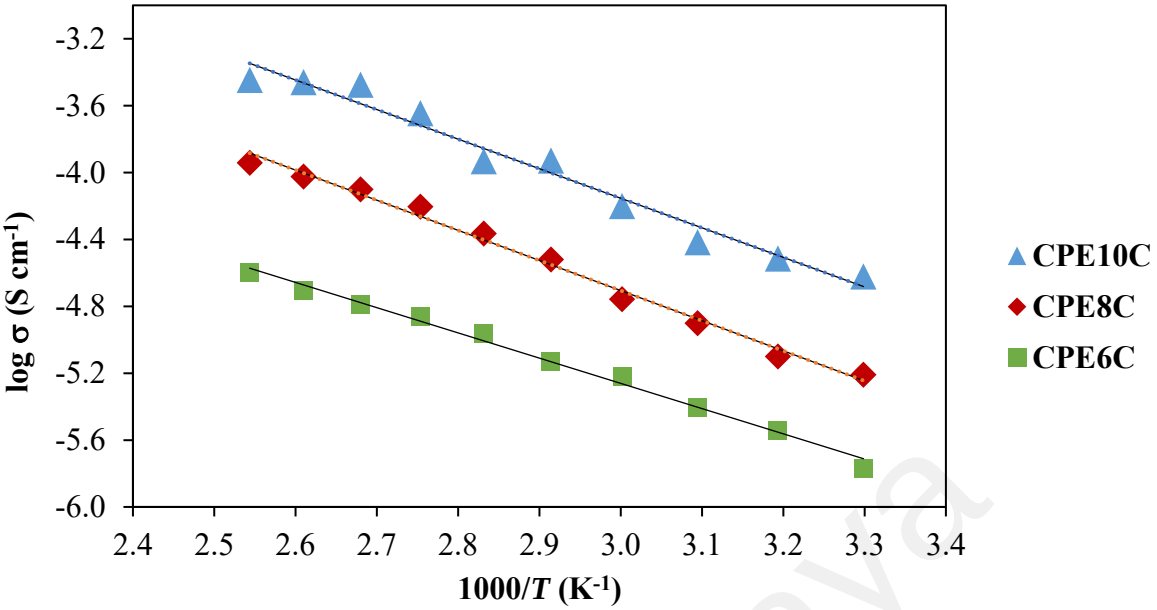

Figure 5.6: Arrhenius plot of ionic conductivity for PAA-$LiClO_4$-$BaTiO_3$ CPE6C, CPE8C, and CPE10C with frequency ranging from 50 Hz to 5 MHz at temperatures from 303 K to 393 K.

Table 5.2: The activation energy of the PAA-$LiClO_4$-$BaTiO_3$ electrolyte systems.

PAA-$LiClO_4$-$BaTiO_3$ Electrolyte Systems	Activation Energy (eV)
CPE6C	3.57×10^{-4}
CPE8C	3.51×10^{-4}
CPE10C	2.99×10^{-4}

5.2.1.5 Dielectric Permittivity Studies of PAA-$LiClO_4$

Figures 5.7(a) and 5.7(b) depict the frequency dependence variation of dielectric permittivity and dielectric loss for the prepared PAA-$LiClO_4$ electrolytes systems: P90-LC10, P85-LC15, and P80-LC20. The plots shown a rapid fall at lower frequency region and saturated at higher frequency region. The fall at the lower frequency region is attributed to the electrode polarization when electrical field was applied across the samples (Liew et al., 2012a). At high frequency region, both dielectric constant and electric loss decreased. This is attributed to the slowing down of the dipoles' orientation

with a fast periodic reversal of the electric field. Thus, the charge density that build up at the electrode-electrolyte interface is decreased. Consequently, the bare polarization effect is occurred at high frequency due to the absence of excessive ion diffusion in the electric field direction (Rajendran et al., 2004). When $LiClO_4$ concentration increased there is a high rise in dielectric constant values. Incorporating more conducting salt resulting a re-association of lithium salt which consequently reduces the availability of mobile ions and thus the dielectric constant values.

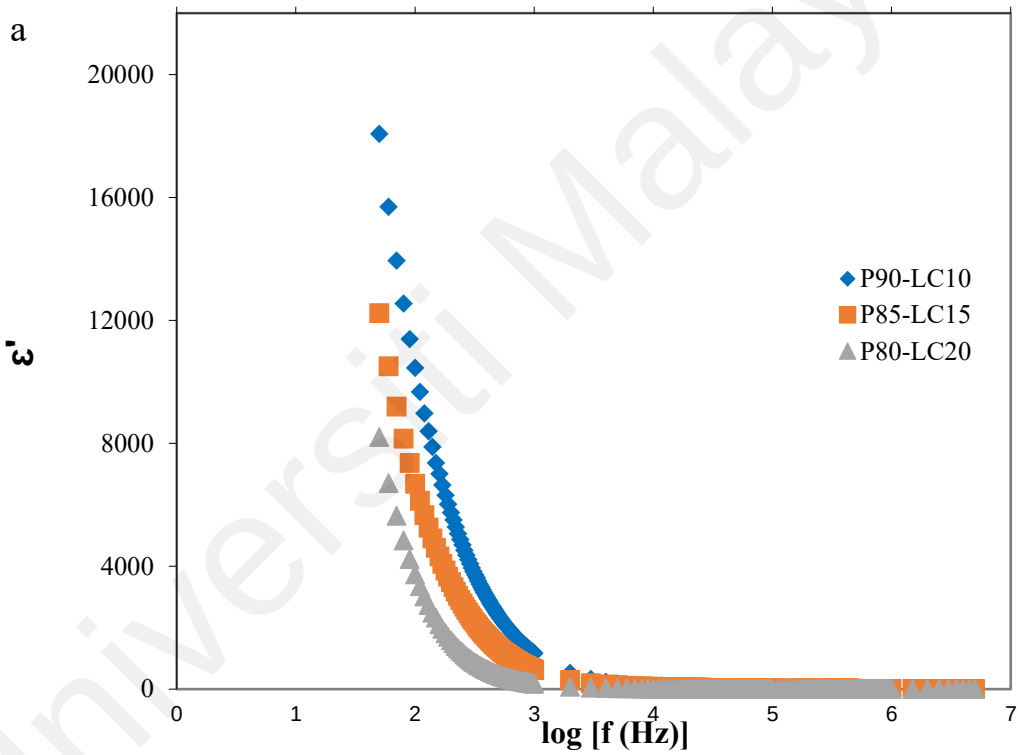

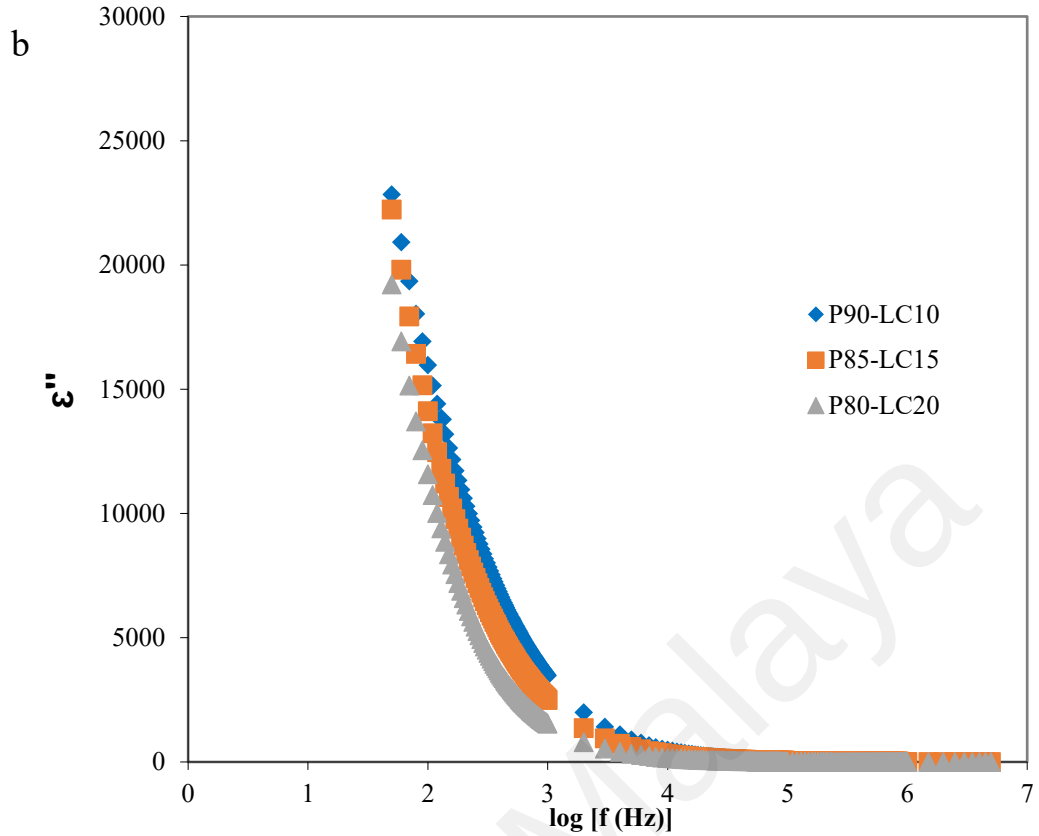

Figure 5.7: Variation of (a) dielectric permittivity and (b) dielectric loss for P90-LC10, P85-LC15, and P80-LC20 as a function of frequency at ambient temperature.

5.2.1.6 Dielectric Permittivity Studies of PAA-$LiClO_4$-$BaTiO_3$

Figures 5.8(a) and 5.8(b) demonstrate the variation of dielectric permittivity and dielectric loss for three PAA-$LiClO_4$-$BaTiO_3$ systems with various dopant composition: CPE2C, CPE6C, CPE10C. The plots demonstrate that all three CPEs exhibit similar patterns where both dielectric permittivity and dielectric loss decrease with the increase of frequency. The fall is rapid at a lower frequency range and becomes saturated at a higher frequency range. This observation is typical in the dielectric study plots of PE or CPE matrices. This phenomenon has been explained in literature clearly. As frequency increases, the dipoles are unable to rotate rapidly which led to a lag between oscillating dipole frequency and the applied field (Awadhia et al., 2006). The figures affirm that

dielectric permittivity increases with the increasing of $BaTiO_3$ content in the PAA-$LiClO_4$-$BaTiO_3$ matrix. At any frequencies, CPE2C shown the lowest dielectric permittivity and also a comparatively lower dielectric loss compared to other CPEs. On the contrary, CPE10C demonstrated the highest dielectric permittivity.

Figure 5.8(a) also demonstrates that CPE10C, with higher dielectric constant is associated with the higher $BaTiO_3$ content. $BaTiO_3$ acts as dopants to dissociate lithium salt into ions in the PAA-$LiClO_4$-$BaTiO_3$ complexes; to enhance polarization; to increase the amorphous nature and thus lead to the enhancement in ion transport properties; and reduce the crystallinity and restrain the recrystallization of the CPE complexes.

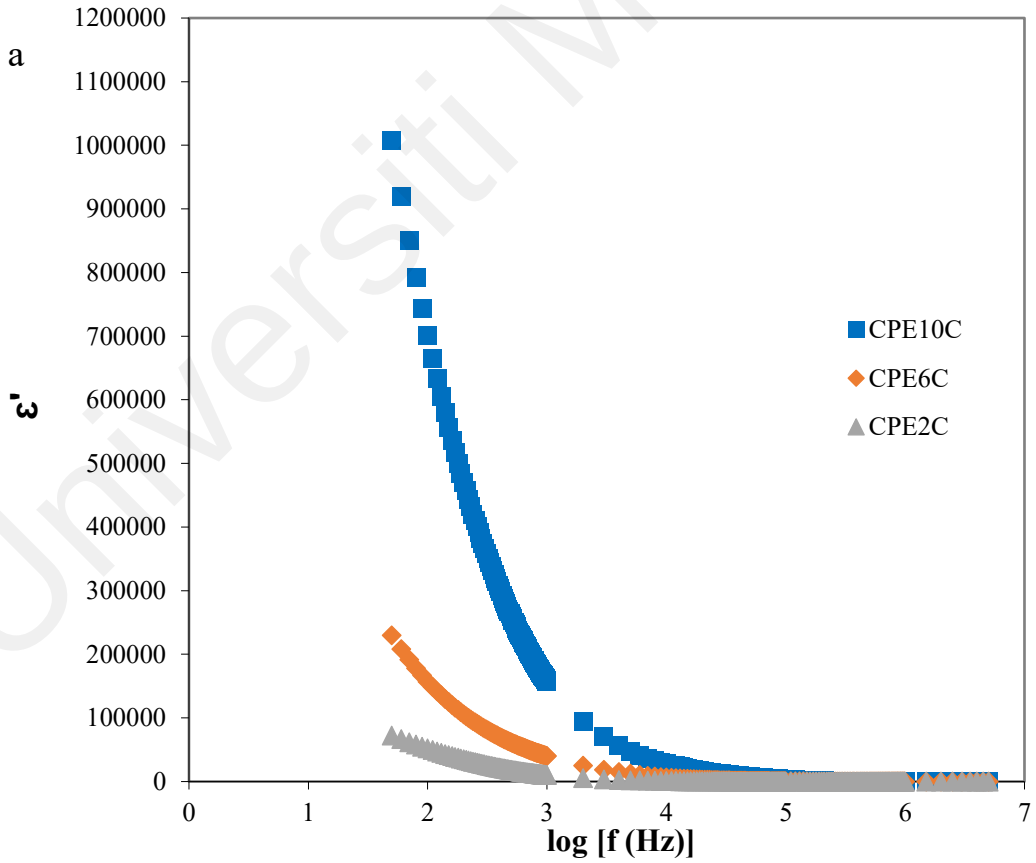

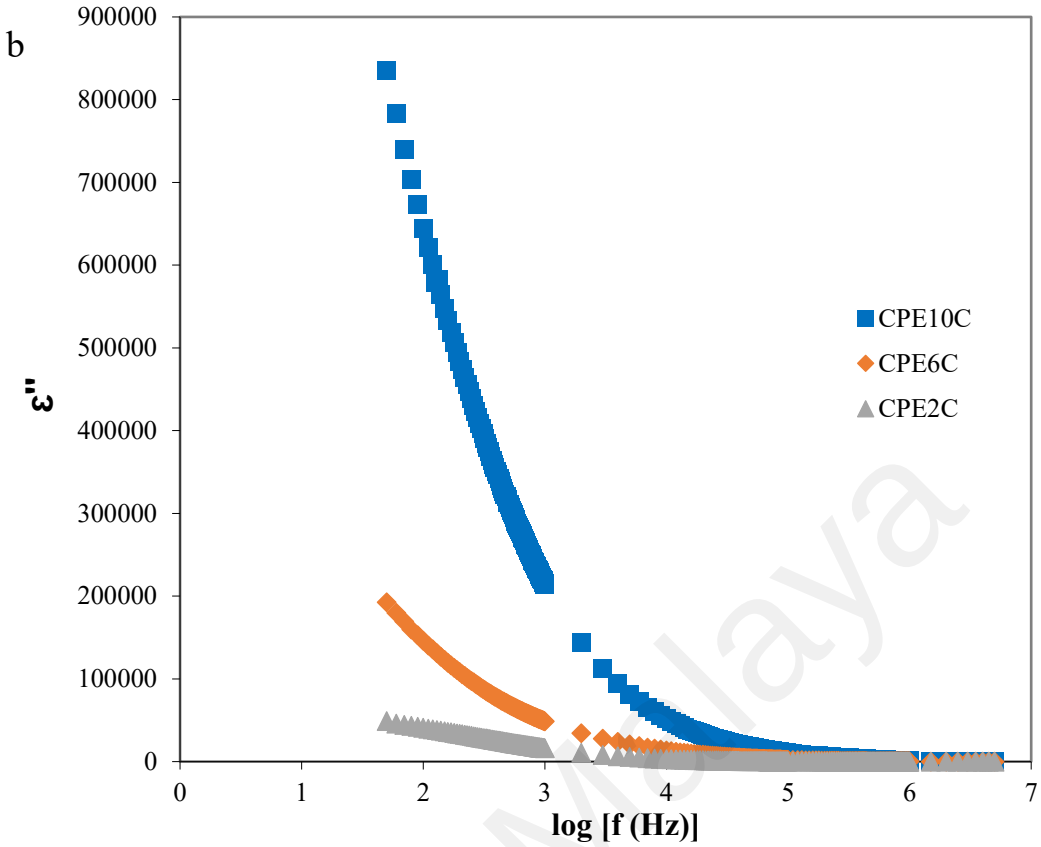

Figure 5.8: Variation of (a) dielectric permittivity and (b) dielectric loss for PAA-$LiClO_4$-$BaTiO_3$ CPE2C (low), CPE6C (medium), and CPE10C (high) as a function of frequency at ambient temperature.

5.2.1.7 Loss Tangent Studies of PAA-$LiClO_4$

Figure 5.9 demonstrates the dielectric loss tangent plot of tested electrolyte matrices of P90-LC10, P85-LC15, and P80-LC20. The relaxation frequencies for all the samples with different $LiClO_4$ content are tabulated in Table 5.3. Based on Figure 5.9, the loss tangent peaks were found shifted towards higher frequency with the increasing of $LiClO_4$ content. The shifting correlates to the mobility of cations and the reduction of relaxation time (Paradhan et al., 2008; Winie et al., 2009; Yahya & Arof, 2003; Jana & Zhong, 2008). Compared to P90-LC10, P80-LC20 possesses higher cation content with lower ionic conductivity. The aggregate of neutral ions formation blocked the existing conducting pathways (Jana & Zhong, 2008) which restrict the cations' mobility that causing the slow

mobility in P80-LC20. The magnitude of tan δ deduces the number of lithium ions which involves in ionic conduction. The magnitude of tan δ is increased upon the decreasing of $LiClO_4$ content. This inferred the increase of the area under the peak which ascribed the increasing in the number of lithium ion that involves in the relaxation process. The availability of lithium ions resulting to the enhancement in ionic conductivity (Norashikin & Ibrahim, 2009). Based on the observation from Figure 5.9, the area under the peak for various PE systems is increased in the following order: P80-LC20 < P90-LC10 < P85-LC15. P85-LC15 exhibits the highest magnitude of tan δ as well as the area under the peak which infers the number of mobile lithium ions that involve in ionic conduction.

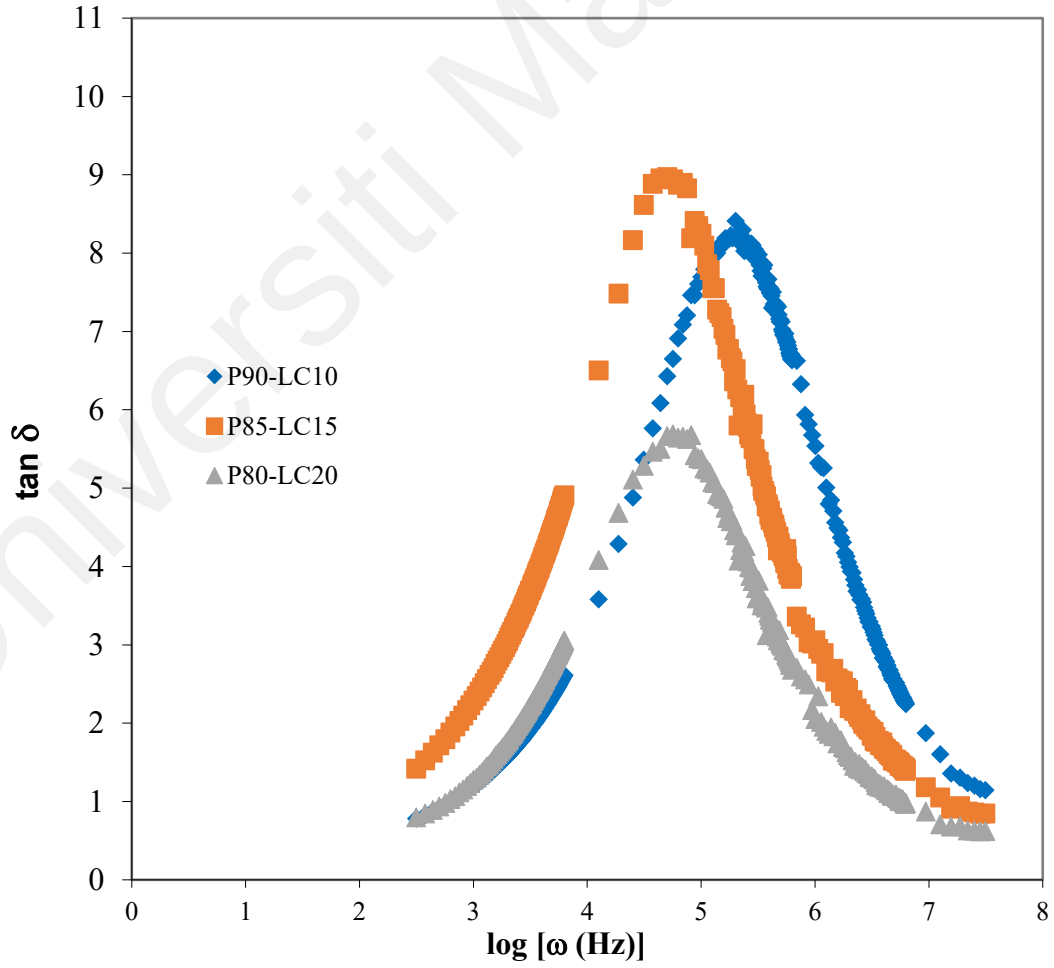

Figure 5.9: Variation of loss tangent (tan δ) against the logarithm of angular frequency (log ω) for P90-LC10, P85-LC15, and P80-LC20 at ambient temperature.

Table 5.3: Relaxation frequencies for P90-LC10, P85-LC15, and P80-LC20 with different $LiClO_4$ content.

PE Sample	Relaxation frequency, log ω_m (Hz)
P90-LC10	5.4
P85-LC15	4.8
P80-LC20	4.9

5.2.1.8 Loss Tangent Studies of PAA-$LiClO_4$-$BaTiO_3$

The frequency dependence of loss tangent plot for CPE2C is illustrated in Figure 5.10. Plots for CPE6C and CPE10C are not shown as the plots appeared as vertical asymptotes instead of valuable relaxation peaks. As can be seen from Figure 5.10, tangent loss peak is 6.0 Hz when the dopant content in CPE is 2 wt.%. Upon the increasing of dopant content in the electrolyte matrices, the amorphous fraction which facilitate the lithium ions' mobility is increased. CPE which possesses an increase portion of amorphous phase is coupled with an increased amount of conducting cations. The ionic conductivity is enhanced when the relaxation time of ions is reduced after the acceleration in mobility. The magnitude of tan δ also correlates to the area under the peak of the tangent loss plot.

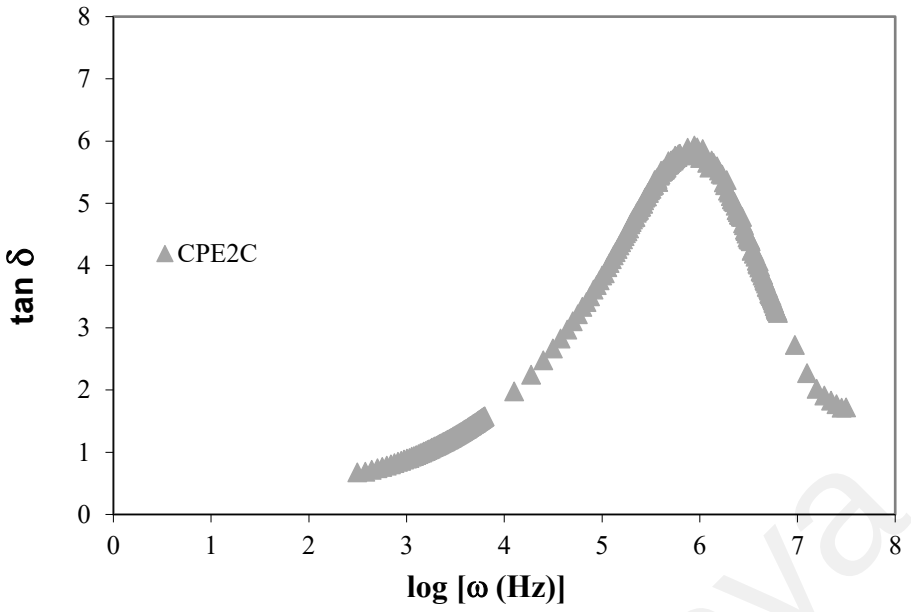

Figure 5.10: Variation of loss tangent (tan δ) against the logarithm of angular frequency (log ω) for PAA-$LiClO_4$-$BaTiO_3$: CPE2C at ambient temperature.

5.2.1.9 Modulus Studies of PAA-$LiClO_4$

The real part of dielectric modulus (M') and the imaginary part of dielectric modulus (M") for P90-LC10, P85-LC15 and P80-LC20 are shown in Figures 5.11(a) and 5.11(b), respectively. As indicated in these plots, the relaxation peaks are absent. An abrupt increase of the curve is observed towards higher frequency range. The plots also demonstrate a long tail approach zero at lower frequency region. As described in the literature, the contribution of electrode polarization is insignificant and the high capacitance is associated with the electrodes (Gogulamurali et al., 1992). As can be observed from Figure 5.11, when the lithium salt concentration is increased, the peak is shifted to lower frequency which reveals the effect of lithium salt in the dielectric properties of PEs. The amount of mobile charge carriers is increased upon the increase in lithium salt content. The re-association of lithium salts occurs when more cations are available in the polymer matrix. The amount of mobile charge carriers is reduced when more cations are involved in the interaction. The ionic hopping mechanism is affected when the participation of charge carriers in the ion conduction is reduced.

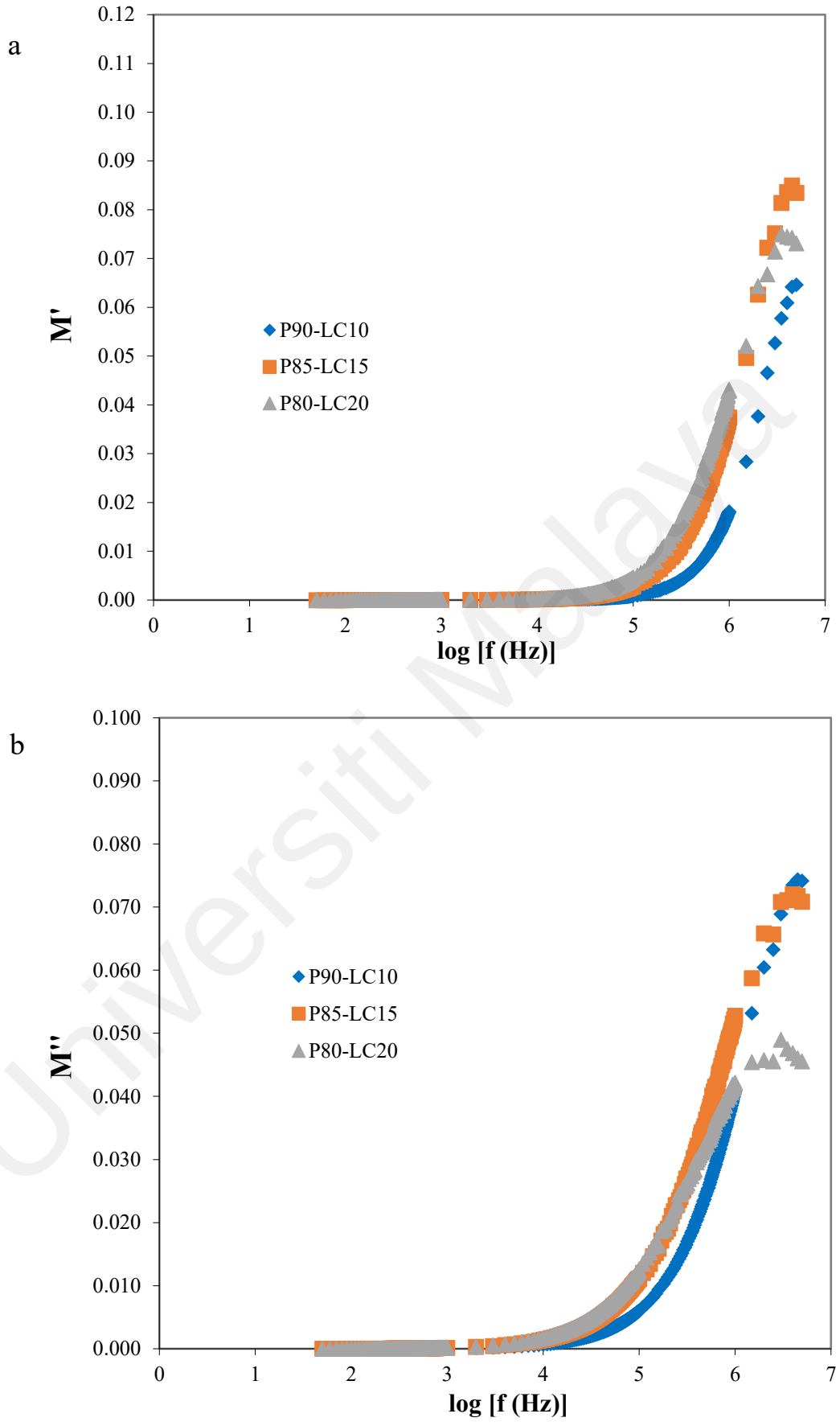

Figure 5.11: The (a) real part and (b) imaginary part of dielectric moduli as a function of logarithmic frequency for P90-LC10, P85-LC15, and P80-LC20 in the frequency range of 50 Hz – 5 MHz at ambient temperature.

5.2.1.10 Modulus Studies of PAA-$LiClO_4$-$BaTiO_3$

Figures 5.12(a) and 5.12(b) depict the frequency dependence of real and imaginary parts of dielectric moduli for different polymer electrolyte complexes: CPE2C, CPE6C and CPE10C. As no characteristic peaks are observed from the figures, this ascribed the narrow experimental frequency window. Based on the figures, all curves tend toward zero at lower frequency regime for both real an imaginary part of dielectric moduli. This implies the negligible contribution of electrode polarization. The decline is suggested attribute by the greater extend of ion-ion interaction when the excessive amount of $BaTiO_3$ is present. The curve indicates a long tail at lower frequency which correlates to the high capacitance is associated with the electrodes (Gogulamurali et al., 1992).

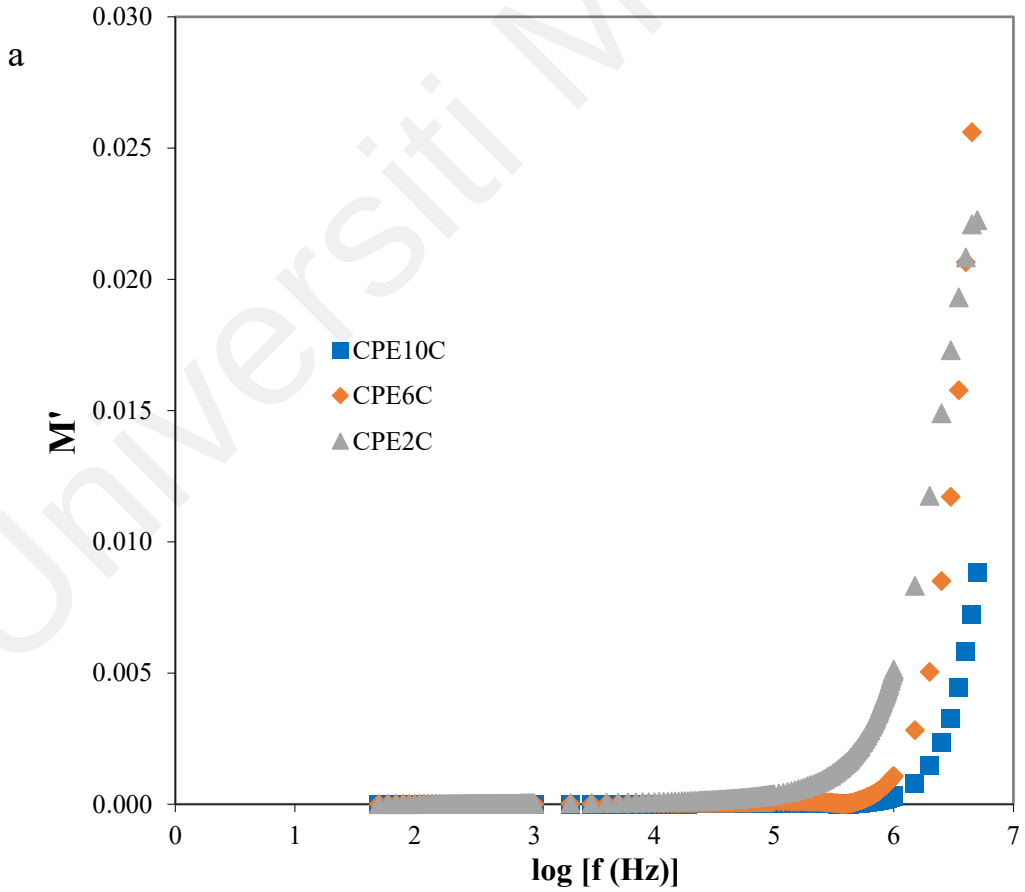

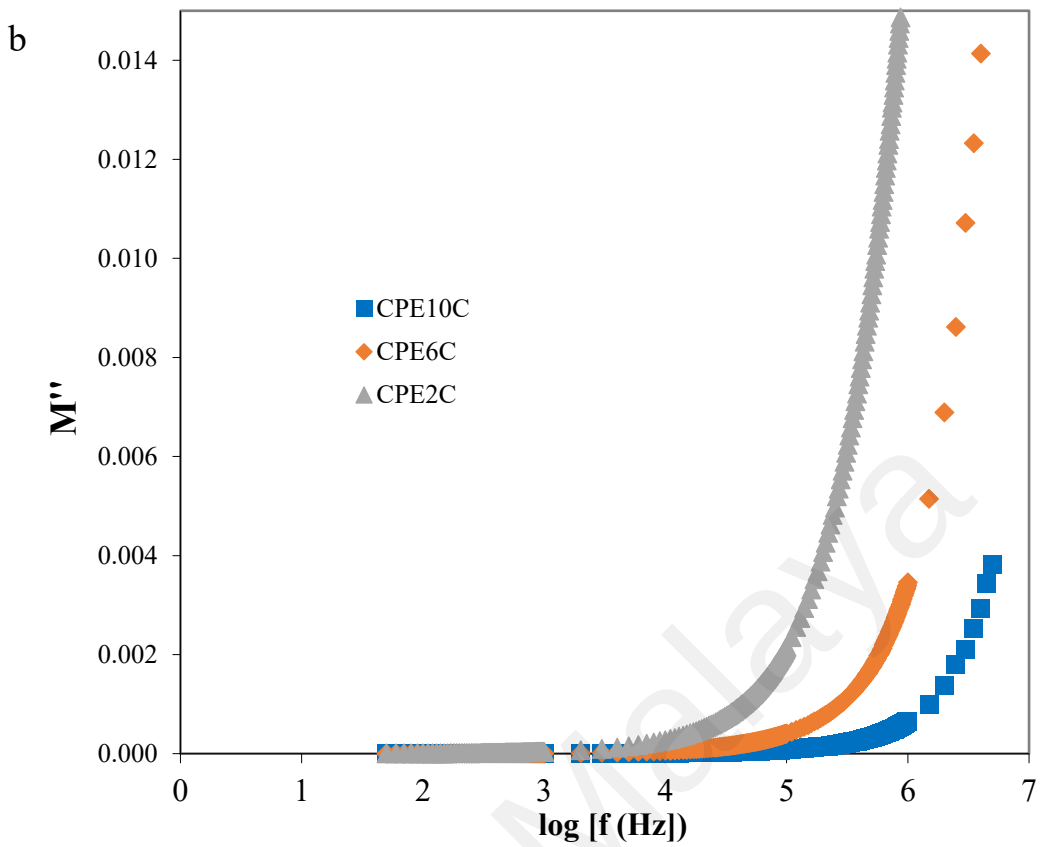

Figure 5.12: The (a) real part and (b) imaginary part of dielectric moduli as a function of logarithmic frequency for PAA-$LiClO_4$-$BaTiO_3$: CPE2C, CPE6C and CPE10C in the frequency range of 50 Hz – 5 MHz at ambient temperature.

5.2.2 Electrochemical Properties

5.2.2.1 Electrochemical Stability Window of PAA-$LiClO_4$

The ESW of the PAA-$LiClO_4$ electrolyte system was determined with linear sweep voltammetry (LSV) in the potential range of -9.0 V to +4.0 V at a scan rate of 5 mV s^{-1}. LSV responses of the stainless-steel electrode/PE cell assembly are shown in Figure 5.13. It was found that PAA-based electrolyte systems exhibited an anodic stability up to 10 V within the selected potential range. Beyond the potential range, the PAA-$LiClO_4$ start to degrade. A previous literature reported an electrochemical stability of 5 V for the PCL/$LiClO_4$ electrolyte (Fonseca et al., 2006). From the result obtained it proved that PAA-$LiClO_4$ has a wider electrochemical stability window compared to the PCL/$LiClO_4$. The enhanced electrochemical stability could attribute by the electron delocalization of

perchlorate anions. The electron delocalization of perchlorate anions is induced by the strong electron withdrawing group to achieve a more stable state which resulting in the electrochemical stability. As stated by Kotz & Carlen, the electrochemical stability window above 3 V is meeting the minimum requirement for the electrochemical device applications (Kotz & Carlen, 2000). These clearly indicate when PAA-$LiClO_4$ electrolyte are applied in the electrochemical devices, it expected to be stable within the operating voltage.

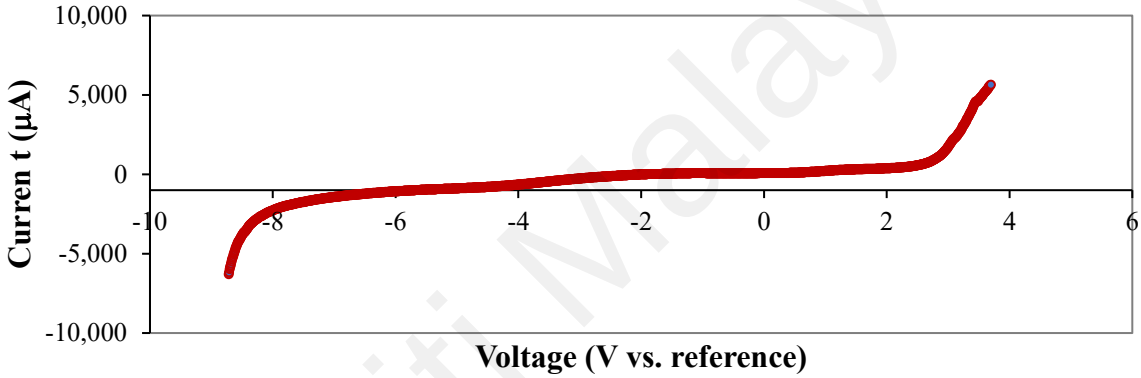

Figure 5.13 Linear Sweep voltammogram of PAA-$LiClO_4$ (10 wt.% $LiClO_4$) electrolyte system (P90-LC10) at ambient temperature. Scan rate: 5 mV s^{-1}.

5.2.2.2 Electrochemical Stability Window of PAA-$LiClO_4$-$BaTiO_3$

Figure 5.14 illustrates the ESW by LSV for PAA-$LiClO_4$-$BaTiO_3$ electrolyte system with 10 wt.% $BaTiO_3$ at ambient temperature. PAA-based electrolyte systems can be operated up to 11.5 V, from -10.0 V to +3.0 V. PAA-$LiClO_4$ doped with $BaTiO_3$ showed a wider electrochemical stability of 11.5 V when in the voltage between -9.5 to 2.0 V compared to the polymer electrolytes without dopant or lithium salt. This may be due to the presence of $BaTiO_3$ and $LiClO_4$ in the polymer matrices. Itoh and co-workers demonstrated a CPE prepared using PEO, $LiN(CF_3SO_2)_2$ and $BaTiO_3$ offered a wide ESW of 4.0 V (Itoh et al., 2003). The electrochemical stability of the lithium perchlorate and di-ureasil matrix

electrolyte was report to be 4.2 V (Silva et al., 2006). ESW of at least 4.0 V was obtained for the polyethylene oxide (PEO)-based CPE comprised of PEO, $LiClO_4$, and $BaTiO_3$ (Sun et al., 1999). As reported by Kotz & Carlen, optimized electrode and electrolyte materials should allow at least 3 V in electrochemical potential windows (Kotz & Carlen, 2000). The results also suggest that the PAA-$LiClO_4$-$BaTiO_3$ electrolyte system with 10 wt.% $BaTiO_3$ could be a promising material for the design and assembly of electrochemical devices.

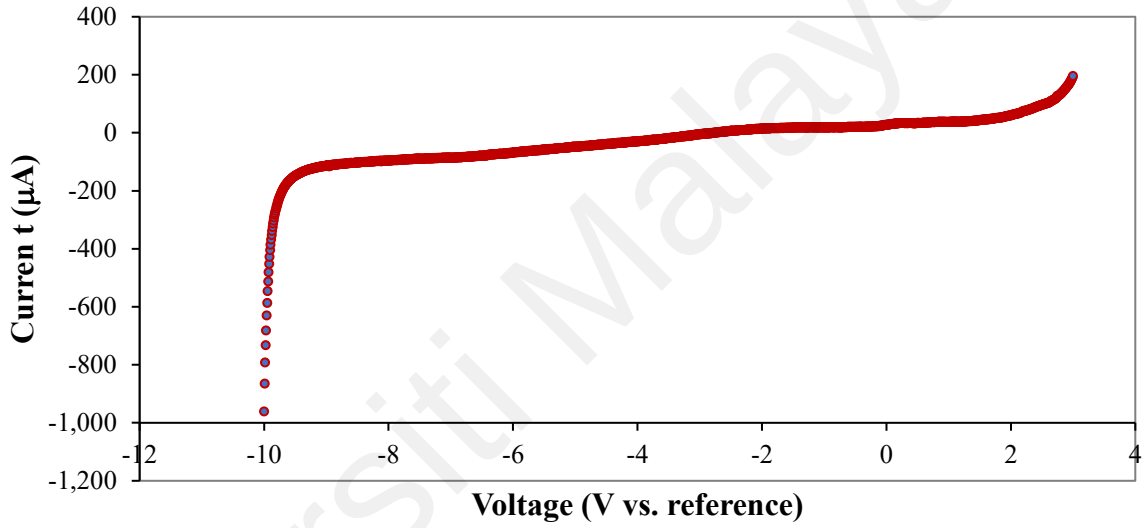

Figure 5.14: Linear Sweep voltammogram of PAA-$LiClO_4$-$BaTiO_3$ electrolyte (with 10 wt.% $BaTiO_3$) at ambient temperature. Scan rate: 5 mV s^{-1}.

5.2.3. Thermal Properties

5.2.3.1 Thermal Studies of PAA-$LiClO_4$

TGA is a thermal technique to examine the thermal stability of PE under inert atmosphere. The overall thermal properties of the PE systems can be investigated by determining the weight loss of the samples over a selective temperature range at a controlled uniform heating rate. The thermal stability of PEs was carried out via TGA under nitrogen atmosphere at a constant heating rate. The thermal properties of the polymer and PE systems are examined by using three selected representative composition. Figure 5.15

shows the overlay of four thermograms of pure PAA, P90-LC10, P85-LC15 and P80-LC20 within the temperature range of 20-600 ^{o}C. In the preparation of PEs, water is used as a solvent. The initial weight loss was due to the evaporation of water molecules that trapped in PAA-$LiClO_4$ film which resulting a total loss of 14%, 10%, 7% for the PAA-$LiClO_4$ systems with 10 wt.%, 15 wt.% and 20 wt.% $LiClO_4$, respectively. As can be seen from the curves, P80-LC20 exhibits a smallest initial weight loss percentage compared to P85-LC15 and P90-LC10.

There are four different stages of weight losses were observed upon heating pure PAA. The PAA degradation is discussed in Chapter 4.2.4.1. As can be seen from Figure 5.15, it is shown that the pure PAA decomposes at a temperature of 270 °C. For the PE samples with different $LiClO_4$ content, the decomposition initiated at a temperature slightly lower than 270 °C. This ascribed the addition of $LiClO_4$ into the PAA matrix reduces the heat resistivity in the decomposition of PE. All samples loss the weight upon subject to continuous heating. The third gradual weight loss starting at 320 °C could be attributed to the decarboxylation process. P80-LC20, P85-LC15, P90-LC10 portray small weight loss in this region. A total weight loss of 30% is measured for the PAA-$LiClO_4$ electrolytes, which is much higher compared to the total weight loss of 20% in PAA at 470 °C. Herewith it can be concluded that PAA-$LiClO_4$ electrolyte systems having better thermal profile than the pure PAA.

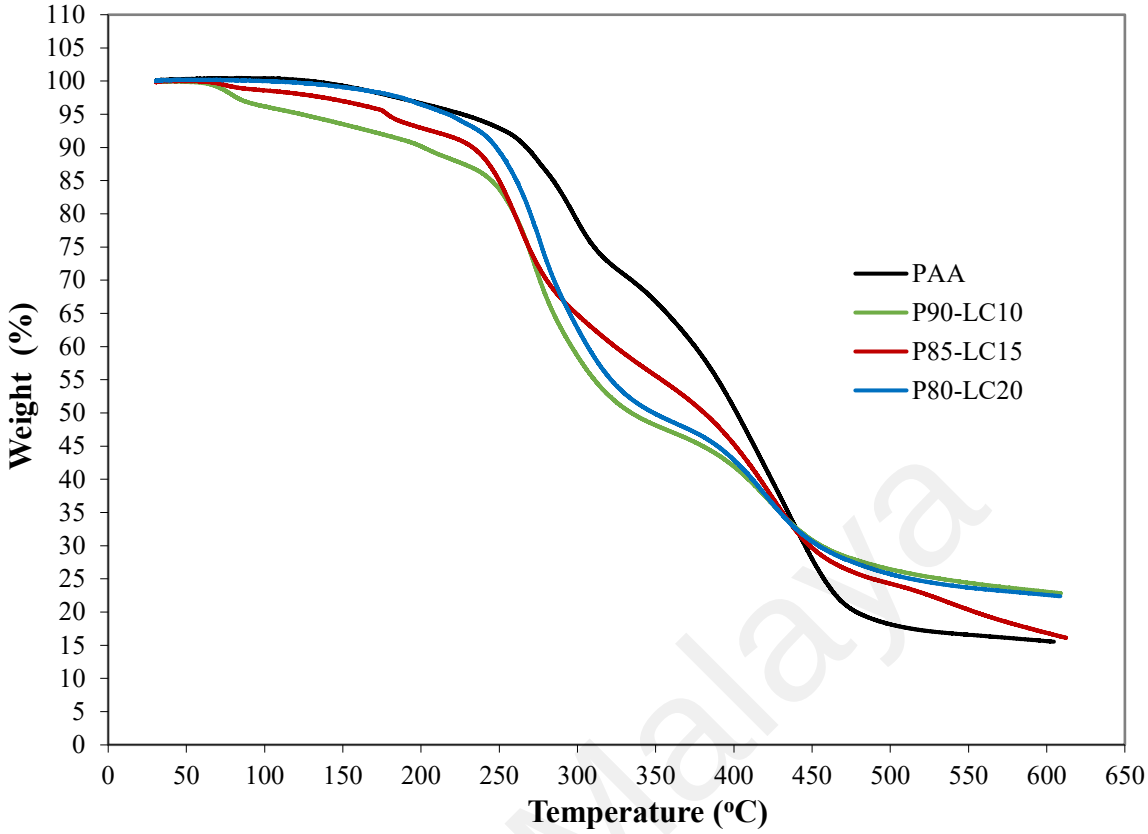

Figure 5.15: TGA thermograms of pure PAA, P90-L10, P85-L15, and P80-L20 in the temperature range of 20–600 °C under inert condition.

5.2.3.2 Thermal Studies of PAA-$LiClO_4$-$BaTiO_3$

Figure 5.16 shows the TGA thermograms in nitrogen gas for PAA, CPE6C, CPE8C, CPE10C which representing pure PAA, PAA-$LiClO_4$-$BaTiO_3$ (6 wt.%), PAA-$LiClO_4$-$BaTiO_3$ (8 wt.%), and PAA-$LiClO_4$-$BaTiO_3$ (10 wt.%), respectively. In the initial dehydration stage, CPE6C shows a weight loss of 5%. On the contrary, 8% of mass loss has been observed for both CPE8C and CPE10C at 225 °C. It can be seen that CPE6C exhibits a smallest initial weight loss compared to CPE8C and CPE10C. The decomposition of the polymer compound led to a sharp weight loss for the subsequent stage. In this stage, all CPEs start to loss about 40% of weight at 320 °C. It was shown in the TGA curves that the residue weights of the CPEs were around 32% at 470 °C. However, the pure PAA attained a residue weight of 20% at 470 °C. At 600 °C, the residual mass of PAA and CPE are 16% and 20%, respectively. The results proven that

incorporation of $BaTiO_3$ improves the thermal stability of polymer electrolyte. A new thermal profile is observed thereafter compared to pure PAA.

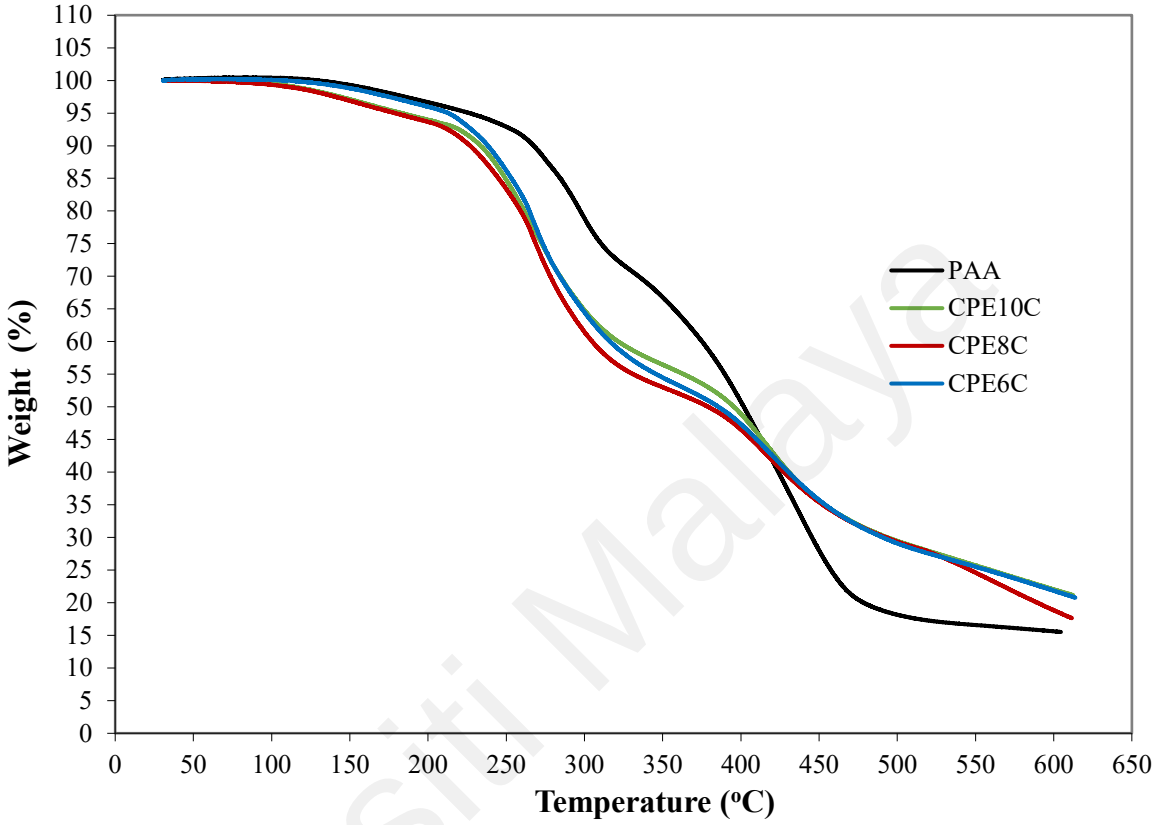

Figure 5.16: TGA thermograms of pure PAA, PAA-$LiClO_4$-$BaTiO_3$ in 6 wt.% (CPE6C), 8 wt% (CPE8C) and 10 wt.% (CPE10C) in the temperature range of 20–600 °C under inert condition.

5.2.4 Structural Properties

5.2.4.1 X-ray Diffraction Studies of PAA-$LiClO_4$

X-ray diffraction is an analytical technique to examine the degree of amorphous nature of testing materials such as polymer electrolytes, and to confirm the complexation among polymers and dissolution salts. Figure 5.17 presented the XRD patterns of pure PAA, pure $LiClO_4$, P90-LC10, P85-LC15 and P80-LC20. The complexation among the constituents in the PE systems can be proven by observing shifting, broadening or shortening in the peaks (Ramesh & Lu, 2012).

As can be observed in Figure 5.17, the sharp intense peaks at 2θ = 21.3°, 31.7° suggests the crystalline behaviour of $LiClO_4$. The amorphous behaviour increases with the increasing of the lithium salt content. It can be seen from the Figure 5.17 that the XRD pattern (c)-(e) of PEs show a significant peak broadening at 21.3°, 23.3°, 31.5°, 35.8°, compare to these peaks at $LiClO_4$. The results confirmed the complexation between PAA and $LiClO_4$ and implied the high degree of amorphous nature in the PAA-$LiClO_4$ electrolytes. By comparing the diffraction patterns between PEs, it is observed that the intensity of these peaks in P90-LC10 is reduced after the impregnation of more $LiClO_4$ to the P85-LC15 and P80-LC20 matrices. The observation implies that the orderly arrangement of the polymer chain is disrupted by the addition of $LiClO_4$. The further increase in the amorphous nature of the polymer matrix initiates the ionic hopping mechanism which leads to a higher ionic conductivity (Ramesh & Liew, 2013).

The observations signify that the incorporation of lithium salt disrupts the orderly arrangement of polymer matrices. In this study, the degree of crystallinity is quantified using full width at half maximum (FWHM) for the sharp intense peaks between 2θ = 23° to 24°, where the values obtained were 0.2860°, 0.2426° and 0.2340° for P90-LC10, P85-LC15 and P80-LC20, respectively. The degree of crystallinity is reduced and in other words the amorphous character increases. Higher loading of lithium salt reveals a higher amorphous degree which improves the ionic transportation in the PE systems leading to higher ionic conductivity.

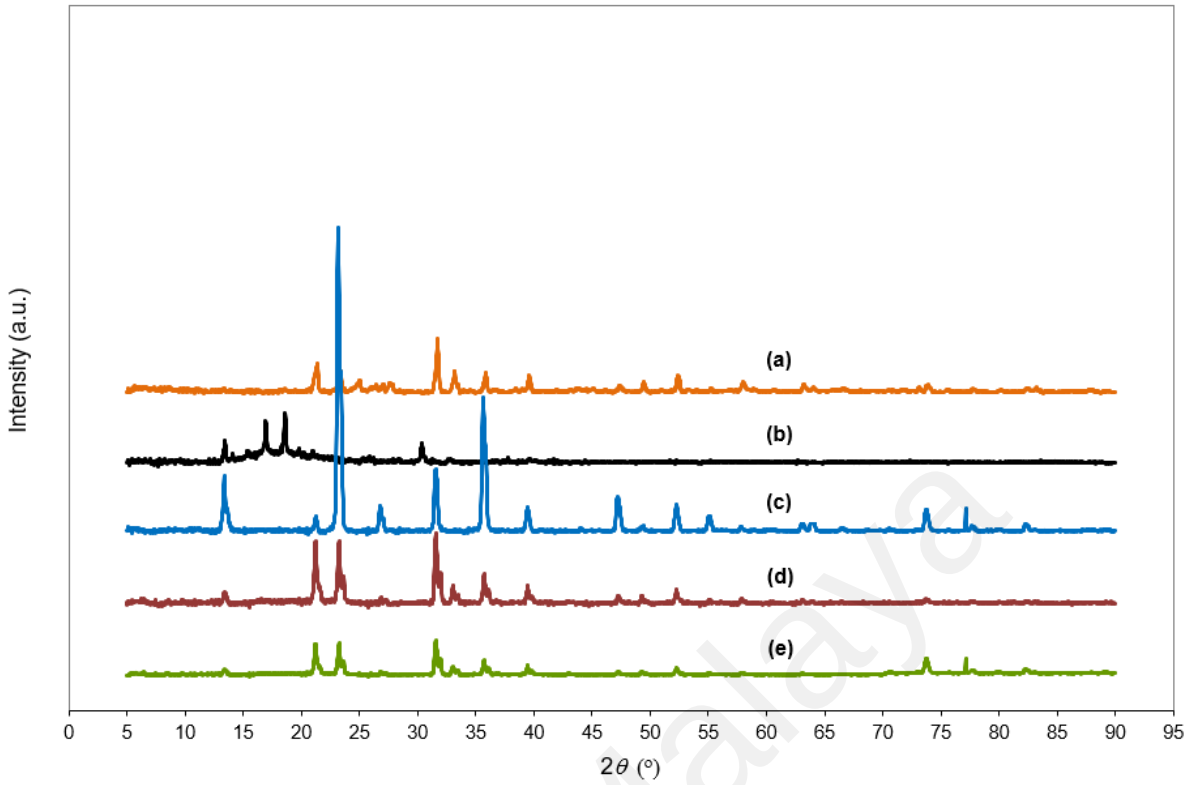

Figure 5.17: XRD patterns of (a) $LiClO_4$, (b) pure PAA, (c) P90-LC10, (d) P85-LC15, and (e) P80-LC20.

5.2.4.2 X-ray Diffraction Studies of PAA-$LiClO_4$-$BaTiO_3$

Inclusion of $BaTiO_3$ would increase the amorphous nature within the CPE matrix by demolishing the orderly arrangement of the polymer backbone. Shifting or broadening of peaks can be an evidence of complexation between the constituents in the electrolyte systems (Ramesh & Lu, 2012). Figure 5.18 shows the X-ray diffractograms of PAA, $LiClO_4$, $BaTiO_3$, CPE10C, CPE8C, and CPE6C.

A highly crystalline behaviour of $BaTiO_3$ is indicated by the intense and sharp crystalline peaks at 2θ = 22.3°, 31.7°, 39.1°, 45.4°, 51.2°, 56.3°, 66.0°, and 75.1°. On the contrary, amorphous character is demonstrated when the composite PE shows peak broadening at the same peaks. Ionic hopping mechanism which initiates by a higher degree of amorphous nature in PE matrix could lead to a higher ionic conductivity due to a more flexible polymer chain. The complexion of CPE is attributed by the presence of

interactions between PAA, $LiClO_4$ and $BaTiO_3$. The interactions within polymer matrix is weakening as a result of the incorporation of $BaTiO_3$ particles, and thus the ordered arrangement of polymer complex is disrupted. The segmental mobility of polymer backbone is enhanced by the increase in amorphous proportion. This further enhances the flexibility of polymer chain and thus improve the ionic conductivity (Ramesh et al., 2011).

The FWHM obtained of the sharp intense peaks between 2θ = 31.0° to 33.0° were 0.3552°, 0.3846° and 0.3999° for CPE6C, CPE8C and CPE10C, respectively. Increases in FWHM of CPE10C indicates reduced in crystallinity degree and thus the amorphous character increases.

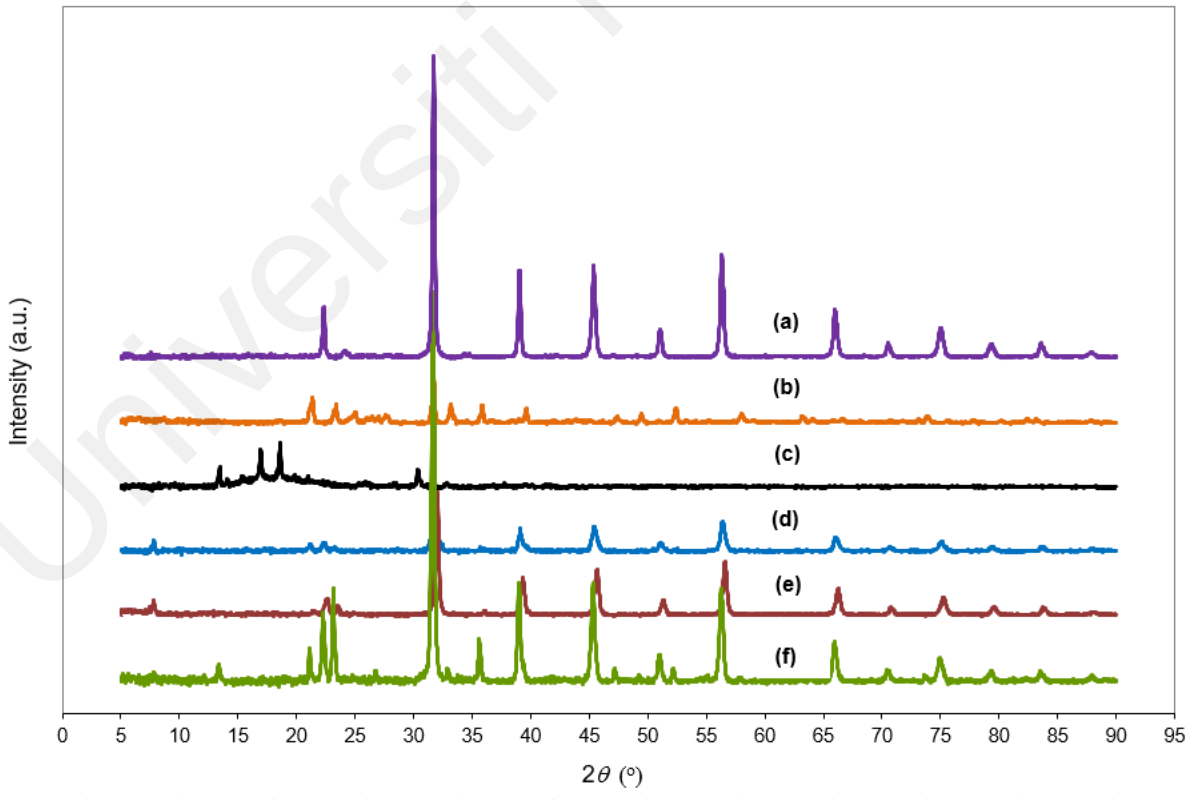

Figure 5.18: XRD pattern of (a) $BaTiO_3$, (b) $LiClO_4$, (c) pure PAA, (d) CPE10C, (e) CPE8C, and (f) CPE6C.

5.2.4.3 ATR-FTIR Studies of PAA-$LiClO_4$

Evidence of complexation between polymer host and inorganic salt could be deduced based on spectroscopic method. The ATR-FTIR spectra of pure PAA, pure $LiClO_4$, P90-LC10, P85-LC15 and P80-LC20 are displayed in Figure 5.19. As reported in the previous literature, the signature vibration bands of $LiClO_4$ were found at 1630, 1368, 1089, 633 and 616 cm^{-1} (Sim et al., 2010). As presented in Figure 5.19, the vibration modes of ClO_4^- ion were observed at the vibration modes at 1627, 1088, 688 and 623 cm^{-1} which is very near to the vibration bands as reported in the literature. As depicted from the Figure 5.19, the characteristic vibration bands of ClO_4^- at 1627 and 1088 cm^{-1} was found in the spectra of PAA-$LiClO_4$ electrolytes indicating the complexation between the PAA and $LiClO_4$. The reduce intensity of the vibration band near 1721 cm^{-1} implies that most of the COO^- groups of the PAA chain are attached to the Li^+ ions from the $LiClO_4$.

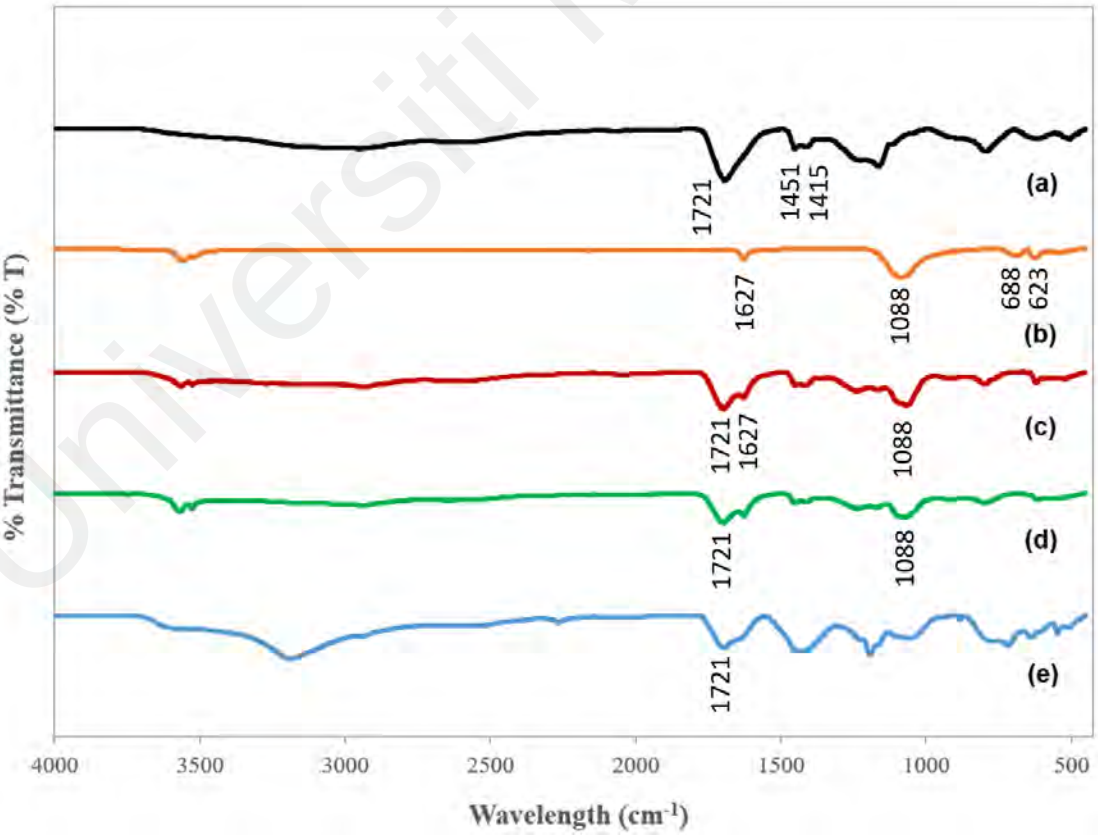

Figure 5.19: ATR-FTIR Spectra of (a) pure PAA, (b) pure $LiClO_4$, (c) P90-LC10, (d) P85-LC15, and (e) P80-LC20.

5.2.4.4 ATR-FTIR Studies of PAA-$LiClO_4$-$BaTiO_3$

ATR-FTIR studies the spectra of pure PAA, pure $LiClO_4$, $BaTiO_3$ and PAA-$LiClO_4$-$BaTiO_3$ electrolyte systems. The complexation can be evidently found via the changes in the vibration modes of the polymer host. As depicted in Figure 5.20(b), the two characteristic vibration bands of $LiClO_4$ near 1627 and 1088 cm^{-1} disappeared in the most spectra of respective CPEs at Figures 5.20(d), (e) and (f). This infers the ClO_4^- anions are involved in the complexation with the groups from PAA. As shown in Figure 5.20(a), the vibration band of pure PAA were observed at 1721, 1451 and 1415 cm^{-1} denoting to the C-O and C=O stretching of COOH in PAA which agreed with the past study reported by Sankar and co-authors (Sankar et al., 2012). The C=O stretching of COOH groups in PAA at 1721 cm^{-1} was reduced in the band intensity along with a slightly shifted to 1695 cm^{-1}. Meanwhile, the ClO_4^- stretching at 1088 cm^{-1} was reduced in band intensity in Figures 5.20(e) and (f) further confirms the interactions between PAA and $LiClO_4$.

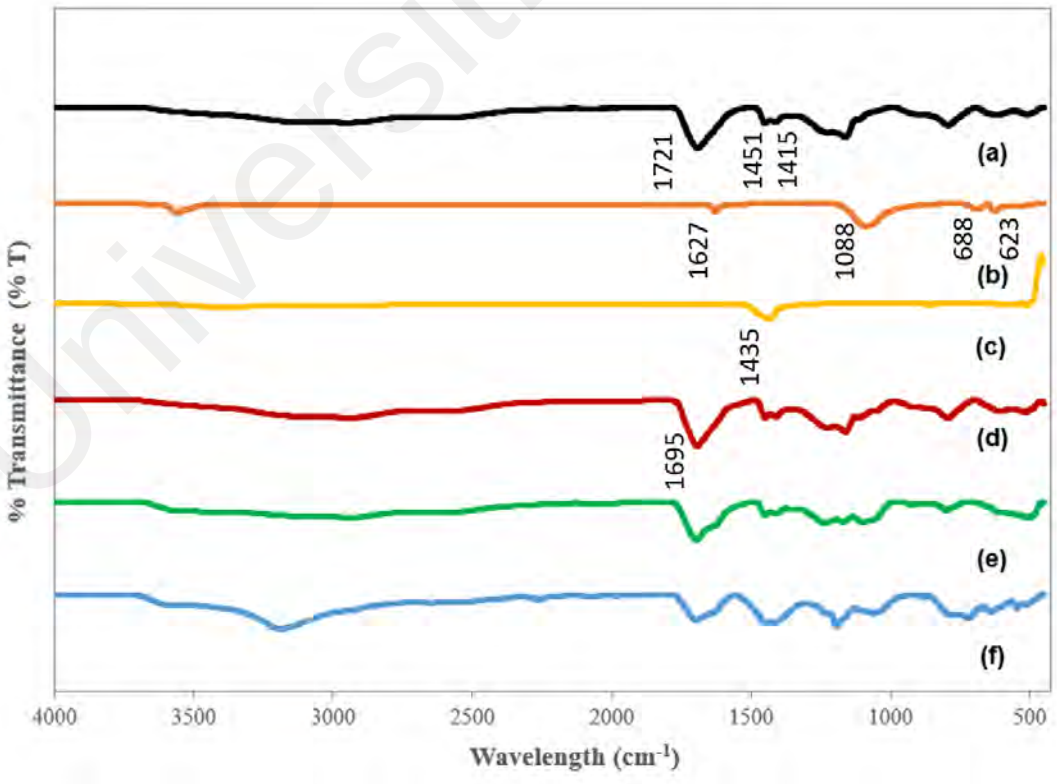

Figure 5.20: ATR-FTIR Spectra of (a) PAA, (b) $LiClO_4$, (c) $BaTiO_3$, (d) CPE10C, (e) CPE8C, and (f) CPE6C.

5.3 Conclusion

Novel PEs/CPEs composed of combinations of PAA, $LiClO_4$ and $BaTiO_3$ were prepared via solvent casting technique. The chemical compositions of the electrolyte materials were optimized by investigating the ratio of PAA, lithium salt and $BaTiO_3$ content on the ionic conductivity. The highest ionic conductivity was found to be 2.4×10^{-6} S cm^{-1} for PE with 90% PAA and 10% $LiClO_4$; and 1.0×10^{-5} S cm^{-1} was obtained found with the addition of 10 wt.% $BaTiO_3$ into this electrolyte system. Temperature dependence study demonstrated that the ionic conductivity obeys Arrhenius equation with a low activation energy in the temperature range of 30 °C to 120 °C. The dielectric permittivity and moduli of the electrolyte materials are studied. The dielectric permittivity is decreased with frequency but increased with $LiClO_4$ content for every frequency. The formation of electrical double layer has been proven in the dielectric permittivity studies.

The optimized PAA-$LiClO_4$ and PAA-$LiClO_4$-$BaTiO_3$ electrolyte systems demonstrated a maximum ESW of 10.0 V and 11.5 V, respectively. Thermal stability study shown that the thermal decomposition was slightly improved with the increases of $LiClO_4$ content in PEs or $LiClO_4$ content in CPEs. Structural study by XRD exhibits highly amorphous fraction of the PAA-$LiClO_4$ based electrolyte materials with increased $LiClO_4$/$BaTiO_3$ content. ATR-FTIR analysis ascertain the presence of interactions between PAA and $LiClO_4$. This study confirmed a promising material of PEs/CPEs with enhanced characteristics which potentially used in the applications in electrical and electrochemical devices.

CHAPTER 6: COMPARATIVE STUDIES BETWEEN DIFFERENT ELECTROLYTE SYSTEMS

6.1 Introduction

Chapters 4 and 5 have presented the results obtained from the characterization study. Critical review and chemistry insight of the materials and their properties are discussed. Chapter 6 reviews the results obtained from both Chapters 4 and 5 in a cross-comparison manner, between PEs with different conducting salts; or between same PE systems with and without the incorporation of dopant. This including the comparison of the properties and characteristics between PAA/$LiBF_4$ and PAA/$LiClO_4$ electrolyte systems; and the comparison of the properties and characteristics between PAA/$LiBF_4$ or PAA/$LiClO_4$ electrolyte systems with the respective CPE systems.

6.2 Results and Discussion

6.2.1 Ambient Temperature-Ionic Conductivity Studies

6.2.1.1 Comparison between Polymer Electrolytes with Different Conducting Salts

Figure 6.1 show the ionic conductivity with different inorganic salt content (wt.%) for the PAA/$LiBF_4$ and PAA/$LiClO_4$ systems at ambient temperature. Even though the same polymer host is used for the preparation of different systems, the change in the trend of the plots in the figure is much depending on the nature of the conducting salts. In PAA/$LiBF_4$ electrolyte system, the highest ionic conductivity is occurred when the PAA/$LiBF_4$ content is at 30 wt.%. However, in PAA/$LiClO_4$ electrolyte system, the highest ionic conductivity is obtained when the PAA/$LiClO_4$ content is at 10 wt.%.

Table 6.1 summarized the ambient temperature ionic conductivity obtained. PAA/$LiBF_4$ system offers higher ionic conductivity compared to PAA/$LiClO_4$ system. The chemical

structure of $LiBF_4$ offers more stable polymerization matrix. $LiClO_4$ may be less stable within the polymer matrix as compared to $LiBF_4$. Figures 6.2(a) and 6.2(b) illustrated the chemical structure of both $LiBF_4$ and $LiClO_4$. Tetrafluoroborate ions (BF_4^-) act as counter ions which participate in the ionic conduction. In the dissociation of PAA/$LiBF_4$ electrolyte to form lithium cations and BF_4^- anions, increase the number of mobile ions and the degree of disorder of the matrix. In the increasing of the lithium salt concentration, the ionic conductivity increases due to the increase of the mobile BF_4^- anions; the excessive conducting salt disrupt the crystalline morphology of the PAA matrix. The amorphous nature of the polymer matrices often correlates with high ionic conductivity. When the $LiBF_4$ content is more than 30 wt.% and $LiClO_4$ content is exceeding 10 wt.%, the lithium salt could have re-associated, and the formation of neutral ion pairs which could reduce the availability of freely mobile ions.

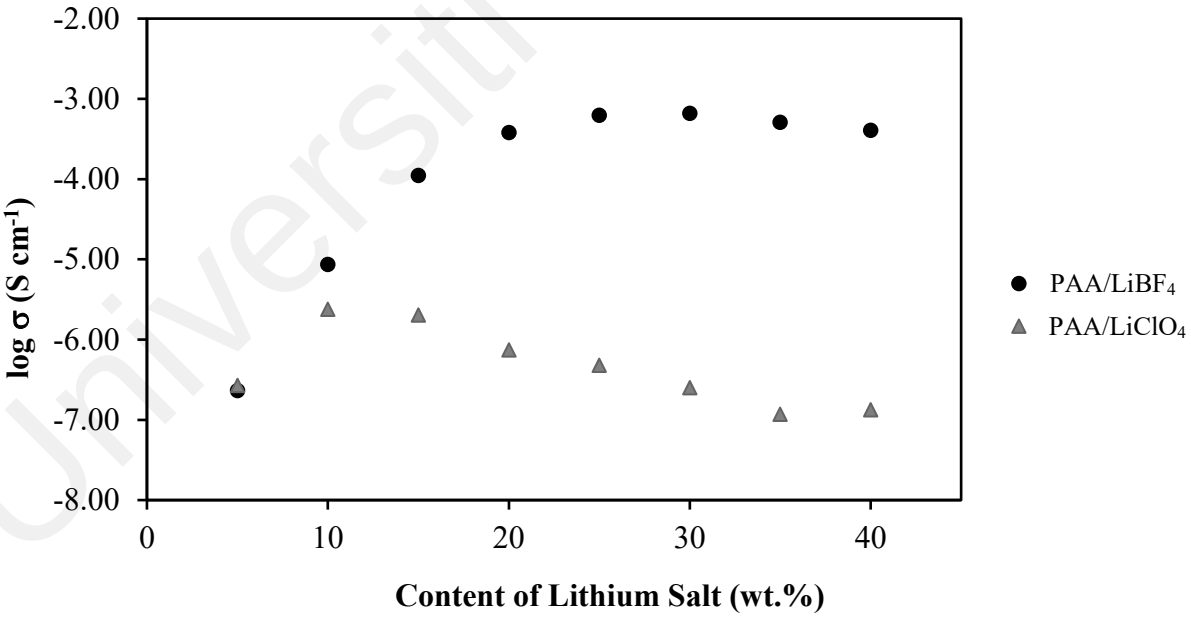

Figure 6.1: Effect of types of conducting salt and respective content on the ionic conductivity of PAA-based electrolytes at ambient temperature.

Table 6.1: Ionic conductivity of poly(acrylic acid) electrolyte systems with optimized lithium salt/barium titanate content at ambiet temperature.

Polymer Electrolyte Systems	Ionic Conductivity, S cm^{-1}
PAA/$LiBF_4$	6.61×10^{-4}
PAA/$LiBF_4$/$BaTiO_3$	8.95×10^{-4}
PAA/$LiClO_4$	2.40×10^{-6}
PAA/$LiClO_4$/$BaTiO_3$	1.00×10^{-5}

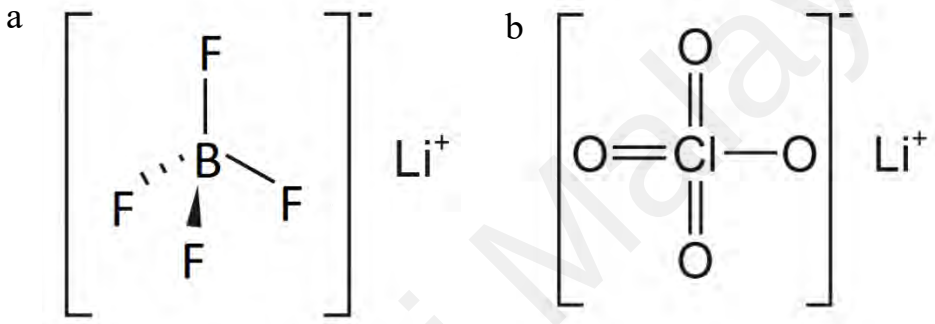

Figure 6.2: The chemical structure of both conducting salts: (a) $LiBF_4$ and (b) $LiClO_4$.

6.2.1.2 Comparison between Polymer Electrolytes with Respective Composite Polymer Electrolytes

Table 6.2 demonstrated that the incorporation of $BaTiO_3$ particles into the PE systems improved the ionic conductivity of the respective electrolyte systems. Dopant content has a direct effect on ionic conductivity of both systems whereas higher dopant content increases the ionic conductivity. The incorporation of $BaTiO_3$ as dopant may assist in dissociating lithium salts into lithium ions. Dopant further disrupts the ordered structure of the polymer matrix increases the amorphous nature of the structure of macromolecules.

Table 6.2: Effect of $BaTiO_3$ content on the ionic conductivity of (a) PAA- $LiBF_4$ and (b) PAA- $LiClO_4$ electrolytes at ambient temperature.

Content of $BaTiO_3$ (wt.%)	Ionic conductivity, log σ (S cm^{-1})	
	PAA-$LiBF_4$-$BaTiO_3$	PAA-$LiClO_4$-$BaTiO_3$
2.0	-3.756	-5.419
4.0	-3.424	-5.251
6.0	-3.225	-5.206
8.0	-3.108	-5.102
10.0	-3.048	-4.998

6.2.2 Temperature Dependent-Ionic Conductivity Studies

The results obtained from temperature dependent-ionic conductivity studies of PAA-$LiBF_4$, PAA-$LiBF_4$-$BaTiO_3$, PAA-$LiClO_4$ and PAA-$LiClO_4$-$BaTiO_3$ indicate that all PE and CPE systems used in the study are thermally-assisted and obey the Arrhenius Theory. As the temperature is increased from 30 °C to 120 °C, the ionic conductivity of all polymer electrolyte systems increased. In the optimum composition of PE/CPE, the high ionic conductivity is associated with the low activation energy of the ion conduction. It can be confirmed that the ion movement in the CPE was faster than in the PE. Upon addition of $BaTiO_3$, the interaction between the polymer system and lithium ions is disturbed. This causes less energy required for the charge carriers hopping process.

6.2.3 Dielectric Permittivity Studies

The dielectric permittivity studies for PAA-$LiBF_4$ and PAA-$LiClO_4$ shown the similar pattern in the dielectric permittivity plot. The observations from both plots showing that when the content of inorganic salts either $LiBF_4$ or $LiClO_4$ in the PE matrices is increased, the respective dielectric permittivity also increased. Incorporating more conducting salt

resulting a re-association of lithium salt which consequently reduces the availability of mobile ions and thus the dielectric constant values.

6.2.4 Modulus Studies

The real and imaginary parts of dielectric moduli for all PAA-$LiBF_4$, PAA-$LiBF_4$-$BaTiO_3$, PAA-$LiClO_4$ and PAA-$LiClO_4$-$BaTiO_3$ electrolyte systems are shown in Figures 4.10, 4.11, 5.11 and 5.12, respectively. As can be seen from figures 4.10 (Chapter 4) and 5.11 (Chapter 5), the frequency dependence of real and imaginary parts of dielectric moduli for PAA-$LiBF_4$ and PAA-$LiClO_4$ electrolyte systems shown the similar pattern in the plots. Both figures shown that the relaxation peaks are absent. The plots also indicate abrupt increments are found in the higher frequency end and a long tail approach zero at lower frequency region. As shown in Figures 4.10 and 5.11, the PAA based electrolytes with highest ionic conductivities (PAA with 30 wt.% $LiBF_4$ and PAA with 10 wt.% $LiClO_4$) are indicated that the abrupt increase in the plot was happened at highest frequency, compared to other compositions.

Figures 4.11 (Chapter 4) and 5.12 (Chapter 5) depict the frequency dependence of real and imaginary parts respectively, of dielectric moduli for PAA-$LiBF_4$-$BaTiO_3$ and PAA-$LiClO_4$-$BaTiO_3$ CPEs. Both figures shown the similar patterns with the respective PE systems. As can be seen from the figure, no characteristic peaks are observed within the experimental frequency window. The long tails which tend to move towards zero at a lower frequency region indicate the suppression of electrical double layer effect at the interface of electrode-electrolyte. This implies the negligible contribution of electrode polarization. The decline suggested that the excessive amount of $BaTiO_3$ could assist in the dissociation of conducting salt into ions which accumulate at the electrode-electrolyte interface in lower frequency range. Another observation for both figures are the CPEs

with highest ionic conductivities shifted at the higher frequency end. This is also aligned with the results obtained from their respective PEs.

6.2.5 Electrochemical Stability Window

Table 6.3 summarized the ESW obtained from all optimized PE and CPE systems. The LSW studies indicate that the ESW for CPE is wider than the respective PE. PAA-$LiBF_4$ resulted an ESW of 3.2 V however the PAA-$LiBF_4$-$BaTiO_3$ have an ESW of 4.0 V. PAA-$LiClO_4$ with an ESW of 10.0 V but the respective CPE, i.e. PAA-$LiClO_4$-$BaTiO_3$ have an ESW of 11.5 V. Therefore, PEs doped with dopant showed a wider electrochemical stability compared to the PEs without dopant. The combination of conducting salt and $BaTiO_3$ in the composite matrix offers a wider electrochemical stability range.

Table 6.3: Electrochemical stability window for PAA-$LiBF_4$, PAA-$LiBF_4$-$BaTiO_3$, PAA-$LiClO_4$ and PAA-$LiClO_4$-$BaTiO_3$ with selected potential range at ambient temperature. Scan rate: 5 mV s^{-1}.

PE/CPE sample	Electrochemical stability window (V)	Potential range (V)
PAA-$LiBF_4$	3.2	-1.5 to +1.7
PAA-$LiBF_4$-$BaTiO_3$	4.0	-2.5 to +1.5
PAA-$LiClO_4$	10.0	-7.5 to +2.5
PAA-$LiClO_4$-$BaTiO_3$	11.5	-9.5 to 2.0

In the comparison between PEs of different conducting salt, PAA-$LiClO_4$ offers a wider ESW compared to PAA-$LiBF_4$. The wider electrochemical stability range of PAA-$LiClO_4$ systems could be attributed by the electron delocalization of perchlorate anions, which is induced by the strong electron withdrawing group. Since the perchlorate anions achieve a more stable state, it is expected that the electrochemical stability would be improved.

The results also suggest that the PAA-$LiClO_4$-$BaTiO_3$ electrolyte system which could be a promising material for the design and assembly of electrochemical devices. Therefore, the changes in the PEs' composition that affected their ability to conduct ions also affected their ESW.

6.2.6 Thermal Studies

Table 6.4 Summarized the residual weight of all tested PEs and CPEs at 600 °C. All tested PEs and CPEs exhibit higher residual weight at 600 °C compared to the pure PAA. This indicates that the incorporation of conducting salt and dopant enhanced the thermal stability of the polymer material. In PAA-$LiBF_4$ electrolyte system, different weight percent of $LiBF_4$ did not have significant effect in the residual weight at 600 °C. However, the doping of $BaTiO_3$ into the PE system resulted a significant changed in the thermal stability, whereas 6, 8 and 10 wt.% of $BaTiO_3$ resulted a 37, 23 and 19% of residual weight. The 37% of residual weight for CPE6B is the highest residual weight obtained among all the tested systems in this study. For PAA-$LiClO_4$ electrolyte system, incorporation of $LiClO_4$ into PAA also increased the thermal stability from 16% to 24%, which is slightly better than the respective CPE. In overall, PAA-$LiBF_4$ chain offers a better thermal stability compared to PAA-$LiClO_4$ system. This could be attributed to the decomposition of PAA-$LiBF_4$ only happened in a very high temperature range.

Table 6.4: Summarized the residual mass of all tested PEs and CPEs at 600°C.

Sample Nature	Tested Sample	Residual weight at 600°C (%)
PAA	PAA	16
PAA-$LiBF_4$	P80-LB20	26
	P75-LB25	27
	P70-LB30	26
PAA-$LiBF_4$-$BaTiO_3$	CPE6B	37
	CPE8B	23
	CPE10B	19
PAA-$LiClO_4$	P90-LC10	24
	P85-LC15	17
	P80-LC20	24
PAA-$LiClO_4$-$BaTiO_3$	CPE6C	20
	CPE8C	17
	CPE10C	20

6.2.7 Structural Studies

The XRD analyses drawn the same conclusion over the PE/CPE systems tested. The study indicates that the crystallinity of the structural have reduced with the evidence of the appears of intense and sharp peaks, or shifting of peaks after the complexation of conducting salts. For PAA-$LiBF_4$ electrolytes, the evidence of the complexation between PAA and $LiBF_4$ is the disappearance of the crystalline peaks of PAA at $2\theta = 13.5^o$, 17.0^o, 18.6^o, and 30.2^o. For PAA-$LiClO_4$ electrolytes, a significant peak broadening at 21.3°, 23.3°, 31.5°, 35.8° confirmed the complexation between PAA and $LiClO_4$ and implied the high degree of amorphous nature in the PAA-$LiClO_4$ electrolytes.

In the XRD plot of PAA-$LiBF_4$-$BaTiO_3$ electrolyte, the absent of the sharp and intense crystalline peaks at 2θ = 22.3°, 31.6°, 39.1°, 45.4°, 56.4° of $BaTiO_3$ and 2θ = 21.2°, 23.6°, 31.6°, 32.8°, 36.3°, 40° of $LiBF_4$ indicate the complete complexation of CPE. CPE6 shows medium sharp peaks at 24.7, 46.3° and broad peak at 28.2° which further divulges the semicrystalline behaviour of the material. For PAA-$LiClO_4$-$BaTiO_3$ electrolyte, amorphous character is demonstrated by the broadening of the intense and sharp crystalline peaks at 2θ = 22.3°, 31.7°, 39.1°, 51.2°, 56.3° and 75.1°.

6.3 Conclusion

The ambient temperature-ionic conductivity studies shown that PAA-based electrolyte mixed with $LiBF_4$ have higher ionic conductivity than the PAA electrolyte mixed with $LiClO_4$. CPEs indicate better ambient temperature ionic conductivity than the respective PEs. Temperature dependence-ionic conductivity studies shown that all PE/CPE systems obey the Arrhenius theory which reveal that ion conduction mechanism is thermally assisted. Typical properties of electric material such as PAA-$LiBF_4$**,** PAA-$LiBF_4$-$BaTiO_3$**,** PAA-$LiClO_4$ and PAA-$LiClO_4$-$BaTiO_3$ are demonstrated by dielectric study via AC-impedance spectroscopy. PAA-$LiClO_4$ and PAA-$LiClO_4$-$BaTiO_3$ have wider ESW compared to PAA-$LiBF_4$ and PAA-$LiBF_4$-$BaTiO_3$.

Thermal study confirmed that all tested PEs and CPEs exhibit higher residual weight at 600 °C compared to the pure PAA. But PAA-$LiBF_4$ chain offers a better thermal stability compared to PAA-$LiClO_4$ system. In structural study via XRD, the confirmation of complexation and increase of amorphous nature is demonstrated via the shifting, disappearing or broadening of the peaks from each individual components of electrolyte systems. In the ATR-FTIR analysis, the confirmation of complexation between polymer

host, lithium salt and $BaTiO_3$ is demonstrated through the reduction, shifting or disappearing of the stretching vibration bands.

CHAPTER 7: CONCLUSION

7.1 Preamble

This research study entitled "Study of Poly(acrylic acid) and Lithium Tetrafluoroborate/Lithium Perchlorate Based Polymer Electrolytes" is conducted. The research study is completed and met the objectives of the project as prescribed in Chapter 1.4 of this thesis. The outcomes of the study are presented in the Chapters 4, 5 and 6 of this thesis, and also presented in some articles and proceedings as listed in the List of Publications and Papers Presented of this thesis. The summary of the research outcomes to meet the objectives stated in this research are as follows:

Objective 1: To formulate polymer electrolytes and composite polymer electrolytes using poly(acrylic acid) as a polymer host, lithium tetrafluoroborate and lithium perchlorate as conducting salts, and barium titanate as dopant/filler.

The materials and methods adopted for the preparation of all electrolyte systems in this research study is presented in Chapter 3. Poly(acrylic acid) is used as a polymer host; which mixed with lithium tetrafluoroborate or lithium perchlorate for the preparation of poly(acrylic acid)/ lithium tetrafluoroborate and poly(acrylic acid)/ lithium perchlorate electrolytes. Barium titanate is incorporated into both electrolyte systems to prepare poly(acrylic acid)/ lithium tetrafluoroborate/barium titanate and poly(acrylic acid)/lithium perchlorate/barium titanate composite polymer electrolytes. All electrolyte systems are prepared via solvent casting technique.

In the preparation of PEs via solvent casting, the respective fraction of PAA and lithium salt are mixed and stirred at 100 °C for 12 h. Then the PE solution is casted on petri dish and dry in oven at 50 °C for 12 h. In the preparation of CPEs via solvent casting, the

respective fraction of PAA, lithium salt and barium titanate are mixed and ultrasonicated for 30 minutes, followed by the stirring at 100 °C for 12 h. Then the CPE solution is cast on petri dish and dry in oven at 50 °C for 12 h.

Objective 2: To perform chemical, electrical, electrochemical, thermal and structural characterization of the prepared polymer electrolytes and composite polymer electrolytes.

Prepared polymer electrolyte and composite polymer electrolyte systems: poly(acrylic acid)/lithium tetrafluoroborate electrolyte, poly(acrylic acid)/lithium tetrafluoroborate/barium titanate electrolyte, poly(acrylic acid)/lithium perchlorate electrolyte, and poly(acrylic acid)/lithium perchlorate /barium titanate electrolyte were characterized using chemical, electrical, electrochemical, thermal and structural studies.

AC-Impedance Spectroscopy is used for ambient temperature-ionic conductivity study, temperature dependent-ionic conductivity study, dielectric permittivity study, loss tangent and modulus studies; linear sweep voltammetry is used for electrochemical stability window study; thermogravimetric analysis is used for thermal study; and X-ray diffraction and ATR-FTIR analyses are used for structural study. The characterization of poly(acrylic acid)/ lithium tetrafluoroborate and poly(acrylic acid)/ lithium tetrafluoroborate/barium titanate presents in Chapter 4. The experimental results and corresponding discussion are written in separated subchapters and sub-subchapters of Chapter 4. PAA-hosted sample with 30 wt.% of $LiBF_4$ (P70-L30) achieved the highest ionic conductivity of 6.61×10^{-4} S cm^{-1}. The highest ionic conductivity of 8.95×10^{-4} S cm^{-1} is obtained with the 10 wt.% of $BaTiO_3$ in optimized composition of PAA/$LiBF_4$. The temperature-dependence ionic conductivity study of both electrolyte systems demonstrated a straight line in the Arrhenius plot which confirmed the increase of

temperature leads to the increase in ionic conductivity. The dielectric permittivity study shown that the dielectric permittivity increases when the content of inorganic salts in the PAA/$LiBF_4$ electrolyte matrices is increased. A higher dielectric constant was found for CPE10, i.e. PAA/$LiBF_4$ with 10 wt.% of $BaTiO_3$. PAA-$LiBF_4$ demonstrated a wide ESW at about 3.2 V within the selected potential range from -1.5 to +1.7 V. PAA-$LiBF_4$-$BaTiO_3$ electrolyte portrays a wide electrochemical stability of 4.0 V, in the potential range from -2.5 to +1.5 V. Incorporation of $LiBF_4$ improved the weight loss of polymer electrolytes where the total weight loss of pure PAA is 84% but reduced to 74% upon addition of 30 wt.% of $LiBF_4$. XRD results indicate that the increases of ionic conductivity of PAA-$LiBF_4$ and PAA-$LiBF_4$-$BaTiO_3$ resulting from the enhancement of the amorphous nature of the electrolyte systems.

The characterization of poly(acrylic acid)/ lithium perchlorate and poly(acrylic acid)/ lithium perchlorate /barium titanate presents in Chapter 5. The experimental results and corresponding discussion are written in separated subchapters and sub-subchapters of Chapter 5. The incorporation of 10 wt.% $LiClO_4$ demonstrated a highest ionic conductivity, which is 2.40×10^{-6} S cm^{-1}. The highest ionic conductivity of 1.0×10^{-5} S cm^{-1} was obtained for PAA-$LiClO_4$-$BaTiO_3$ electrolyte. From the temperature-dependence ionic conductivity study of both electrolyte systems, Arrhenius plot confirms the increase of ionic conductivity with the increase in temperature. From dielectric study, when $LiClO_4$ concentration of PAA-$LiClO_4$ electrolyte increased there is a high rise in dielectric constant values. The result also demonstrates that PAA-$LiClO_4$-$BaTiO_3$ electrolyte with higher dielectric constant is associated with the higher $BaTiO_3$ content. In the loss tangent studies of PAA-$LiClO_4$, the loss tangent peaks were found shifted towards higher frequency with the increasing $LiClO_4$ content. PAA-$LiClO_4$-$BaTiO_3$ electrolyte with 10 wt.% $BaTiO_3$ (CPE10C) exhibits the highest magnitude of tan

δ compared to CPE6C and CPE2C which could be attributed to the increase in number of lithium ions that participate in the ion conduction. The modulus study confirmed the effect of $LiClO_4$ in the dielectric properties of PAA-$LiClO_4$ electrolyte. From the electrochemical stability window study, PAA-$LiClO_4$ electrolyte system exhibited an anodic stability up to 10 V in the potential range of -9.0 V to +4.0 V at a scan rate of 5 mV s^{-1}. PAA-$LiClO_4$-$BaTiO_3$ electrolyte systems can be operated up to 11.5 V, from -10.0 V to +3.0 V. The thermal decomposition study shown that a total weight loss of 30% is measured for the PAA-$LiClO_4$ electrolytes, which is much higher compared to the total weight loss of 20% in PAA at 470 °C. It was shown in the study that the residue weights of the PAA-$LiClO_4$-$BaTiO_3$ electrolyte with 10 wt.% $BaTiO_3$ (CPE10C) was around 32% at 470 °C. The results proven that incorporation of $BaTiO_3$ improves the thermal stability of PE. The structural study indicates that higher loading of $LiClO_4$ reveals a higher amorphous degree which improves the ionic transportation in the PAA-$LiClO_4$ electrolyte systems leading to higher ionic conductivity. The increased complexion of PAA-$LiClO_4$-$BaTiO_3$ is attributed to the incorporation of $BaTiO_3$.

Objective 3: To compare the chemical, electrical, electrochemical, thermal and structural properties between polymer electrolytes with different lithium salts; and between the polymer electrolyte with/without the incorporation of dopant.

The properties and characteristics between PAA/$LiBF_4$ and PAA/$LiClO_4$ electrolyte systems; and the properties and characteristics between PAA/$LiBF_4$ or PAA/$LiClO_4$ electrolyte systems with their respective CPE systems are compared and discussed in Chapter 6. PAA-$LiBF_4$ based electrolytes systems exhibit higher ionic conductivity and thermal stability compared to PAA-$LiClO_4$ based electrolytes systems. However, PAA-$LiClO_4$ based electrolytes systems indicate wider ESW compared to PAA-$LiBF_4$ based

electrolytes systems. All PE and CPE systems demonstrated similar properties in the temperature dependence-ionic conductivity studies and dielectric studies. The complexation of the conducting salt ($LiBF_4$ and $LiClO_4$) with/without dopant ($BaTiO_3$) is confirmed by ATR-FTIR study and the increases of amorphous nature in the respective CPEs are demonstrated via XRD study.

7.2 Recommendations for Further Research

A sustainable source of renewable energy is highly demanded. A potential renewable material should fulfill the commercial requirements such cost effective, energy efficient, able to produce in bulk, low cost and high performance with desired properties. The electrochemical energy is one of the most effective, inexpensive, convenient, simple configure, and high mobility renewable energy source. EDLC presents an emerging technology that plays a vital role in fulfilling the requirements and demands of advanced electrochemical devices. Even though many have been achieved for the past decades, the further improvement of the high-performance device is still required. More efforts are required to ensure the realization of EDLCs with high ionic conductivity, high power density, high capacitance value, with a wide operative voltage.

Solid electrolytes are potentially the best solution for batteries or EDLCs attributed to their enhanced properties and also overcoming most the drawbacks of liquid electrolytes. One of the drawbacks using liquid electrolytes is the incompatibility of the electrolyte and electrodes which could affect the behaviour of the EDLC. Due to the fact that the working principle of EDLC is based on the interaction between electrode and electrolyte, thus the compatibility of both material plays a vital role in the development of advanced EDLC. The solid electrolytes are more compatible with the electrode materials compared to the liquid electrolytes.

The next generation EDLC is expected to have excellent properties such as high power density, high energy density, and desirable operative voltage. The innovation of the structural design of the device can be strategies via electrode component as well as electrolyte. Among most of the electrode materials, transition metal oxide and the composite of transition metal oxide with carbon could be among the research options. For the electrolyte materials, scientists could explore into new materials or composites that involved of new salt, ionic liquid, nanoparticles, functional chemicals, and new solvents.

A systematic research protocol should be developed and published to offer a standard and best practice in performing research for the new materials for EDLC. Besides the development of the new materials, the evaluation and improvement of the existing in-used materials also required further research efforts. When the materials are on board for application, the performance monitoring, evaluation and improvement should be in-placed so that either the electrode/electrolyte materials can be continuously worked out to meet the expected requirements.

A database of all the polymer hosts, solvents, conducting salts, dopants should be developed. Besides, it is ideally to have some matching and forecasting tools/software to perform screening of those material properties; make prediction of the expected properties and performance; perform simulation of the electrolyte/electrode material in the desired device. The digitalization of the electrochemical data could be used to identify the research gap and thus complete the research study to rule out what are not working and working. There are many of the components are yet to explore by the researchers. A gap analysis also recommended to establish for the prediction of the problem could occur when the new materials are produced in bulk. In the mass production, the purity of the chemicals used will be reduced. The study should determine whether the new grade of

chemicals used will affect the performance of the devices. The doping process is a process to introduce the dopant into the electrolyte system. The dopant could act as impurities either to enhance the electrolyte properties or the device performance.

The development and advancement of the electric double layer technology is a continuous state of act to meet the industrial requirements. In the changing world, continuous technology advancement is the important rule to sustain and create more values to mankind.

REFERENCES

Ahmad, Z., Al-Awadi, N. A., Al-Sagheer, F. (2007). Morphology, thermal stability and visco-elastic properties of polystyrene–poly(vinyl chloride) blends. *Polym. Degrad. Stabil., 92:* 1025–1033.

Ahn, J. H., Wang, G. X., Liu, H. K., Dou, S. X. (2003). Nanoparticle-dispersed PEO polymer electrolytes for Li batteries. *J. Power Sources, 119–121:* 422–426.

Alamgir, M. and Abraham, K. (1993). Li ion conductive electrolytes based on poly(vinyl chloride). *J. Electrochem. Soc., 140:* L96–L97.

Almond, D. P. and West, A. R. (1983). Impedance and modulus spectroscopy of 'real' dispersive conductors. *Solid State Ionics, 11:* 57–64.

Appetecchi, G. B., Croce, F., Persi, L., Ronci, F., Scrosati, B. (2000). Transport and interfacial properties of composite polymer electrolytes. *Electrochim. Acta 45:* 1481–1490.

Arslan, A., Kıralp, S., Toppare, L., Bozkurt, A. (2006). Novel conducting polymer electrolyte biosensor based on poly(1-vinylimidazole) and poly(acrylic acid) networks. *Langmuir, 22:* 2912–2915.

Awadhia, A., Patel, S. K., Agrawal, S. L. (2006). Dielectric investigations in PVA based gel electrolytes. *Prog. Cryst. Growth Charact. Mater., 52:* 61–68.

Bloise, A. C., Tambelli, C. C., Franco, R. W. A., Donoso, J. P., Magon, C. J., Souza, M. F., Rosario, A. V., Pereira, E. C. (2001). Nuclear magnetic resonance study of PEO-based composite polymer electrolytes. *Electrochim. Acta, 46:* 1571–1579.

Bocharova, V. and Sokolov, A. P. (2020). Perspectives for polymer electrolytes: A view from fundamentals of ionic conductivity. *Macromolecules, 53*(11): 4141–4157.

Bruce, P. G. (1995). *Solid State Electrochemistry*. Cambridge University Press.

Buraidah, M. H., Teo, L. P., Majid, S. R., Arof, A. K. (2009). Ionic conductivity by correlated barrier hopping in NH_4I doped chitosan solid electrolyte. *Physica B, 404:* 1373–1379.

Capiglia, C., Mustarelli, P., Quartarone, E., Tomasi, C., Magistris, A. (1999). Effects of nanoscale SiO_2 on the thermal and transport properties of solvent-free, poly(ethylene oxide) (PEO)-based polymer electrolytes. *Solid State Ionics, 118:* 73–79.

Capuano, F., Croce, F., Scrosati B. (1991). Composite polymer electrolytes. *J. Electrochem. Soc., 139:* 1918–1922.

Carlberg, J. C. and Inganäs, O. (1997). Poly(3,4-ethylenedioxythiophene) as electrode material in electrochemical capacitors. *J. Electrochem. Soc., 144:* 61–63.

Chen-Yang, Y. W., Chen, H. C., Lin, F. J., Chen, C. C. (2002). Polyacrylonitrile electrolytes: A novel high-conductivity composite polymer electrolyte based on PAN, $LiClO_4$ and α-Al_2O_3. *Solid State Ionics, 150:* 327–335.

Choe, H. S., Giaccai, J., Alamgir, M., Abraham, K. M. (1995). Preparation and characterization of poly(vinyl sulfone) and poly(vinylidene fluoride)-based electrolytes. *Electrochim. Acta, 40:* 2289–2293.

Choi, B. and Shin, K. (1996). Effects of SiC fillers on the electrical and mechanical properties of $(PEO)_{16}LiClO_4$ electrolytes. *Solid State Ionics, 86–88:* 303–306.

Chung, S. H., Wang, Y., Persi, L., Croce, F., Greenbaum, S. G., Scrosati B., Plichta E. (2001). Enhancement of ion transport in polymer electrolytes by addition of nanoscale inorganic oxides. *J. Power Sources, 97–98:* 644–648.

Croce, F., Appetecchi, G. B., Persi, L., Scrosati, B. (1998). Nanocomposite polymer electrolytes for lithium batteries. *Nature, 394:* 456–458.

Croce, F., Persi, L., Ronci, F., Scrosati, B. (2000). Nanocomposite polymer electrolytes and their impact on the lithium battery technology. *Solid State Ionics 135*: 47–52.

Croce, F., Persi, L., Scrosati, B., Serraino-Fiory, F., Plichta, E., Hendrickson, M. A. (2001). Role of the ceramic fillers in enhancing the transport properties of composite polymer electrolytes. *Electrochim. Acta, 46:* 2457–2461.

Croce, F., Scrosati, B., Mariotto, G. (1992). Electrochemical and spectroscopic study of the transport properties of composite polymer electrolytes. *Chem. Mater., 4:* 1134–1136.

Dai, Y., Wang, Y., Greenbaum, S. G., Bajue, S. A., Golodnitsky, D., Ardel, G., Strauss, E., Peled, E. (1998). Electrical, thermal and NMR investigations of composite solid electrolyte based on PEO, LiI and high surface area inorganic oxides. *Electrochim. Acta, 43:* 1557–1561.

Dasenbrock, C. O., Ridgway, T. H., Seliskar, C. J., Heineman, R. W. (1998). Evaluation of the electrochemical characteristics of a poly(vinyl alcohol)/poly(acrylic acid) polymer blend. *Electrochimi. Acta, 43:* 3497–3502.

Dionisio, M., Fernandes, A. C., Mano, J. F., Carreia, N. T., Sovsa, R. C. (2000). Relaxation studies in PEO/PMMA blends. *Macromolecules, 33:* 1002–1011.

Du, X., Guo, P., Song, H., Chen, X. (2010). Graphene nanosheets as electrode material for electric double-layer capacitors. *Electrochim. Acta, 55:* 4812–4819.

Fenton, D. E., Parker, J. M., Wright, P. V. (1973). Complexes of alkali metal ions with poly(ethylene oxide). *Polymer, 14:* 589–589.

Feuillade, G. and Perche, P. (1975). Ion-conductive macromolecular gels and membranes for solid lithium cells. *J. Appl. Electrochem., 5:* 63–69.

Fonseca, C. P., Rosa, D. S., Gaboardi, F., Neves, S. (2006). Development of a biodegradable polymer electrolyte for rechargeable batteries. *J. Power Sources, 155:* 381–384.

Fusalba, F., Gouérec, P., Villers, D., Bélanger, D. (2000). Electrochemical characterization of polyaniline in nonaqueous electrolyte and its evaluation as electrode material for electrochemical supercapacitors. *J. Electrochem. Soc., 148:* A1–A6.

Gogulamurali, N., Suthanthiraraj, S. A., Maruthamuthu, P. (1992). In: Chowdari BVR, Chandra S, Singh S, Srivastava PC (eds) Solid state ionics: materials and applications. *World Scientific,* Singapore, 373–373.

Golodnitsky, D., Ardel, G., Strauss, E., Peled, E., Lareah, Y., Rosenberg, Y. (1997). Conduction mechanism in concentrated LiIpolyethylene oxide Al_2O_3-based solid electrolytes. *J. Electrochem. Soc., 144:* 3484–3491.

Gray, F. M. (1991). Solid polymer electrolytes: Fundamentals and technological applications. New York: VCH Publishers.

Gray, F. M. (1997). Polymer electrolytes, RSC materials monographs, Cambridge: The Royal Society of Chemistry 1–30.

Gupta, V. and Miura, N. (2005). Electrochemically deposited polyaniline nanowire's network: A high-performance electrode material for redox supercapacitor. *Electrochem. Solid State Lett., 8:* A630–A632.

Gurkaynak, A., Tubert, F., Yang, J., Matyas, J., Spencer, J. L., Gryte, C. C. (1996). High-temperature degradation of polyacrylic acid in aqueous solution. *Polym. Chem., 34:* 349–355.

Hao, J., Li, X., Yu, S., Jiang, Y., Luo, J., Shao, Z., Yi, B. (2015). Development of proton-conducting membrane based on incorporating a proton conductor 1,2,4-triazolium methanesulfonate into the Nafion membrane. *J. Energy Chem., 24:* 199–206.

Huang, Y., Li, H., Wang, Z., Zhu, M., Pei, Z., Xue, Q., Huang, Y., Zhi, C. (2016). Nanostructured polypyrrole as a flexible electrode material of supercapacitor. *Nano Energy, 22:* 422–438.

Hu, J., Luo, J., Wagner, P., Agert, C., Conrad, O. (2011). Thermal behaviours and single cell performance of PBI-OO/PFSA blend membranes composited with lewis acid nanoparticles for intermediate temperature DMFC application. *Fuel Cells, 11*: 756–763.

Hu, J., Luo, J., Wagner, P., Conrad, O., Agert, C. (2009). Anhydrous proton conducting membranes based on electron-deficient nanoparticles/PBI-OO/PFSA composites for high-temperature PEMFC. *Electrochem. Commun., 11:* 2324–2327.

Itoh, T., Ichikawa, Y., Uno, T., Kubo, M., Yamamoto, O. (2003). Composite polymer electrolytes based on poly(ethylene oxide), hyperbranched polymer, $BaTiO_3$ and $LiN(CF_3SO_2)_2$. *Solid State Ionics, 156:* 393–399.

Jana, S. and Zhong, W. H. (2008). Electrical conductivity enhancement of a polymer using butyl glycidyl ether (BGE)–lithium hexafluorophosphate ($LiPF_6$) complex. *J. Mater. Sci., 434:* 4607–4617.

Javaid, A. (2017). Activated Carbon Fiber and Textiles, Woodhead Publishing Series in Textiles, 281–303.

Kam, W., Liew, C. W., Lim, J. Y., Ramesh S. (2014). Electrical, structural, and thermal studies of antimony trioxide-doped poly(acrylic acid)-based composite polymer electrolytes. *Ionics, 20*: 665–674.

Katsaros, G., Stergiopoulos, T., Arabatzis, I. M., Papadokostaki, K. G., Falaras. P. (2002). A solvent-free composite polymer/inorganic oxide electrolyte for high efficiency solid-state dye-sensitized solar cells. *J. Photochem. Photobiol. A, 149:* 191–198.

Khanmirzaei, M. H. and Ramesh, S. (2013). Ionic transport and FTIR properties of lithium iodide doped biodegradable rice starch based polymer electrolytes. *Int. J. Electrochem. Sci., 8:* 9977–9991.

Khanmirzaei, M. H. and Ramesh, S. (2014). Nanocomposite polymer electrolyte based on rice starch/ionic liquid/TiO_2 nanoparticles for solar cell application. *Measurement, 58:* 68–72.

Khiar, A. S. A., Puteh, R., Arof, A. K. (2006). Conductivity studies of a chitosan-based polymer electrolyte. *Phys. B, 373:* 23–27.

Kim, H. S., Kum, K. S., Cho, W. I., Cho, B. W., Rhee, H. W. (2003). Electrochemical and physical properties of composite polymer electrolyte of poly(methyl methacrylate) and poly(ethylene glycol diacrylate). *J. Power Sources, 124:* 221–224.

Kim, J. H, Kang, M. S., Kim, Y. J., Won, J., Park, N. G., Kang, Y. S. (2004). Dye-sensitized nanocrystalline Solar cells based on composite polymer electrolytes containing fumed silica nanoparticles. *Chem Commun., 14:* 1662–1663.

Kim, J. K., Cheruvally, G., Li, X., Ahn, J. H., Ki, K. W., Ahn, H. J. (2008). Preparation and electrochemical characterization of electrospun, microporous membrane-based composite polymer electrolytes for lithium batteries. *J. Power Sources, 178:* 815–820.

Ko, J. M. and Kim, K. M. (2009). Electrochemical properties of MnO_2/activated carbon nanotube composite as an electrode material for supercapacitor. *Mater. Chem. Phys., 114:* 837–841.

Kotz, R. and Carlen, M. (2000). Principles and applications of electrochemical capacitors. *Electrochim. Acta, 45:* 2483–2498.

Liew, C. W. and Ramesh, S. (2014). Comparing triflate and hexafluorophosphate anions of ionic liquids in polymer electrolytes for supercapacitor applications. *Materials, 7:* 4019–4033.

Liew, C. W., Ramesh, S., Arof, A. K. (2014b). Good prospect of ionic liquid based-poly(vinyl alcohol) polymer electrolytes for supercapacitors with excellent electrical, electrochemical and thermal properties. *Int. J. Hydrogen Energy, 39:* 2953–2963.

Liew, C. W., Ramesh, S., Durairaj, R. (2012a). Impact of low viscosity ionic liquid on PMMA PVC LiTFSI polymer electrolytes based on Ac impedance, dielectric behavior and HATR FTIR characteristics. *J. Mater. Res., 27:* 2996–3004.

Liew, C. W., Ramesh, S., Ramesh, K., Arof A. K. (2012b). Preparation and characterization of lithium ion conducting ionic liquid-based biodegradable corn starch polymer electrolytes. *J. Solid State Electrochem., 16:* 1869–1875.

Liquan, C., Chowdari, B. V., Radhakrishna S. (1988). Materials for solid-state batteries. Singapore: *World Scientific,* 69–69.

Li, Q., Sun, H. Y., Takeda, Y., Imanishi, N., Yang J., Yamamoto O. (2001). Interface properties between a lithium metal electrode and a poly(ethylene oxide) based composite polymer electrolyte. *J. Power Sources, 94:* 201–205.

Li, W., Yuan, M., Yang, M. (2006). Dual-phase polymer electrolyte with enhanced phase compatibility based on Poly(MMA-g-PVC)/PMMA. *Eur. Polym. J., 42:* 1396–1402.

Luo, J., Conrad, O., Vankelecom, I. F. J. (2013). Imidazolium methanesulfonate as a high temperature proton conductor. *J. Mater. Chem. A, 1:* 2238–2247.

MacCallum, J. R. and Vincent, C. A. (1987). Polymer electrolytes reviews, vol.2. London: Elsevier.

Madhurjya, M. B., Thokchom, J., Bhat, S. V. (2010). Studies on a nanocomposite solid polymer electrolyte with hydrotalcite as a filler. *Solid State Ionics, 181:* 964–970.

McGaugh, M. C. and Kottle, S. (1967). The thermal degradation of poly(acrylic acid). *J. Polym. Sci. Part C: Polym. Letters, 5:* 817–820.

Mi, H., Zhang, X., Yang, S., Ye, X., Luo, J. (2008). Polyaniline nanofibers as the electrode material for supercapacitors. *Mater. Chem. Phys., 112:* 127–131.

Nicotera, I., Coppola, L., Oliviero, C., Castriota, M., Cassanelli E. (2006). Investigation of ionic conduction and mechanical properties of PMMA–PVdF blend-based polymer electrolytes. *Solis State Ionics, 177:* 581–588.

Norashikin, N. Z. and Ibrahim, M. Z. (2009). The potential of natural waste (corn husk) for production of environmental friendly biodegradable film for seedling. *World Acad. Sci. Eng. Technol., 58:* 176–180.

Osman, Z., Ibrahim, Z. A., Arof, A. K. (2001). Conductivity enhancement due to ion dissociation in plasticized chitosan based polymer electrolytes. *Carbohydr. Polym., 44:* 167–173.

Paradhan, D. K., Choundhary, R. N. P., Samantaray, B. K. (2008). Investigations on the effect of various plasticizers in PVA–PMMA solid polymer blend electrolytes. *Int. J. Electrochem. Sci., 3:* 597–608.

Parikh, P., Sina, M., Banerjee, A., Wang, X., D'Souza, M. S., Doux, J. -M., Wu, E. A., Trieu, O. Y., Gong, Y., Zhou, Q., Snyder, K., Meng, Y. S. (2019). Role of polyacrylic acid (PAA) binder on the solid electrolyte interphase in silicon anodes. *Chem. Mater., 31*(7): 2535–2544.

Prasad, K. R. and Miura, N. (2004). Potentiodynamically deposited nanostructured manganese dioxide as electrode material for electrochemical redox supercapacitors. *J. Power Sources, 135:* 354–360.

Qian, Y., Lu, S., Gao, F. (2011). Preparation of MnO_2/graphene composite as electrode material for supercapacitors. *J. Mater. Sci., 46:* 3517–3522.

Quartarone, E., Mustarelli, P., Magistris, A. (1998). PEO-based composite polymer electrolytes. *Solid State Ionics, 110:* 1–14.

Raghavan, S. R., Riley, M. W., Fedkiw, P. S., Khan, S. A. (1998). Composite polymer electrolytes based on poly(ethylene glycol) and hydrophobic fumed silica: Dynamic rheology and microstructure. *Chem. Mater., 10:* 244–251.

Ragupathy, P., Park, D. H., Campet, G., Vasan, H. N., Hwang, S. J., Choy, J. H., Munichandrajah, N. (2009). Remarkable capacity retention of nanostructured manganese oxide upon cycling as an electrode material for supercapacitor. *J. Phys. Chem. C., 113:* 6303–6309.

Rajendran, S., Kannan, R., Mahendran, O. (2001). An electrochemical investigation on PMMA/PVdF blend-based polymer electrolytes. *Mater. Lett., 49:* 172–179.

Rajendran, S., Mahendran, O., Kannan, R. (2002). Ionic conductivity studies in composite solid polymer electrolytes based on methylmethacrylate. *J. Phys. Chem. Solids, 63:* 303–307.

Rajendran, S., Sivakumar, M., Subadevi, R. (2004). Investigations on the effect of various plasticizers in PVA–PMMA solid polymer blend electrolytes. *Mater. Lett., 58:* 641–649.

Rajendran, S. and Uma, T. (2000). Lithium ion conduction in PVC-$LiBF_4$ electrolytes gelled with PMMA. *J. Power Source, 88*: 282–285.

Ramesh, S. and Bing, K. N. (2012). Conductivity, mechanical and thermal studies on PMMA based polymer electrolytes complexed with $Li_2B_4O_7$ and PC. *J. Mater. Eng. Perform., 21:* 89–94.

Ramesh, S. and Liew, C. W. (2013). Development and investigation on PMMA-PVC blend-based solid polymer electrolytes with LiTFSI as dopant salt. *Polym. Bull., 70:* 1277–1288.

Ramesh, S. and Liew, C. W. (2010). Investigation on the effects of addition of SiO_2 nanoparticles on ionic conductivity, FTIR, and thermal properties of nanocomposite PMMA- $LiCF_3SO_3$- SiO_2. *Ionics, 16:* 255–262.

Ramesh, S., Liew C. W., Morris E., Durairaj R. (2010). Effect of PVC on ionic conductivity, crystallographic structural, morphological and thermal characterizations in PMMA PVC blend-based polymer electrolytes. *Thermochim, Acta, 511:* 140–146.

Ramesh, S. and Lu, S. C. (2012). Enhancement of ionic conductivity and structural properties by BMIMTf ionic liquid in P(VdF-HFP)-based polymer electrolytes, *J. Appl. Polym. Sci., 126:* 484–492.

Ramesh, S., Lu, S. C., Morris, E. (2012). Towards magnesium ion conducting poly (vinylidenefluoride-hexafluoropropylene)-based solid polymer electrolytes with great prospects: Ionic conductivity and dielectric behaviours. J. *Taiwan Inst. of Chem. Eng., 43:* 806–812.

Ramesh, S., Shanti, R., Morris, E. (2013). Employment of [Amim] Cl in the effort to upgrade the properties of cellulose acetate based polymer electrolytes. *Cellul., 20:* 1377–1389.

Ramesh, S., Yin, T. S., Liew, C. W. (2011). Effect of dibutyl phthalate as plasticizer on high molecular weight poly (vinyl chloride) lithium tetraborate based solid polymer electrolytes. *Ionics, 17:* 705–713.

Reddy, R. N. and Reddy, R. G. (2003). Sol–gel MnO_2 as an electrode material for electrochemical capacitors. *J. Power Sources, 124:* 330–337.

Reddy, R. N. and Reddy, R. G., (2006). Porous structured vanadium oxide electrode material for electrochemical capacitors. *J. Power Sources, 156:* 700–704.

Rhoo, H. J., Kim, H. T., Park, J. K., Hwang, T. S. (1997). Ionic conduction in plasticized PVC/ PMMA blend polymer electrolytes. *Electrochim. Acta, 42:* 1571–1579.

Ruiz, V., Blanco, C., Santamaria, R., Ramos-Fernández**,** J. M., Martínez-Escandell, M., Sepúlveda-Escribano, A., Rodríguez-Reinoso, F. (2009). An activated carbon monolith as an electrode material for supercapacitors. *Carbon, 47:* 195–200.

Saikia, D., Chen-Yang, Y. W., Chen, Y. T., Li, Y. K., Lin S. I. (2008). Investigation of ionic conductivity of composite gel polymer electrolyte membranes based on P(VDF-HFP), $LiClO_4$ and silica aerogel for lithium ion battery. *Desalination, 234:* 24–32.

Saikia, D. and Kumar, A. (2004). Ionic conduction in (PVdFHFP)PC+DEC-$LiClO_4$ polymer gel electrolytes. *Electrochim Acta, 49*: 2581–2589.

Sankar, S., Hazra, C., Chatti, M., Sudarsan, V., Mahalingam, V. (2012). Enhanced quantum efficiency for Dy^{3+} Emissions in water dispersible PbF_2 nanocrystals. *RSC Advances, 2*: 8269–8272.

Scrosati, B. (1993). Applications of Electroactive Polymers, Chapman Hall, London.

Scrosati, B., Croce, F., Persi, L. (2000). Impedance spectroscopy study of PEO-based nanocomposite polymer electrolytes. *J. Electrochem. Soc., 147:* 1718–1721.

Shastry, M. C. R. and Rao, K. J. (1991). Ac conductivity and dielectric relaxation studies in AgI-based fast ion conducting glasses. *Solid State Ionics, 44:* 187–198.

Shin, J. H., Lim, Y. T., Kim, K. W., Ahn H. J., Ahn J. H. (2002). Effect of ball milling on structural and electrochemical properties of $(PEO)_nLiX$ (LiX = $LiCF_3SO_3$ and $LiBF_4$) polymer electrolytes, *J. Power Sources, 107*: 103–109.

Silva, M. M., Nunes, S. C., Barbosa, P. C., Evans, A., Bermudez, V. Z., Smith, M. J., Ostrovskii, D. (2006). Sol–gel preparation of a di-ureasil electrolyte doped with lithium perchlorate. *Electrochim. Acta, 52*: 1542-1548.

Sim, L. H., Gan, S. N., Chan, C. H., Yahya, H. (2010). ATR-FTIR studies on ion interaction of lithium perchlorate in polyacrylate/poly(ethylene oxide) blends. *Spectrochim. Acta Part A, 76*: 287-292.

Singh, M., Ranjan, A., Yadav, B. C., Kaur, M. (2017). Synthesis and characterization of perovskite barium titanate thin film and its application as LPG sensor. *Sens. Actuators, B, 241*: 1170–1178.

Singh, S., Arora, N., Paul, K., Kumar, R., Kumar, R. (2019). FTIR and rheological studies of PMMA-based nano-dispersed gel polymer electrolytes incorporated with $LiBF_4$ and SiO_2. *Ionics, 25*: 1495-1503.

Sivakkumar, S. R., Kim, W. J, Choi, J. A., MacFarlane, D. R., Forsyth, M., Kim, D. W. (2007). Electrochemical performance of polyaniline nanofibres and polyaniline/multi-walled carbon nanotube composite as an electrode material for aqueous redox supercapacitors. *J. Power Sources, 171:* 1062–1068.

Smitha, B., Sridhar, S., Khan, A. A. (2004). Polyelectrolyte complexes of chitosan and poly(acrylic acid) as proton exchange membranes for fuel cells. *Macromol., 37:* 2233–2239.

Stamenkovic, J. V., Premovic, P. I., Mentus, S. V. (1997). Electrical conductivity of poly(acrylic acid*)* gels. *J. Serb. Chem. Soc., 62:* 945–950.

Stephan, A. M. Renganathan, N. G., Kumar T. P., Thirunakaran R., Pitchumani S., Shrisudersan, J., Muniyandi N. (2000). Ionic conductivity studies on plasticized PVC/PMMA blend polymer electrolyte containing $LiBF_4$ and $LiCF_3SO_3$. *Solid State Ionics, 130:* 123–132.

Stephan, A. M. (2006). Review on gel polymer electrolytes for lithium batteries. *Eur. Polym. J., 42:* 21–42.

Stevens, J. R. and Wieczorek, W. (1996). Ionically conducting polyether composites. *Can J. Chem., 74:* 2106–2113.

Subramanian, V., Hall, S. C., Smith, P. H., Rambabu, B. (2004). Mesoporous anhydrous RuO_2 as a supercapacitor electrode material. *Solid State Ionics, 175:* 511–515.

Subramaniam, V., Zhu, H., Wei, B. (2006). Nanostructured MnO_2: Hydrothermal synthesis and electrochemical properties as a supercapacitor electrode material. *J. Power Sources, 159:* 361–364.

Sukeshini, M., Nishimoto, A., Watanabe, M. (1996). Transport and electrochemical characterization of plasticized poly(vinyl chloride) solid electrolytes. *Solid State Ionics, 86:* 385–393.

Sun, H. Y., Sohn, H. J., Yamamoto, O., Takeda, Y., Imanishi, N. (1999). Enhanced lithium-ion transport in PEO-based composite polymer electrolytes with ferroelectric $BaTiO_3$. *J. Electrochem. Soc. 146*: 1672-1676.

Sun, H. Y., Takeda, Y., Imanishi, N., Yamamoto, O., Sohn, H. -J. (2000). Ferroelectric materials as a ceramic filler in solid composite polyethylene oxide-based electrolytes. *J. Electrochem. Soc. 147*: 2462–2467.

Susan, M. A. B. H., Kaneko, T., Noda, A., Watanabe, M. (2005). Ion gels prepared by in situ radical polymerization of vinyl monomers in an ionic liquid and their characterization as polymer electrolytes. *J. Am. Chem. Soc., 127:* 4976–4983.

Suthanthiraraj, S. A., Sheeba, D. J., Paul, B. J. (2009). Impact of ethylene carbonate on ion transport characteristics of PVdF–$AgCF_3SO_3$ polymer electrolyte system. *Mater. Res. Bull., 44:* 1534–1539.

Teoh, K. H, Ramesh S., Arof, A.K. (2012). Investigation on the effect of nanosilica towards corn starch lithium perchlorate based polymer electrolytes. *J. Solid State Electrochem., 16:* 3165–3170.

Tsunemi, K., Ohno, H., Tsuchida, E. (1983). Mechanism of ionic conduction of PvDF-lithium perchlorate hybrid films. *Electrochim. Acta, 28:* 833–837.

Venkateswarlu, M., Reddy, K. N., Rambabu, B., Satyanarayana, N. (2000). A.c. conductivity and dielectric studies of silver-based fast ion conducting glass system. *Solid State Ionics, 127:* 177–184.

Vincent, C. A. (1987). Polymer electrolytes. *Prog. Solid State Chem., 17:* 145–261.

Vondrak, J., Sedlarikova, M., Velicka, J., Klapste, B., Novak, V., Reiter, J. (2001). Gel polymer electrolytes based on PMMA. *Electrochim. Acta, 46:* 2047–2048.

Walls, H. J., Zhou, J., Yerian, J. A., Fedkiw, P. S., Khan, S. A., Stowe M. K., Baker G. L. (2000). Fumed silica-based composite polymer electrolytes: synthesis, rheology, and electrochemistry. *J. Power Sources, 89:* 156–162.

Watanabe, M., Kanba, M., Nagaoka, K., Shinohara, I. (1983). Ionic conductivity of hybrid films composed of polyacrylonitrile, ethylene carbonate and $LiClO_4$. *J. Polym. Sci. Part B: Polym. Phys., 21:* 939–948.

Watanabe, M., Nagano, S., Sanui, K., Ogata, N. (1986). Ionic conductivity of network polymers from poly(ethylene oxide) containing lithium perchlorate. *Polymer J., 18*: 809-817

Wei, Y.Z., Fang, B., Iwasa, S., Kumagai, M. (2005). A novel electrode material for electric double-layer capacitors. *J. Power Sources 141:* 386–391.

Wen, Z., Itoh, T., Uno, T., Kubo, M., Yamamoto, O. (2003). Thermal, electrical, and mechanical properties of composite polymer electrolytes based on cross-linked poly(ethylene oxide-co-propylene oxide) and ceramic filler. *Solid State Ionics, 160:* 141–148.

Weston, J. E. and Steele, B. C. H. (1983). Effects of inert filler s on the mechanical and electrochemical properties of lithium salt-poly(ethylene oxide) polymer electrolytes. *Solid State Ionics, 7:* 75–79.

Winie, T., Ramesh S., Arof A. K. (2009). Studies on the structure and transport properties of hexanoyl chitosan-based polymer electrolytes. *Physica B. Condensed Matter, 404:* 4308–4311.

Wright, P.V. (1975). Electrical conductivity in ionic complexes of poly(ethylene oxide). *Br. Polym. J., 7:* 319–327.

Wu, G. M., Lin, S. J., Yang, C. C. (2006). Preparation and characterization of PVA/ PAA membranes for solid polymer electrolytes. *J. Membr. Sci*., *275*: 127–133.

Xiong, H. G., Tang, S. W., Tang, H. L., Zou P. (2008). The structure and properties of a starch-based biodegradable film. *Carbohydr. Polym., 71:* 263–268.

Xu, K., Ding, S. P., Jow, T. R. (1999). Toward reliable values of electrochemical stability limits for electrolytes. *J. Electrochem. Soc., 146:* 4172–4178.

Xu, M. W., Zhao, D. D., Bao, S. J., Li, H. L. (2007). Mesoporous amorphous MnO_2 as electrode material for supercapacitor. *J. Solid State Electrochem., 11:* 1101–1107.

Yahya, M. Z. A. and Arof, A. K. (2003). Effect of oleic acid plasticizer on chitosan-lithium acetate solid polymer electrolytes. *Euro Polym. J., 39:* 897–902.

Yang, I., Yoo, J., Kwon, D., Choi, D., Kim, M. -S., Jung, J. C. (2020). Improvement of a commercial activated carbon for organic electric double-layer capacitors using a consecutive doping method. *Carbon, 160*: 45-53.

Yang, M., Cheng, B., Song, H., Chen, X. (2010). Preparation and electrochemical performance of polyaniline-based carbon nanotubes as electrode material for supercapacitor. *Electrochim. Acta, 55:* 7021–7027.

Ye, L. and Feng, Z. (2010). Polymer Electrolytes – Fundamentals and applications, woodhead publishing series in electronic and optical materials, 550–582.

Yin, L., Li, S., Liu, X., Yan T. (2019). Ionic liquid electrolytes in electric double layer capacitors. *Science China Materials, 62*: 1537-1555.

Yoon, D. H. and Lee, B. I. (2002). $BaTiO_3$ properties and powder characteristics for ceramic capacitors. *J. Ceram. Process. Res., 3:* 41-47.

You, X., Misra, M., Gregori, S., Mohanty, A. K. (2018). Preparation of an Electric double layer capacitor (EDLC) using *Miscanthus*-derived biocarbon. *ACS Sustainable Chem. Eng., 6(1)*: 318-324.

Yu, S., Liu, Z., Xu, N., Chen, J., Gao, Y. (2020). Influencing factors for determining the crystallinity of native cellulose by X-ray diffraction. *Anal. Sci., 36*: 947-951.

Zhang, D., Zhang, X., Chen, Y., Yu, P., Wang, C., Ma, Y. (2011a). Enhanced capacitance and rate capability of graphene/polypyrrole composite as electrode material for supercapacitors. *J. Power Sources, 196:* 5990–5996.

Zhang, F. B., Zhou, Y., Li, H. (2004). Nanocrystalline NiO as an electrode material for electrochemical capacitor. *Mater. Chem. Phys., 83:* 260–264.

Zhang P., Yang L. C., Li L. L., Ding M. L., Wu Y. P., Holze R. (2011b). Enhanced electrochemical and mechanical properties of P(VDF-HFP)-based composite polymer electrolytes with SiO_2 nanowires. *J. Membr. Sci., 379:* 80–85.

Zhang, Y., Li, G., Lv, Y., Wang, L., Zhang, A., Song, Y., Huang, B. **(**2011c). Electrochemical investigation of MnO_2 electrode material for supercapacitors. *Inter. J. Hydrogen Energy, 36:* 11760–11766.

Zhao, X., Tian, H., Zhu, M., Tian, K., Wang, J. J., Kang, F., Outlaw, R. A. (2009). Carbon nanosheets as the electrode material in supercapacitors. *J. Power Sources, 194:* 1208–1212.

Zheng, J. P., Cygan, P. J., Jow, T. R. (1995). Hydrous ruthenium oxide as an electrode material for electrochemical capacitors. *J. Electrochem. Soc., 142:* 2699–2703.

Zheng, Y., Ding, H., Zhang, M. (2009). Preparation and electrochemical properties of nickel oxide as a supercapacitor electrode material. *Mater. Res. Bull., 44:* 403–407.